Contributions

of

Utrecht University, Faculty of Science

to

21st European Photovoltaic Solar Energy Conference and Exhibition (EPSEC21) 4-8 September, 2006, Dresden, Germany

Collected by

W.G.J.H.M. van Sark (Science, Technology and Society)
R.E.I. Schropp (Surfaces, Interfaces and Devices)

September 2006, NWS-E-2006-120

[Faculteit Bètawetenschappen]

Universiteit Utrecht

ORAL PRESENTATIONS

3AO.8.4
R.H. Franken, R.L. Stolk, H. Li, C.H.M. van der Werf, J.K. Rath, R.E.I. Schropp
Correlation Between the Surface Morphology and the Current Enhancement in n-i-p Solar Cells

6BO.7.2
A.C. de Keizer, W.G.J.H.M. van Sark, S. Stettler, P. Toggweiler, E. Lorenz, A. Drews, D. Heinemann, G. Heilscher, M. Schneider, E. Wiemken, W. Heydenreich, H.G. Beyer
PVSAT-2: Results of Field Test of the Satellite-Based PV System Performance Check

8CO.1.3
E.A. Alsema, M.J. de Wild-Scholten, V.M. Fthenakis
Environmental Impacts of PV Electricity Generation - A Critical Comparison of Energy Supply Options

1CO.6.2
W.G.J.H.M. van Sark
Optimization of the Performance of Solar Cells With Spectral Down Converters

7DO.5.5
E.W. ter Horst, C. Zhang
PV market and industry development in China - Impacts of the China REDP project, other PV programs and technology

POSTER PRESENTATIONS:

5BV.1.20
N.H. Reich, W.G.J.H.M. van Sark, E.A. Alsema
Simulation of PV-powered product: iPV-Sim

5BV.1.21
N.H. Reich, M. Veefkind, E.A. Alsema, W.G.J.H.M. van Sark, B. Elzen
Industrial Design of a PV Powered Consumer Application - Case Study of a Solar Powered Wireless Computer Mouse

7BV.5.30
W.G.J.H.M. van Sark, E.H. Lysen, D. Cocard, P. Beutin, G.F. Merlo, B. Mohanty, J. van den Akker, A. Razzak Idris, A. Firag, A. Waheed, A. Shaheed, M. Latheef, A. Wajeeh
The First PV-Diesel Hybrid System in the Maldives Installed at Mandhoo Island

3DV.3.48
R.H. Franken, R.L. Stolk, H. Li, C.H.M. van der Werf, J.K. Rath, R.E.I. Schropp
Control of the Growth of Textured Ag and Ag:AlO_x Back Reflectors for n-i-p Solar Cells

3DV.3.51
H. Li, F. Rubinelli, J. Rath, R.E.I. Schropp
Observation of Photogating Effect in Microcrystalline Silicon Solar Cells and its Contribution to Device Optimization

7DV.5.15
M.J. de Wild-Scholten, E.A. Alsema, E.W. ter Horst, M. Bächler, V.M. Fthenakis
A cost and environmental impact comparison of grid-connected rooftop and ground-based PV systems

CORRELATION BETWEEN THE SURFACE MORPHOLOGY AND THE CURRENT ENHANCEMENT IN N-I-P SILICON SOLAR CELLS

R.H. Franken, R.L. Stolk, H. Li, C.H.M. van der Werf, J.K. Rath*, R.E.I. Schropp
Utrecht University, Debye Institute, SID - Physics of Devices, P.O. Box 80.000, 3508 TA Utrecht, The Netherlands,
Tel : 0031 (0)30 2532964, Fax 0031 (0)30 2543165, email: R.H.Franken@phys.uu.nl,

For substrate type n-i-p solar cells rough reflecting back contacts are used in order to enhance the short-circuit currents. The roughness at the interfaces is considered to be the key to efficient light trapping. Root-mean-square (*rms*) roughness, angular resolved scattering (*ars*) intensity and haze are normally used to indicate the amount of scattering, but they do not quantitatively correlate with the current enhancement. It is proposed that the lateral dimensions should also be taken into account. Based on fundamental considerations, we have analyzed by atomic force microscopy (AFM) specific lateral dimensions that are considered to have a high scattering efficiency. For textured back reflectors with widely varying morphologies, both the value of the *rms* roughness as well as the integrated intensity of *ars* under wide angles have been weighted with the lateral dimensions of the effective scattering features. A clear correlation is found in the current generation under red light in microcrystalline n-i-p solar cells with the weighted *rms* value as well as with the weighted *ars* intensity of the Ag back contacts. Furthermore, the surface plasmon absorption of the rough Ag back contact has been considered to be a significant limiting factor for the current enhancement.
Keywords: Micro-crystalline Si, light trapping, back contact

1. INTRODUCTION

In order to enhance the generated photocurrent in thin microcrystalline silicon solar cells, effective light trapping schemes are needed. In case of thin microcrystalline layers, rough interfaces at the front or back of the active material can increase the path length of the light by scattering and consequently increase the absorption. The morphology at the interfaces is considered to be the key to efficient light trapping. However, a better understanding of the relation between this surface morphology and light scattering properties is important to develop optimized structure roughness. Root-mean-square (*rms*) roughness, angular resolved scattering (ARS) distribution and haze values are micro- and macroscopic quantities of the morphology that are commonly used to indicate the amount of scattering, but they do not quantitatively correlate with the current enhancement in the solar cell [1,2]. It has so far been difficult to determine experimentally specific morphology related properties that uniquely correlate with the current enhancement in thin film solar cells.

This paper experimentally identifies and fundamentally discusses two specific properties of the surface morphology of Ag back contacts that are considered to be important for light scattering. Taking into account these two effects results in a clear correlation between the Ag surface morphology and the long wavelength current enhancement of the measured external collection efficiency (ECE) curves.

First, we consider that also the lateral properties of the surface play an important role in the light trapping process [1,3]. This paper describes how both vertical as well as lateral properties of the surfaces can be combined in order to obtain a better indicator for the light induced current generation potential of solar cells.

Secondly, we indicate the influence of the light absorption from the surface plasmons of the Ag back contact in terms of a limitation of the current enhancement and show that a unique correlation with the current enhancement can be obtained after correcting for the plasmon absorption losses.

2 EXPERIMENTAL

This paper presents results that are obtained on n-i-p type 1.5 μm thick hot-wire chemical vapour deposition (HWCVD) μc-Si:H solar cells deposited on texture-grown highly reflecting Ag or Ag:AlO_x layers. A large variety in the surface morphology of the back contacts is obtained [4]. In order to increase the reflection from the metal back contact, a conformal 100 nm thick low refractive index ZnO:Al interlayer is used. The microscopic parameters of the back contact such as *rms* roughness and lateral feature size are obtained by AFM measurements and power spectral density (PSD) evaluation. The integration of the wide-angle *ars* intensity results in a different quantitative parameter that also relates to the light scattering. The current density considered in this paper is the integrated current density obtained from negatively biased ECE measurements in the wavelength range between 650-1100 nm convoluted with the AM1.5 spectrum. The plasmon absorption of the Ag contact is calculated from total reflection measurements in air.

3 FUNDAMENTAL

The interaction of light with the various interfaces inside a solar cell is dependent on the effective wavelength (λ_{eff}) in the respective media used in the cell and the dimensions of the morphology of the interface. For surface feature dimensions larger than λ_{eff} the interaction can be described by geometrical optics. For dimensions in the order of the wavelength the interaction should be treated as a scattering (diffraction) problem, which is best described by Mie theory [5]. Therefore, apart from vertical characteristics, such as *rms* roughness, also the lateral properties of the surface play an important role in the light trapping process. In thin film solar cells only the scattering of the light can result in effective reflection and transmission at wide angles and thus, longer path lengths. Therefore, the surface feature dimensions of the interfaces should preferably have sizes close to λ_{eff}

Through each different medium, the light travels with

* Corresponding Author: J.K.Rath@phys.uu.nl

a different λ_{eff}, with which it encounters the successive interfaces. Therefore, we consider that each interface can be separately optimized with respect to its morphology. However, in case of thin film solar cells it is considered that the morphology of all the interfaces is mainly determined by the morphology of the substrate on which the solar cell is deposited.

Furthermore, absorption loss occurs at the back electrode due to surface plasmon (SP) absorption at the highly reflecting Ag surface. This SP absorption peak occurs at a wavelength of 350 nm. However, the peak can be broadened and affect the absorption at long wavelength region. The broadening and intensity of this peak is dependent on the material used and the surface feature dimensions [6]. Moreover, it is known from the literature that there are two ways by which plasmon absorption can be increased: grating coupling [7] and attenuated total reflection [8]. A rough surface can result in effective grating coupling and therefore limit the light scattering. A low refractive index ZnO:Al interlayer on top of the Ag surface results in a weaker plasmon coupling than with the high refractive index μc-Si:H i-layer. In order to limit the surface plasmon absorption losses at rough Ag layers this plasmon coupling should be avoided.

4 RESULTS

4.1 Texture properties of the Ag back reflector

Common correlations simply between *rms* roughness and J_{sc} or integrated EQE current such as done in Figure 1 do not include any lateral dimension parameter. The lateral dimension, however, is inherently correlated with the given roughness parameter as is presented in this conference [4]. Therefore, a fair one to one correlation between J_{sc} and only the *rms* roughness cannot be made. A positive correlation is observed up to a certain roughness, in this case 60 nm. Larger roughness also includes increased lateral sizes that can be one order of magnitude larger than the effective wavelength, which is considered not to be effective for light scattering. A quantitative correlation between the *rms* roughness of the Ag back contact morphology with the current enhancement, therefore, does not hold.

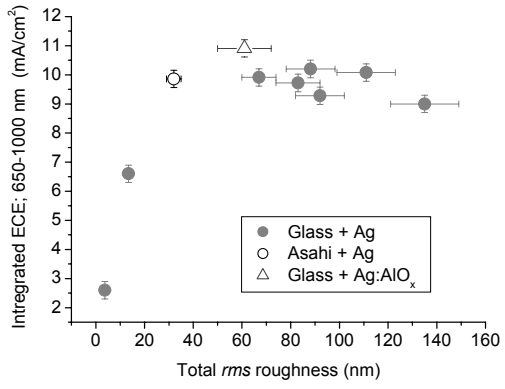

Figure 1: The relation between the total *rms* roughness of the Ag back contacts and the current density at long wavelengths.

4.2 Angle resolved scattering

One could expect that the light that is scattered at the surface of the back contact into angles wider than the angle of total internal reflection (> 30° for n-i-p μc-Si:H i-layers with front ITO) contributes directly to the light trapping in the solar cells. However, we observed that the *ars* intensity is related to the surface morphology and dependent on both the vertical sizes, σ as well as the lateral sizes, L as is depicted in Figure 2.

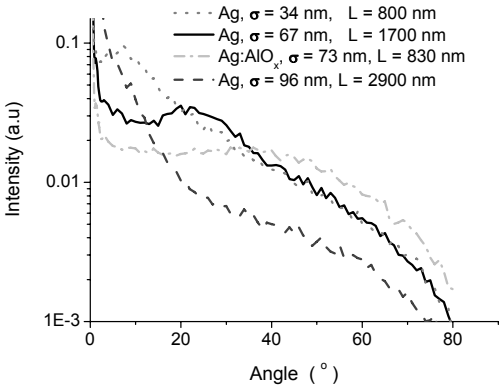

Figure 2: The dependency of the ARS distibution on the morphology of various Ag back contacts.

The reflected ARS distribution is measured in air at a wavelength of 633 nm. As the measurements at wide angles were virtually independent of the wavelength between 400 and 1000 nm, the measurements should reflect the scattering inside the solar cell. However, as can be seen in Figure 3, for a large variety of surface morphologies the integrated *ars* intensity does not quantitatively correlate with the current generation, as has also been observed in the literature [9].

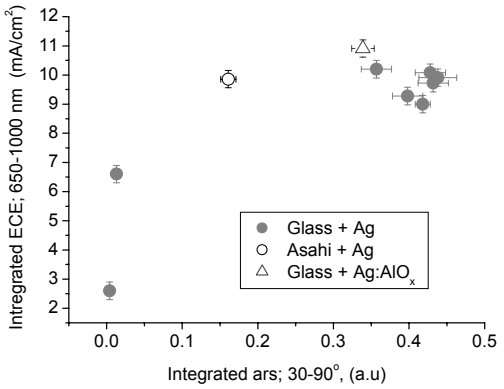

Figure 3: The relation between the intensity of the wide angle ARS measurement and the current density at long wavelengths.

4.3 Power Spectral Density

If we look closer at the AFM image of any of the Ag back contacts, it appears that various feature sizes from 50 to 5000 nm can be present at the surface. This makes it difficult to describe such a surface or to identify the feature sizes that are relevant for light scattering. The sizes that scatter most effectively will be around the effective wavelength that encounters the Ag surface: $\lambda_{scat} = \lambda_{eff} = \lambda_{air}/n_{ZnO:Al}$. Because the light in the wavelength

range between 650 - 1100 nm is considered to reach the back contact, we should also consider a range of the effective scattering feature sizes (λ_{scat}). With a PSD profile the AFM scanned surface profile is resolved into sine profiles of various wavelengths, depending on the lateral feature sizes present on the surface. The power of these spatial features can be interpreted as the amount of dominancy of this specific size. In order to achieve improved light scattering at wide angles it is considered that a surface should have dominating values of the PSD profile in the region of the λ_{scat} range. For the case presented in Figures 1, 2, this occurred at the intermediate *rms* values and the intermediate *ars* intensities. At larger *ars* values the surface profile is dominated by feature sizes much larger than the effective wavelength, which will result in more geometrical reflection and less scattering into wide angles. Figure 4 shows the PSD profiles of Ag back contacts with various *rms* roughness. The Ag layer with a small roughness of 33 nm shows a large contribution in the λ_{scat} range (indicated as B), whereas, the larger *rms* roughness layers show mainly dominating features sizes above 2000 nm.

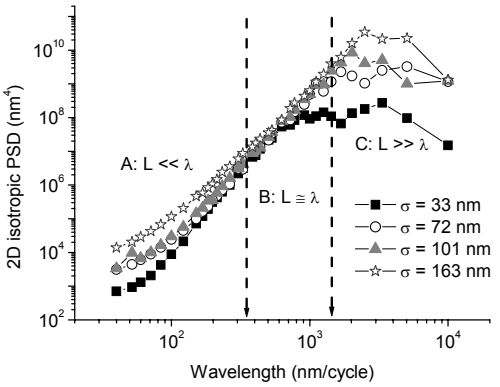

Figure 4: The 2D isotropic PSD spectra of Ag back contacts with various morphologies. The x-scale length resembles the lateral feature sizes present on the surface. The PSD intensity of that wavelength represents the σ^4 roughness of these features. The features with a higher power value are more dominantly present on the surface.

4.4 Weighing with lateral dimensions

We quantified the contribution of the features within region B, as indicated in Figure 4, and calculated the fraction of the power from this region with respect to the total power. The fraction will be used as a weighing factor for the total *rms* roughness value which is calculated from the PSD measurement, resulting in a value of the weighted *rms* roughness, $\sigma_{weigh} = \sigma_{tot}*PSD(\lambda_{scat})/PSD_{tot}$. Additionally the wide angle intensity of the ARS measurements is also weighted with the contribution of the specific light scattering sizes. This recalculation of the *ars* intensity resembles the weighted *ars* intensity reported in the literature [9].

In both cases the weighted *rms* and the weighted *ars* values resulted in an improved correlation with the long wavelength generated current, as is shown in Figure 5. It is observed that the solar cells with a back reflector of very high *rms* and *ars* values and additional with large lateral dimensions, the weighted parameters are shifted to lower values. As the cells with these back reflector layers also showed lower current density in the long wavelength region, the figures showed an improved positive correlation and the maximum that appeared in Figures 1,2 is now less pronounced.

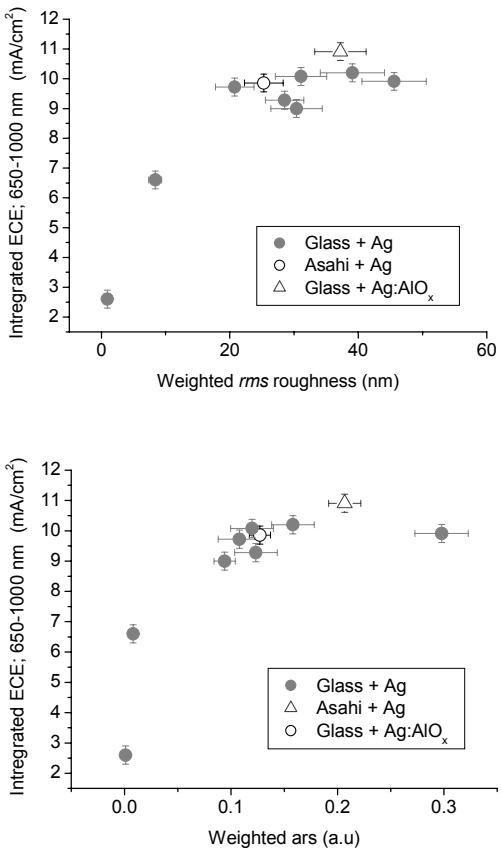

Figure 5: The correlation between the weighted *rms* roughness (top), weighted *ars* values (bottom) and the long wavelength current density.

4.5 Plasmon absorption

We consider that the absorption losses due to the surface plasmons of the back contact can limit the current generation of the solar cells significantly. As was mentioned in section 3; because of the effective plasmon absorption due to grating coupling, it is expected that surfaces with specific roughness exhibit an increased plasmon absorption loss compared to layers without roughness. This grating will be most effective if the lateral (peak to peak) surface dimensions are in the range of the effective wavelength [7]. The losses of the plasmon absorption will therefore partly compensate the increased scattering at these surfaces. We measured the plasmon absorption indirectly by total reflection measurements of the various Ag back contact layers. The measurements are done in air and therefore they do not completely resemble the solar cell situation, in which case a higher refractive index ZnO:Al layer on top of the Ag back contact will result in a larger plasmon absorption [10]. Therefore, we compared the various Ag and Ag:AlO_x contacts relative to each other. The results of the plasmon absorption are depicted in Figure 6. It is indeed observed that the layers with features of optimized light scattering dimensions, such as the Ag:AlO_x layers, exhibit a larger plasmon absorption and

shift in the SP absorption peak than that of a smooth layer. The plasmon absorption can extend up to the long wavelength region that will encounter the back contact in a solar cell.

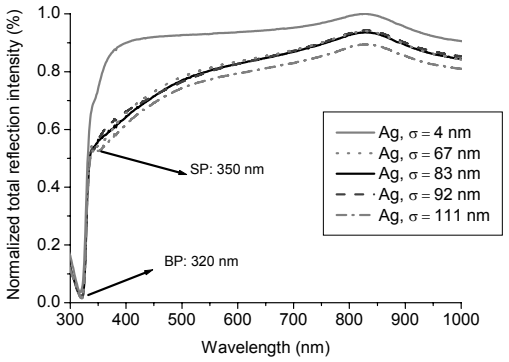

Figure 6: The absorption peaks of the surface (SP) and bulk (BP) plasmon indirectly measured by the total reflection. The intensity of the SP is dependent on the dimensions of the morphology of the back contacts.

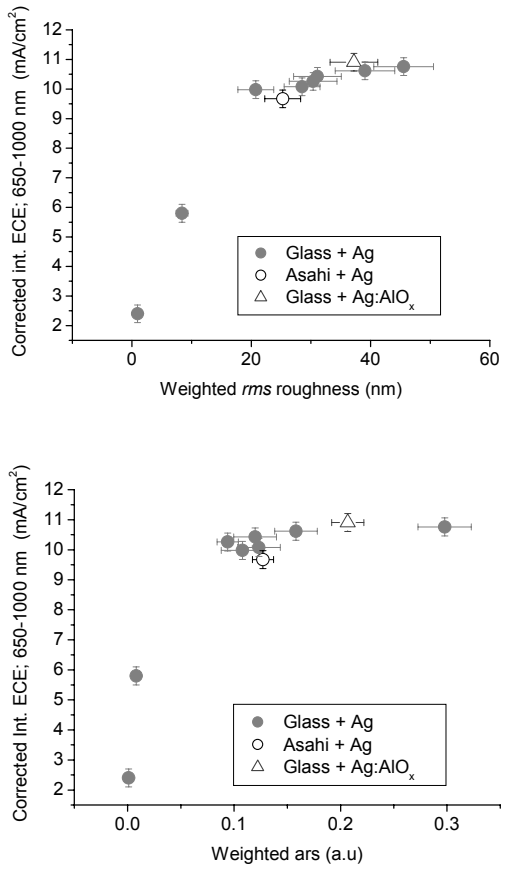

Figure 7: The correlation between the plasmon corrected long wavelength generated current density and the weighted *rms* (top), weighted *ars* intensity (bottom).

The generated current is corrected for the relative absorption losses due to SP absorption and depicted in Figure 7. The correlation indeed improved for both cases. Furthermore, saturation in the generated current appears. From this we conclude that other factors are also limiting the light scattering and current enhancement, such as absorption losses in the TCO layers, in the n- and p-layers, reflection losses on the front of the solar cell and recombination losses in the i-layer.

4.6 High efficiency HWCVD μc-Si:H solar cell

By using an optimized back reflector and hydrogen profiling steps for the i-layer we obtained a 8.5 % efficiency solar cell, comprising a 2.0 μm μc-Si:H HWCVD i-layer, which is presently the highest efficiency HWCVD μc-Si:H n-i-p type solar cell reported in the literature. The J-V data is shown in Table 1.

Table 1: J-V data of a 2.0 μc-Si:H n-i-p solar cell on an optimized textured Ag/ZnO:Al back reflector.

Efficiency (%)	**J_{sc} (mA/cm²)**	**V_{oc} (V)**	**FF**
8.5	23.4	0.55	0.67

Acknowledgements

The authors thank the Netherlands agency for Energy and the Environment (SenterNovem) for financial support.

5 CONCLUSIONS

Based on both fundamental considerations and observed data measurements, we have explained the importance of feature sizes of both dimensions (lateral and vertical) for light scattering. We have shown that neither *rms* roughness nor *ars* values can give a quantitative correlation with the current generated inside n-i-p solar cells with Ag/ZnO:Al back reflectors.

We propose a method that takes into account the lateral sizes in combination with the *rms* roughness and integrated wide angle *ars* values. A weighing factor is used to correlate these values with the current generated from the long wavelength region in n-i-p μc-Si:H solar cells. For both *rms* roughness and integrated *ars* values the use of the weighing factor led to an improved correlation over a wide range of different morphologies, indicating that for optimized scattering back reflectors both surface dimensions should be controlled.

A further correction of the generated current for the plasmon absorption resulted in an improved correlation over a wide range of weighted *rms* roughness and integrated *ars* values. This quantitative correlation between the surface morphology and the current generation in n-i-p microcrystalline solar cells gives us a better indication of the the limiting factors in current enhancement. With this understanding we are paving the way for improved light trapping schemes, which are needed for thin film solar cells.

A high efficiency 8.5% μc-Si:H solar cell is obtained on optimized Ag/ZnO:Al back reflectors.

REFERENCES

[1] T. Dekker, J.W. Metselaar, R. Schaltmann, B. Stannowksi, R.A.C.M.M. van Swaaij and M. Zeman, in *Proc. of 20th EUPVSEC, Barcelona,*(2005) pp 1517.
[2] P. Lechner, R. Geyer, H. Schade, B. Rech, O. Kluth, H. Stiebig, in *Proc.19th EUPVSEC,Paris,*(2004) pp 1591.

[3] O. Kluth, C. Zahren, H. Stiebig, B. Rech, H. Schade, in *Proc.19th EUPVSEC, Paris, France*, (2004) pp. 1587.
[4] R.H. Franken, R.L. Stolk, H.Li C.H.M. van der Werf, J.K. Rath, R.E.I. Schropp**,** in *21st EUPVSEC, Dresden, 2006, this conference.*
[5] G. Mie, Annular Physics **25** (1908) 377.
[6] A. Liebsch, Phys. Rev. Let. **71** (1993) 145.
[7] G.R. Aizin, N. J. M. Horing, L. G. Mourokh, et al. J. Appl. Phys. **96** (2004) 4225.
[8] D.B. Singh, V.K. Tripathi, J. Appl. Phys. **98** (5), (2005) 1.
[9] H. Schade, P. Lechner, R. Geyer, H. Stiebig, B. Rech, O. Kluth, in *Proceedings of 31st IEEE Photovoltaic Specialists Conference,* (2005), pp 1436.
[10] J. Springer, A. Poruba, L. Mullerova, M. Vanecek, O. Kluth, B. Rech, J. Appl. Phys. **95**, (3), 1427

PVSAT-2: RESULTS OF FIELD TEST OF THE SATELLITE-BASED PV SYSTEM PERFORMANCE CHECK

A.C. de Keizer[1], W.G.J.H.M. van Sark[1], S. Stettler[2], P. Toggweiler[2], E. Lorenz[3], A. Drews[3], D. Heinemann[3], G. Heilscher[4], M. Schneider[4], E. Wiemken[5], W. Heydenreich[5], H.G. Beyer[6]
[1]Dept. Science, Technology and Society, Copernicus Institute, Utrecht University, Heidelberglaan 2, 3584 CS Utrecht, the Netherlands, tel: +31 30 253 7736, fax: +31 30 253 7601, email: A.C.deKeizer@chem.uu.nl
[2]Enecolo AG, Lindhofstr. 52, 8617 Mönchaltorf, Switzerland
[3]Energy and Semiconductor Research Laboratory, Institute of Physics, Carl von Ossietzky University Oldenburg, 26111 Oldenburg, Germany
[4]Meteocontrol, Spicherer Str. 48, 86157 Augsburg, Germany
[5]Fraunhofer ISE, Heidenhofstr. 2, 79110 Freiburg, Germany,
[6]Inst. of Electrical Engineering, University of Applied Sciences (FH) Magdeburg-Stendal, 39114 Magdeburg, Germany,

ABSTRACT: Within the EU funded project PVSAT-2 an automated performance check for grid-connected PV systems has been developed. Measured energy yield and simulated yield that is based on satellite-derived irradiation data, are used for the automatic detection of malfunctions in a PV system. It is especially suited for small (< 5 kWp) systems to help avoiding the use of expensive monitoring equipment. The designed method was evaluated for 100 small PV systems in a field test that took place from February to September 2005. We found that incorrect system descriptions caused inaccurate simulations for several systems; solutions are proposed in this paper. The effectiveness of the failure detection is determined by the accuracy of the irradiation information. The uncertainty in the simulated energy yield can be high for cloudy weather situations and at low sun elevation. Under these weather conditions it is more difficult to detect a malfunction than under clear sky conditions. On days with a high irradiation, such as clear sky days in summer, a daily energy loss of circa 15 % can be identified within a day.
Keywords: PV system; performance; monitoring

1 INTRODUCTION

The number of grid-connected photovoltaic systems in Europe is rapidly increasing. In 2005 645 MWp of photovoltaic systems was installed, which leads to a total installed amount of 1.8 GWp in Europe [1]. The large majority of these systems are small and often not monitored. Many larger systems use system surveillance with irradiation sensors, data loggers, or other monitoring devices to prevent economic loss due to malfunctioning. This is not economical for small (< 5 kWp) systems. Furthermore, PV laymen might not discover a partial malfunction of their system, since the energy yields are fluctuating with weather conditions. Jahn [2] states that on average a failure happens once every 4.5 years for PV systems installed between 1991 and 1994 of which inverters contributed 63 %, PV modules 15 % and other failures 23 %. Monitoring of small PV systems leads to a rapid discovery of malfunctions. This leads to a higher energy gain and especially in countries with a feed-in tariff also to a financial benefit.

Therefore, within the PVSAT-2 project a low-cost and reliable method was developed to automatically and daily check the performance of a PV system. Irradiance values are determined from meteorological satellite data, thereby excluding costs for use of relatively expensive (installation of) reference cells. The measured and simulated energy yields are automatically compared, thereby excluding expensive operator time to analyse measurements. During the last year of the project the effectiveness and quality of the PVSAT-2 routine was thoroughly checked in a field test; the results will be presented here. In section 2 an overview of the methodology and the set up of the field test is presented. In section 3 the quality of the simulation of the energy yield is discussed, also some examples of the effectiveness of the failure detection routine in the test phase are given. The conclusions are presented in section 4.

2 METHODOLOGY

2.1 General PVSAT-2 methodology

In Figure 1 the set up of the PVSAT-2 routine is shown. Hourly values of solar irradiance are derived from Meteosat-7 (during the development and test phase) and Meteosat-8 (for the marketed product) satellite images. A description of the system characteristics (tilt, azimuth, module types, inverter, latitude, longitude, distance of system to roof) together with hourly irradiation and temperature information is used to calculate a reference hourly energy yield [3]. This is compared to the measured energy yield by a 'failure detection routine', which in a first step determines, if a failure occurred. In the second step it identifies possible causes for the malfunction [4]. The whole routine is fully automated; monitored energy yield is sent automatically by a data logger to a central server. There the failure detection routine runs automatically every day. The owner of the PV system can check the performance of his or her PV system via an Internet communication portal; feedback is provided in case of detection of a malfunction.

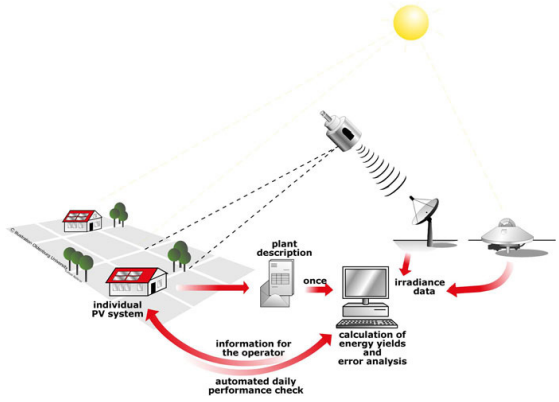

Figure 1: PVSAT-2 routine

2.2 Field test

In the test phase 100 small and mostly privately owned PV systems were monitored between February and October 2005 in Switzerland, Germany and the Netherlands. During the development phase of the procedure, the PVSAT-2 routine was tested with data from well-described and monitored PV systems. During the field test, improvements on the method were introduced directly. The quality and effectiveness of the different steps of the routine was thoroughly analysed.

3 RESULTS

3.1 Importance of correct PV system specifications

For the majority of the monitored PV-systems the PV simulation works well, the accuracy for well-working systems is described in section 3.2.

Initially the simulated hourly energy yield did not correspond well with the measured energy yield for 48 of the PV systems without 'failures'. This mismatch was caused by different factors, which are shown in Figure 2 and discussed in the following paragraphs.

Errors in installation
- *Undersized cables*

Errors in system descriptions
- *Wrong azimuth orientation given*
- *Wrong installation type given (roof top with large/small spacing, roof integrated, free standing,..)*
- *Incorrect module and inverter specifications*

Figure 2: Causes for simulation mismatch found in the test phase

One cause for a mismatch is an erroneous installation of the PV system, thereby reducing the system efficiency. As example, in the test phase for one of the German systems undersized cables were used, which caused an energy loss of circa 10 %. This was discovered in a detailed study that was triggered by the low yields of this system [5]. Although the owner of the system might not immediately decide to replace these cables, it is useful to know there is an energy and financial loss for this reason.

Errors in the system description turned out to be an important reason for a simulation mismatch. The system description forms were filled out by the owners of the PV systems. As the test users were no PV experts, significant uncertainties in the specification of the tilt angle and azimuth were found. For a quarter of the systems in the test phase the azimuth was wrongly specified. An example of this is shown in Figure 3; the original indicated azimuth of 180 degrees (exactly south) was corrected to 155 degrees (towards south east) on basis of measurements and feed-back from the test user. This effect is quite easily observed, when looking at the hourly measured and simulated energy yield of a clear day, but it is more difficult to correct this automatically because of e.g. clouds and shading effects. An incorrect azimuth has only a minor influence on the daily energy yield. But since hourly energy yields are used for identification of the failure type, the failure detection routine may detect shading, because of a wrongly specified azimuth. This can be seen in Figure 3 in the afternoon hours where the measured yield is significantly lower than the uncorrected simulated energy yield (Psim180) for several hours. After correction the small remaining differences between the measured and simulated energy yield at e.g. 13h00 are covered by the general error margins in the simulated energy yield.

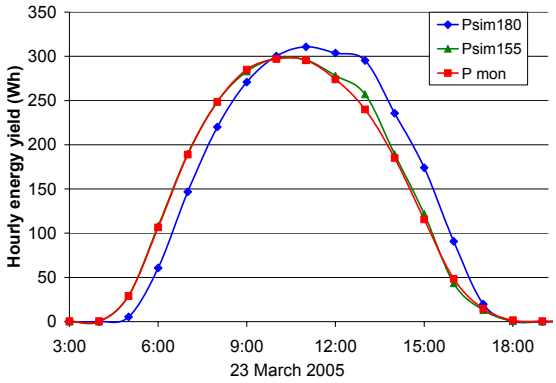

Figure 3: Measured (Pmon) and simulated hourly energy yield before (Psim155) and after (Psim180) correction of azimuth

A wrong description of other input parameters is more difficult to find. A detailed analysis revealed for a German system that the installation type was not 'small distance from the roof', but 'roof integrated' [5]. Therefore the temperature at higher irradiation values was higher than assumed, resulting in a perceived energy loss of ca. 10 %.

The module and inverter specific information, used for simulation of the energy yield are derived from datasheets. An uncertainty is therefore introduced by not having module specific flash test power; this uncertainty of 5 or 10 % is usually specified in the datasheets. Furthermore especially for older systems (some of the systems in the test phase were installed in 1994) degradation effects could be relevant. Without a detailed investigation it is difficult to quantify the effect of this on individual systems.

For this reasons an initial phase is proposed, before the automatic monitoring process starts. In this phase it would be possible to check the system description and simulation. Possible reasons for energy loss could be identified. Furthermore, module and inverter characteristic parameters could be optimized. This phase would guarantee that the monitoring starts with correct parameter settings and therewith, increase the possibility of a correct detection of possible future failures. Also other options like involving the installation company would help in ensuring a correct system description. For newly installed systems, the above-mentioned problems would play a less important role.

3.2 Accuracy of irradiance data and PV simulation

The failure detection routine is based on the comparison of measured and simulated hourly energy yield; therefore, information on the quality of hourly-simulated energy yield is needed. The uncertainty in the simulated energy yield is dominated by uncertainties in the irradiance values. Within the PVSAT-2 project the

data quality of Meteosat-7 and Meteosat-8 have been evaluated for 20 meteorological stations of the German Weather Service for the year 2005. The relative standard errors for hourly, daily and monthly data and the bias are presented in Table 1. The absolute standard error (σ, equation 1) is defined as the standard deviation of the irradiance, which is based on the difference between the satellite value (G_{sat}) and the measured value (G_{meas}). The bias is the systematic error between satellite-derived and measured irradiation for the whole year.

$$\sigma = \sqrt{\frac{\sum_{i=1}^{N}(G_{sat} - G_{meas})^2}{N}} \qquad (1)$$

	Met-7	Met-8
Stderr, hourly	19.4	17.5
Stderr, daily	10.7	9.8
Monthly	5.2	4.7
Bias	1.3	-0.5

Table 1: Accuracy of satellite-derived irradiance data (%)

The table shows that the accuracy of the irradiance data has improved with Meteosat 8. It also shows that for failure evaluation it is important to consider longer time intervals, since uncertainties are smaller for daily and monthly time intervals compared to hourly intervals. Furthermore, it is important to note that the accuracy differs per season. The relative errors are much larger in the winter months and therefore it will take a longer time to identify a failure. The absolute errors are smaller than in summer, since also power production is lower. The standard deviation of the PV simulation is dominated by the standard deviation of the satellite-derived irradiance [6].

The previous given standard errors are based on measurement data, which is obviously not available in real use of the PVSAT-2 routine. Therefore, in the PVSAT-2 method situation specific uncertainty margins are provided with the hourly-simulated irradiance, in order to decide if the difference between measured and simulated energy yield is caused by uncertainty in irradiance or by a failure. These situation specific uncertainty margins are based on an extensive empirical weather-dependent error assessment. The uncertainty is dependent on the situation specific sun elevation, cloud cover and variability of cloud cover (how quickly the cloud cover situation changes). For clear sky situations at high sun elevations uncertainties can be as low as 5 % for hourly-simulated irradiance. Under unfavourable weather conditions, like high cloud cover, high variability of clouds, and low sun elevation, uncertainties can be as high as 50 % for a single hourly value.

The shape of the probability density function of the hourly energy yield was found to resemble a Gaussian shape. To cover a 95 % interval of the simulated hourly energy yield, an error margin of two times the uncertainty was used. This means that for an energy loss to be identified as significant in the failure detection routine the difference between measured and simulated energy yield has to be larger than 2σ, i.e. the error margin.

3.3 Example of assigned error margins

The error margins discussed in the previous section depend on weather circumstances and are, therefore, location specific. In this section the error margins are applied to one test system in South Germany for 2005. This will clarify the uncertainty margins present at different time scales. It is important to know how large the energy loss has to be, to be detected by the failure detection routine.

In Figure 4 an overview of hourly error margins is presented. On the *x*-axis the simulated hourly energy yield, normalized by the nominal power of the PV plant is shown; on the *y*-axis the error margin of the simulated energy yield normalized by the nominal power. The blue triangles represent the situation specific error margin for all hourly-simulated energy yield values of 2005. The red crosses show the mean error margin for 2005 relative to the nominal power. The solid diagonal line represents an error margin being equal to the simulated hourly energy yield. The dashed lines represent error margins of 30 and 15 % of the simulated hourly energy yield, for the top and bottom line, respectively. The figure illustrates that the absolute error margins are lower for lower simulated power, but that this is much larger in relative terms. It can be concluded that only for a small part of the measurements (when power production is high due to high irradiation and therefore low error margins because of clear sky conditions exist) failures that produce an energy loss of 15 % and less can be detected. The detectable share increases with a higher hourly energy loss.

In Figure 5 the daily-normalized error margins are shown. The daily error margins are much lower; failures

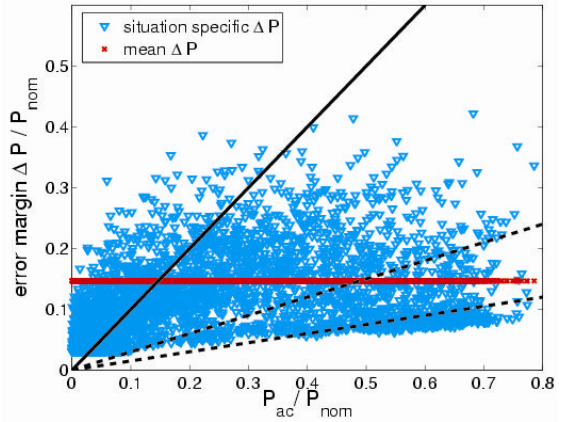

Figure 4: Hourly normalized error margins

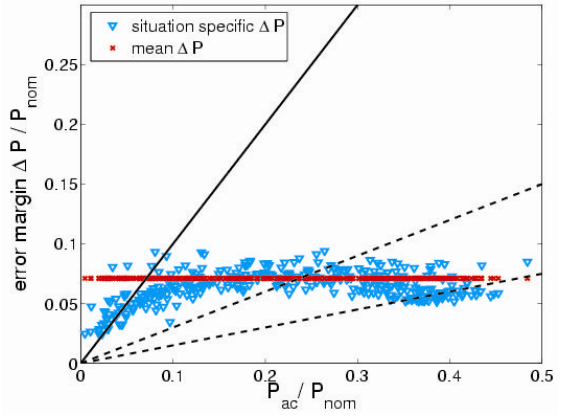

Figure 5: Daily normalized error margins

causing a daily energy loss of 30 % should be detected for days with quite good weather. In Figure 6 the monthly-normalized error margins are presented. Continuous constant failures that cause an energy loss of over 30 % for a whole month can even be detected in winter. In summer, system faults leading to energy losses of circa 15 % can also be detected on a monthly basis. This shows again that it is important to also use longer time intervals for failure detection.

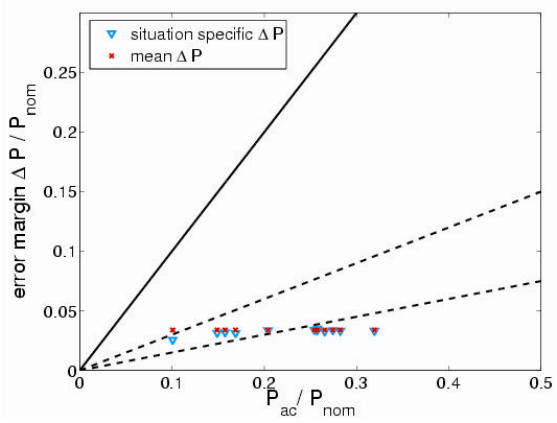

Figure 6: Monthly normalized error margins

3.4 Examples from the test phase

During the field test 100 systems were monitored. The following 'malfunctions' occurred during the test phase: snow, shading, total blackout, power limitation by the inverter and string errors. The detectable failures in the failure detection routine are listed in Table 2 sorted by their general failure type.

General failure type	Failure
Constant energy loss	Degradation
	Soiling
	Module defect
	String defect
Changing energy loss	Shading
	Grid Outage
	High losses at low power
	Power limitation
	MPP tracking
	Hot inverter
	High temperature
Snow cover	Snow cover
Total blackout	Defect inverter
	Defect control devices

Table 2: Detectable failures

The failure detection routine consists of two parts. The failure profiling method checks if there is a significant daily energy loss; if so it sorts the failures in four categories: snow, changing energy loss, constant energy loss and a total blackout. A changing energy loss is for example shading or power limitation of which the energy loss is changing over the day, while a constant energy loss, refers to a defined percentage (with uncertainty) of energy loss caused by e.g. a string error.

The second method, the so-called footprint method, applies a statistical approach for averaging normalized power over three domains: power, time and sun elevation for a one, seven and thirty-day period [3]. Based on this approach the footprint method detects morning or evening shading, permanent power loss and power limitation by the inverter.

One string error detected during the test phase will be discussed as an example. Also general results will be given.

In the Netherlands AC-systems are common, this means the inverter is mounted on the back of the module. 9 of the 29 Dutch test users had an AC system with between 4 and 12 modules and inverters. The described system consists of six AC-modules and inverters (570 Wp). Measurements for this system are available from 20 February to 30 September 2005, with some weeks of missing data, due to a communication problem of the data logger.

One of the inverters broke down in the end of March; another one broke down in the second week of August. Figure 7 presents the simulated and the measured hourly energy yield for 23 March (no failure), 1 April (1 broken inverter) and 16 August (2 broken inverters). It can be seen that the energy loss at 1 April is not significant on an hourly basis, while at 16 August a significant deviation between measurements and simulation is seen at almost every hour. All hourly measured and simulated energy values are shown versus the hourly irradiation in Figure 8. Three lines can be clearly distinguished. From top to bottom they are, respectively, the simulated energy yield, the measured yield with respectively one and two broken inverters. The traces of these errors are equivalent to those of 'string failures' in bigger systems. At high irradiance values the lines are clearly distinguishable and therefore failures can easily be detected. For irradiances lower than 400 Wh/m^2 the different situations cannot be distinguished.

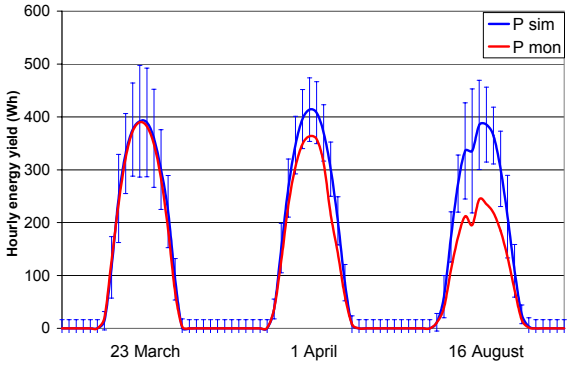

Figure 7: Hourly measured (red) and simulated (blue) energy yield with error margins for a day without a failure (23 March), with one (1 April) and two (16 August) broken inverters

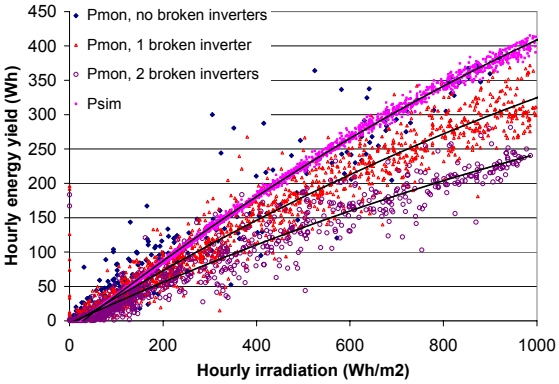

Figure 8: Hourly simulated (Psim) and measured (Pmon) energy yield for total monitored period

Consistent with the results in 3.3, the failure profiling method only detects a constant energy loss when the daily irradiation is very high (~>7000 Wh/m^2) for the period with one broken inverter (17% energy loss). After the second inverter broke down, the frequency of detection of the malfunction increased, since a 33 % energy loss is detected at days with a daily irradiation larger than circa 3000 Wh/m^2.

The footprint method detects a permanent power loss by checking if there are enough intervals on the relative power range with a significant energy loss, for a period of a day, a week, and a month. For the intervals in the higher power range, for example between 70 and 80 percent of nominal power, uncertainties are small. Therefore, an error point is easily found. Since this is not the case for low power categories, it takes some time before a defect inverter is discovered. The averaging approach for 7 and 30 days reduces the uncertainty in the simulation. The footprint detects the permanent power loss from half June onwards.

Also other failures were detected. The footprint method detects shading if there is an hourly significant energy loss, when the sun elevation is lower than 20 degrees, so in the early morning and in the late evening. The failure profiling method detects shading if it causes a significant daily energy loss; in the test phase shading was detected because of some major shading of a tree in mid-day. Intermediate shading (limited energy loss, not in early morning, late evening) is not yet detected. We are looking further into including more options in the footprint for this. Another option is to include shading obstacles in the system descriptions and calculate simulated energy yield including shading.

Furthermore snow was frequently detected for Dutch, German and Swiss systems in winter. Also total power blackouts are detected if the simulated energy yield is larger than 1000 Wh/m^2. Also power limitation was detected for a few systems.

4 CONCLUSIONS

The field test has shown that the detection of failures by the PVSAT-2 routine is strongly dependent on the uncertainty in the satellite-derived irradiance. On clear days in summer the uncertainty is relatively low and failures resulting in a daily energy loss of 15 % can be detected. However in cloudy weather partial malfunctions will take much longer to be detected. Therefore it is important to consider the monthly time scale. Dependent on weather conditions and size and continuity of the failures, it can take between 1 day and several months to detect a failure. The hourly time scale is important for the identification of the specific failure type.

Furthermore, it is very important that the technical system description is correct. It is being considered to introduce an introductory phase.

PVSAT-2 is marketed by Meteocontrol AG, Augsburg Germany under the name safer'Sun Satellite (www.meteocontrol.de) and by Enecolo AG, Mönchaltorf, Switzerland under the name SPYCE (www.spyce.de). More information can also be found at www.pvsat.com.

5 ACKNOWLEDGEMENTS

The PVSAT-2 research project was supported by the European Commission under contract number: ENK5-CT-2002-00631. We also would like to thank the test users, who contributed voluntarily to the success of the project.

6 REFERENCES

[1] Observ'ER, Photovoltaic barometer (April 2006).
[2] U. Jahn, W. Nasse, Prog. Photovolt: Res. Appl. 12 (2004) 441–448.
[3] A. Drews, A.C. de Keizer, *et al.*: Solar Energy, in Press.
[4] S. Stettler, *et al.,* Proceedings 20th European Photovoltaic Solar Energy Conference, (2005) 2490.
[5] O. Prignitz, Begleitung der Testphase des Projekts PVSAT-2, Diploma Thesis, Univ. Of Applied Sciences, Magdeburg-Stendal, Germany
[6] A. Drews, *et al.*, Proceedings Eurosun2006, (2006)

ENVIRONMENTAL IMPACTS OF PV ELECTRICITY GENERATION - A CRITICAL COMPARISON OF ENERGY SUPPLY OPTIONS

E.A. Alsema, e.a.alsema@chem.uu.nl, Phone +31 30 2537618 Fax +31 30 2537601
Copernicus Institute, Utrecht University, Heidelberglaan 2, 3584 CS Utrecht, The Netherlands
M.J. de Wild-Scholten, m.dewild@ecn.nl, Phone +31 224 564736, Fax +31 224 568214
Energy research Centre of the Netherlands ECN, Unit Solar Energy, P.O. Box 1, 1755 ZG PETTEN, the Netherlands
V.M. Fthenakis, vmf@bnl.gov, Phone +1 631 344 2830, Fax +1 631 344 4486,
National Photovoltaic EH&S Research Center, Brookhaven National Laboratory, Upton, NY 11973, USA

ABSTRACT: An overview is given of the environmental impacts of different PV technologies both at the present status of technology and for future technology. Crystalline silicon PV systems presently have energy pay-back times of 1.5-2 years for South-European locations and 2.7-3.5 yr for Middle-European locations. For silicon technology clear prospects for a reduction of energy input exist, and an energy pay-back of 1 year may be possible within a few years. Thin film technologies now have energy pay-back times in the range of 1-1.5 years (S.Europe). Greenhouse gas emissions are now in the range of 25-32 g/kWh and this could decrease to 15 g/kWh in the future. Therefore PV energy systems have a very good potential as a low-carbon energy supply technology.

Keywords: environmental effect, Life Cycle Assessment, c-Si, a-Si, Cu(InGa)Se2, CdTe

1 INTRODUCTION

In the last years considerable progress has been made in the assessment of environmental impacts from photovoltaic systems. In this paper we will give an overview of recent results, identify remaining gaps in knowledge and compare the environmental performance of PV energy generation with other (future) energy supply options.
The following issues are generally perceived as important when discussing the environmental impacts of PV technology:

- Energy Pay-Back Time
- Greenhouse gas (GHG) mitigation
- Toxic emissions
- Resource supply
- Health & Safety risks

We will focus on the first two subjects in this paper and touch briefly on toxic emissions. For a discussion of resource supplies we refer to [6,7]. Health and safety issues are being discussed in a separate paper at this conference [5].
After covering some methodological issues, we will discuss the environmental impacts of PV systems based on crystalline silicon technology. This is followed by a review of thin film technologies. Balance-of-System components are not discussed here, an extensive comparison of roof-top and ground-based BOS options is presented in [4].

2 METHODOLOGY

All environmental impacts results generated by the authors were obtained by a full Life Cycle Assessment, using the software SimaPro 7 and the database Ecoinvent 1.2. For PV *modules* the end-of-life phase was excluded from the analyses because only pilot recycling processes are available at present. An LCA study on one of these pilot process can be found in [9]. Waste issues are also not discussed in this paper.
Two impact types receive the most attention: primary energy requirement and greenhouse gas emission. The primary energy use is calculated by means of the method Cumulative Energy Demand (v. 1.03) as implemented in Ecoinvent. For presentation purposes all energy requirements, fossil, nuclear and renewable are summed into one primary energy figure. The greenhouse gas emissions are evaluated by means of the IPCC 2001 GWP 100a method (version 1.02).
Unless stated otherwise we use the following assumption for system location and performance:

- application type: grid-connected system, with modules installed in-roof (see [4] for details)
- location: either South-Europe with irradiation 1700 kWh/m2/yr, or Middle-Europe with irradiation 1000 kWh/m2/yr;
- system Performance Ratio: 0.75
- system lifetime: 30 years, except the inverter which has a 15 year life.

All electricity supplied to PV-specific production processes, except silicon feedstock production, is assumed to be supplied by the average electricity system for continental Europe (UCTE region, medium voltage level) as modelled in Ecoinvent. For silicon feedstock production which is a highly energy-intensive process and thus usually located at sites with low electricity cost, we assume a specific mix of hydro power and high-efficiency Combined Cycle gas turbines. Electricity generated by the PV systems is also assumed to *displace* the UCTE-average supply mix.

3. CRYSTALLINE SILICON TECHNOLOGY

With respect to crystalline technology the European CrystalClear project has provided the conditions for generating up-to-date Life Cycle Assessments. In cooperation with major European and US manufacturers a set of Life Cycle Inventory data has been collected covering the entire value chain from silicon production to module manufacturing. After averaging data from different sources (i.e. manufacturers) the data set has been made publicly available [3]. Based on these data a transparent and up-to-date analysis can be made of

multicrystalline, monocrystalline and ribbon silicon module manufacturing. Probably the new LCI data will also be incorporated in the next official update of Ecoinvent, a much-used database for LCA studies [14]. In this way comparative analyses of PV will at least be based on data that really reflect the current technology status.

After initial publication of the data in December 2005 we have updated some elements of it in preparation of a full update, which latter is planned for end 2006. One major improvement is that we have included a recycling process for the sawing slurry, the cutting fluid that is used in the wafer sawing process. This recycling process, which is usually performed by the slurry supplier, is able to recover 80-90% of the silicon carbide and of the polyethylene glycol and thus realizes significant reductions in the environmental impacts related to these materials. Because of the cost savings it offers, the use of recycled slurry materials has probably been adopted by the large majority of wafer producers. On a module level the resulting impact reductions have been found to be as high as 15%.

One other area with updated data is the energy consumption of the Czochralski process for monocrystalline ingot production. We received new data from 4 European and one US mono-Si manufacturer that allowed us to make a new, more reliable estimate which turned out to be significantly lower than the previous value [2]. Note that wafer thicknesses have not been updated yet, although significant changes have occurred since the year of our previous data collection (2004). (Such an update is not trivial as we also have to account for changes in cutting yield). Neither have data for ribbon technology been updated, thus these figures still reflect the technology status for 2004.

In figure 1 a key result is shown in the form of Energy Pay Back Times for roof-top systems based on one of the three silicon technologies and located either in Middle- or Southern-Europe (for system assumptions see section 2).

Energy pay back time is now in the order of 1.5-2 years for systems installed in South-Europe and 2.7-3.5 years for Middle-Europe. In comparison with previous evaluations monocrystalline silicon results have come down significantly, due to improved data for Cz growing. Both mono- and multi-Si profit from inclusion of the slurry recycling process in our process flow scheme.

Within the CrystalClear project we do not look at present-day technology only. Evaluation of expected technology improvements in the field of silicon technology is performed regularly. Of course major advances are expected with regard to wafer thickness and cell efficiency, driven by cost reduction targets and (current) silicon shortages. We assume wafer thicknesses of 150 µm for our case study of future mono and multi-Si and 200 µm for ribbon silicon. In line with the targets formulated in the latest CrystalClear roadmap we have set cell efficiencies at 15%, 17%, and 19% for ribbon, multi- and mono-Si respectively.

Other technology developments that can significantly affect the environmental impacts are:

- New silicon feedstock processes, especially the deposition of polycrystalline silicon in a Fluidized Bed Reactor could reduce by at least 70% the electricity consumption in comparison with the (modified) Siemens process that presently dominates the market. Note however, that the cell efficiencies of 17% respectively 19% we assume for multi- and mono-Si have not been demonstrated yet with FBR material;
- Improved energy-efficiency in new ingot growing facilities. In the data we collected from various manufacturers we observe quite significant differences in energy consumption for both casting of multicrystalline ingots as for Czochralski growing of monocrystalline crystals, which can even amount a factor 3. However, careful consideration is always required if all data refers to the same unit output (i.e. with or without yield losses; before or after squaring, etc). Not surprisingly newer facilities appear to have lower energy consumption. We therefore assume for our evaluation of future production that today's best technology will become the standard.

Given the fast developments in crystalline silicon production we believe that most of these improvements may be realised within a few years.

Table 1 below summarizes our main assumptions for future technology and figure 2 shows the effects on energy input per m^2 module area. Observe that no changes for the energy input of the cell and module assembly process have been assumed here. If the assumed high efficiencies requires extended use and/or a higher class of clean room conditions for the cell line, this would increase energy consumption for the cell process. On the other hand the recent introduction of the new fast-cure EVA formulations will probably decrease energy consumption for the module.

Figure 3 shows the reduced impacts in terms of energy pay-back time and figure 4 in terms of GHG emissions.

Under the present assumptions all three silicon technologies could in the near future realize an EPBT below 1 year and a greenhouse gas emission of only 15 g/kWh. Differences in impacts between technologies tend to disappear as common processes and materials get an increasing share in the overall impact. Below we will compare the GHG emissions with those of competing low-carbon energy options.

4. THIN FILM TECHNOLOGIES

Currently thin film technology has a much smaller market share than crystalline silicon. Worldwide there are only a few commercial-scale production facilities. Therefore, only a few LCA studies of thin film industrial production processes exist. For the same reason publication of an LCI data set for major thin film technologies, following the recent example of c-Si industry, has not been possible yet. With the growing investments in thin film production facilities such an action should become easier though.

One of the best-documented thin-film LCA studies has been conducted by Fthenakis and Kim, on the production of CdTe modules by First Solar [1, 10]. Key results are depicted in figures 5 and 6, showing respectively the Energy Pay-Back Time and the GHG emissions. PV systems are as discussed in section 2, except that a ground-mounted installation was considered instead of a roof-top system. For module impacts, though, this makes no difference. Because these modules are produced in the USA the background database is also specifically chosen to reflect the USA production environment (Franklin

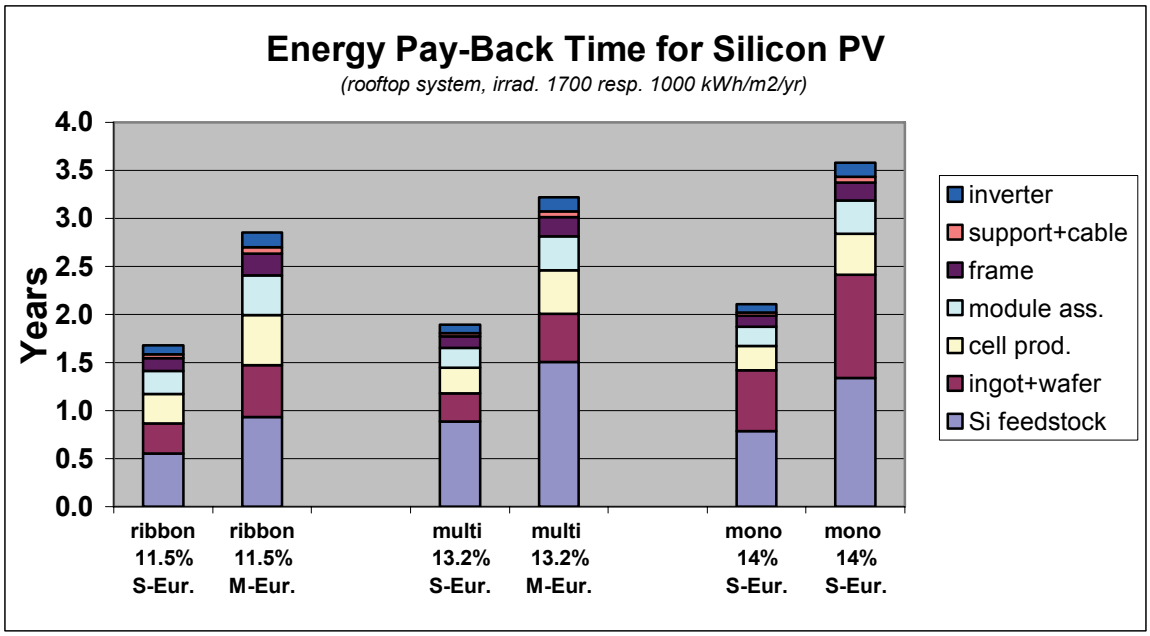

Figure 1: Energy Pay-Back Time (in year) of rooftop PV systems based on crystalline silicon technology at two different locations, South-Europe with 1700 kWh/m2/yr irradiation and Middle-Europe with 1000 kWh/m2/yr. Module efficiencies are shown for each technology; system Performance Ratio 0.75

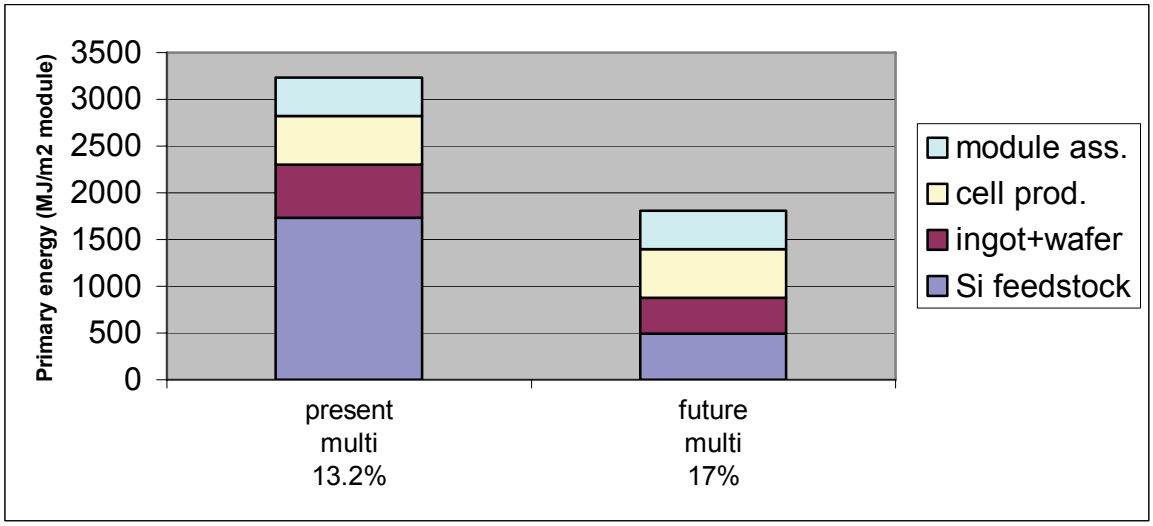

Figure 2: Comparison of primary energy input (MJ per m2 module) of present with future multicrystalline silicon module.

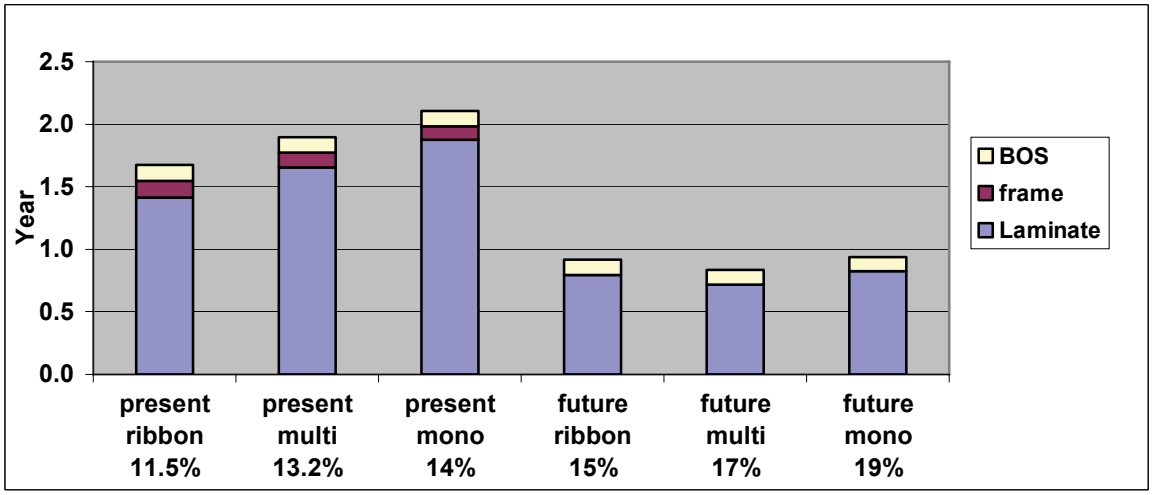

Figure 3: Energy Pay-Back Time for future silicon PV systems. System installed in South-Europe

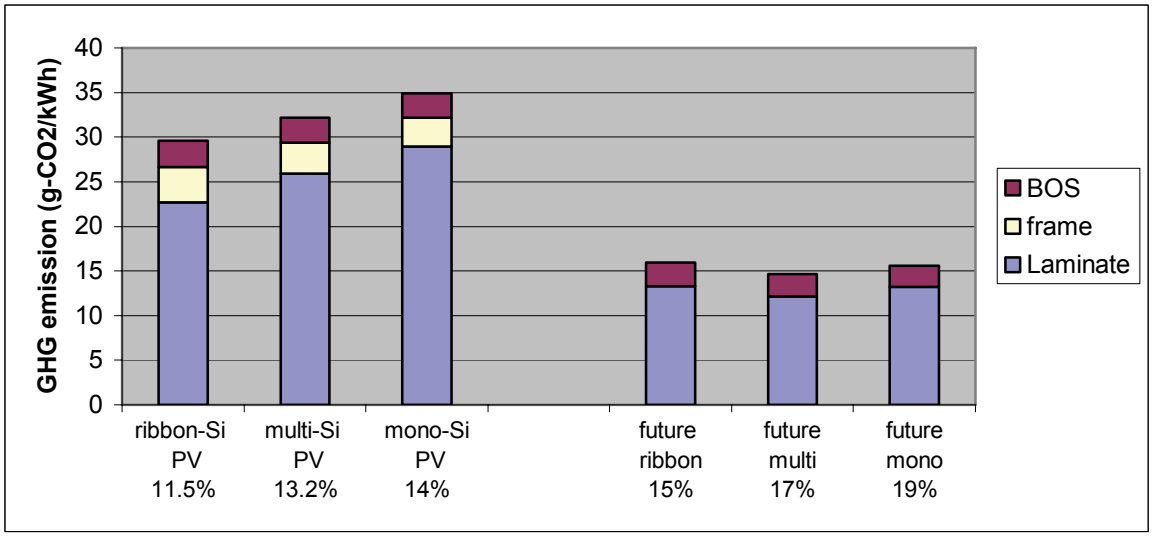

Figure 4: Life-cycle GHG emissions of present and future silicon PV systems, at a S.-European location.

Table 1: Assumptions for future multi-Si, mono-Si and ribbon technology

	Ribbon-Si	**Multi-Si**	**Mono-Si**
Si Feedstock	"Solar-grade" silicon produced with Fluidized Bed Reactor technology		
Crystallisation	Standard Technology 2004	Best Available Technology 2004	Best Available Technology 2006
Wafer thickness	300 -> 200 um	285 -> 150 um	300->150 um
Module efficiency	11.5 -> 15 %	13.2 -> 17%	14->19%
Module assembly	Frameless module	Frameless module	Frameless module

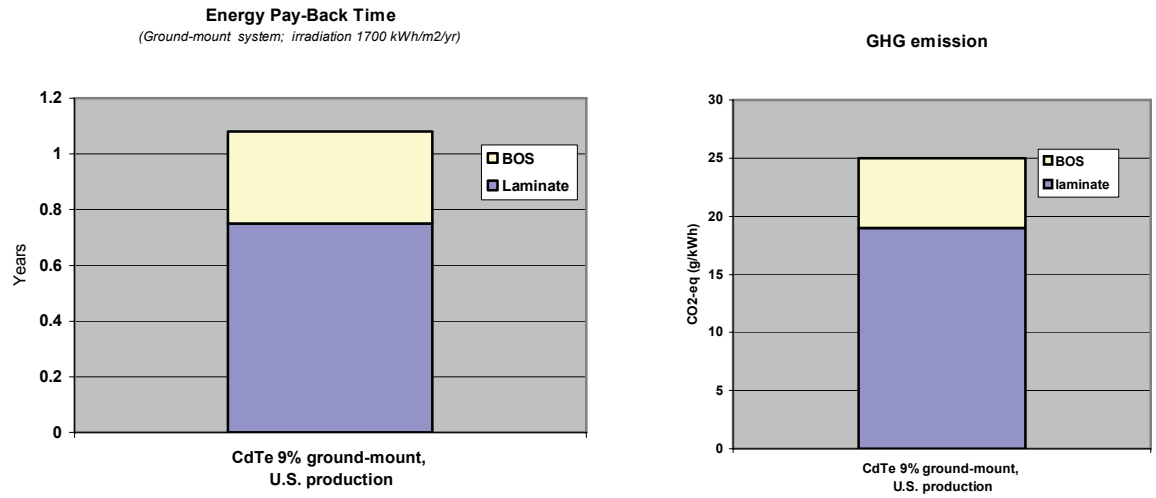

Figures 5 and 6: Environmental indicators for CdTe technology, ground-mounted system in South-Europe, PR=0.75

database). Among others the CO2 emissions of US electricity production is higher than in Europe.
We observe that for this technology an EPBT of about 1 year is already accomplished, despite the lower module efficiency in comparison with c-Si technology. Also GHG emissions are comfortably low. In an European project, named SENSE, three thin film production processes were analysed in cooperation with manufacturers. Although a final report has not been published yet, some preliminary results are shown below, with thanks to SENSE project team (figure 7). Because these results were generated with a different LCA database at the background (i.e. GaBi LCA software and database) and possibly with different LCA system boundaries, the results cannot be compared one-to-one with those of for example Fthenakis and Kim. Again we can observe that EPBT values are relatively low in comparison with crystalline silicon, and that the contribution of BOS is a bit higher, due to the somewhat lower module efficiency. Of course BOS material quantities may also differ from the c-Si case.
If we also consider future possible reductions in EPBT and GHG emission for silicon technology we can observe that the difference between thin-film and c-Si technology might well disappear into the error margin. Improvements in the energy consumption and related GHG emissions are less obvious for thin film production. Thin film module efficiency will undoubtedly increase but if we assume a module efficiency of 15% for CdTe modules the GHG emission will come down to about 15 g/kWh, i.e. in the same range as future c-Si PV.

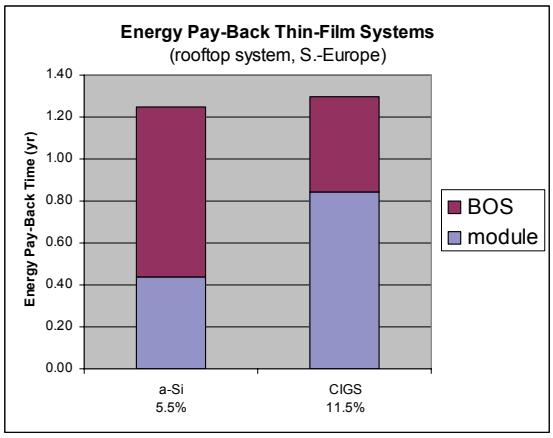

Figure 7: Energy Pay-Back Time for two thin film technologies, as reported by the SENSE project [8]. Rooftops system in S. Europe, Performance Ratio= 0.75. (Preliminary data).

One issue that has often raised concerns is the use of cadmium in CdTe modules. Cadmium in its metallic form is a toxic substance that has the tendency to accumulate in ecological food chains. However, one should be aware that the compound CdTe is more stable than most other cadmium compounds and is not soluble in water, so that risks of cadmium leaching i.e. from broken modules are small. Moreover the amount of cadmium used in PV modules is small (5-10 g/m2) and the material is completely encapsulated in the module. Risks of cadmium emission in fires have been shown to be very small, provided that double-glass encapsulation is used [11,18]. With proper emission control techniques in place the cadmium emissions from module production can be almost zero and emissions from zinc/cadmium winning have also been reduced substantially over the last decades [15]. It has even been argued that CdTe modules form an environmentally safe way of sequestering cadmium that is produced anyway (as an unavoidable by-product of zinc winning). Essential prerequisite for such a thesis is that a closed loop for cadmium can be realised, i.e. that (almost) all cadmium can be recovered from CdTe modules.
Currently a module take-back system has been set up by at least one manufacturer (First Solar) and CdTe modules are being recycled in a pilot scale process or used as a flux agent in metal smelters. First experiments with a different, more efficient recycling process have shown promising results [12].
Based on a comprehensive LCA performed by Fthenakis and Kim [17], the life-cycle cadmium emissions of CdTe-based PV systems have been compared with those of other module types and also with other energy technologies (see figure 8). According to this study the cadmium emissions of CdTe technology are among the lowest, and even lower than those of silicon PV technology. This result which at first sight may seem counter-intuitive, is caused by the cadmium emissions in electricity production plants that are fuelled by coal or oil. In other words because the *direct* cadmium emissions in the CdTe module production are very low, it is actually the electricity input for module production - and the related *indirect* cadmium emissions - which determines the total life-cycle emission for a PV system.
This again highlights the importance of reducing energy input for (c-Si) module production.

5. COMPARISON WITH OTHER ENERGY SUPPLY OPTIONS

In order to attain a sustainable energy supply system it is very important that a portfolio of low-carbon energy technologies with a reasonable cost level becomes available as quickly as possible. Most probably there will finally not be one single “best technology” but depending on the local resources (e.g. irradiation), application (e.g. stationary or moving), power demand and available infrastructure a choice among available sustainable energy options will be made.
Can PV technology be considered one of those sustainable energy options? In figure 9 we have depicted the life-cycle greenhouse gas emission of different energy supply options. Among these options we also included fossil-fuelled power plants that are combined with carbon capture and sequestration (CSS) technology. Early experiments with CSS have been promising and there appears to be a sufficiently large potential in underground reservoirs where CO2 can be stored safely for long periods [13].
Also nuclear energy is included in the figure, separately for Europe and for the US. This difference between European and US nuclear is mainly due to the different fuel processing technologies used in these two regions. In Europe the more energy-efficient ultracentrifuge process is dominant, while in the mostly uses gas diffusion at this time. It seems likely though that in the future the US will also gradually switch over to the ultracentrifuge process [16].

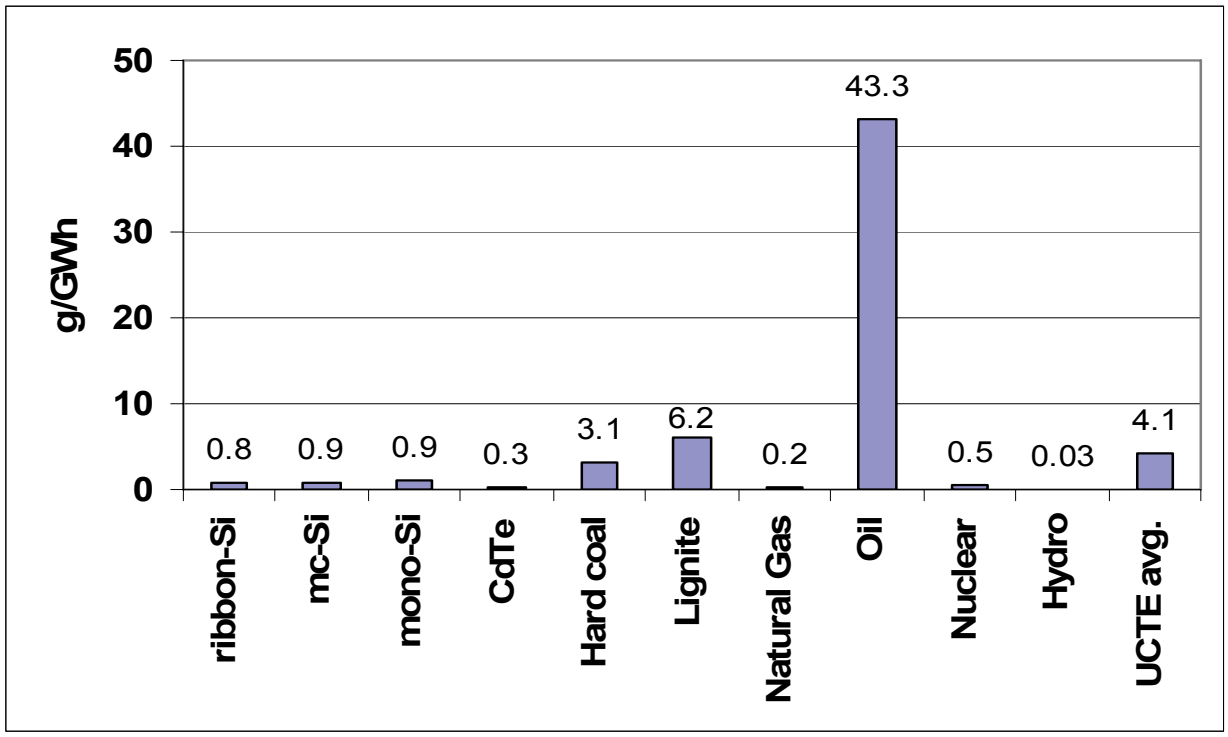

Figure 8: Life-cycle cadmium emissions (in g/kWh) from different energy technologies. PV systems located in S.-Europe, PR=0.80. Non-PV technologies based on Ecoinvent database.

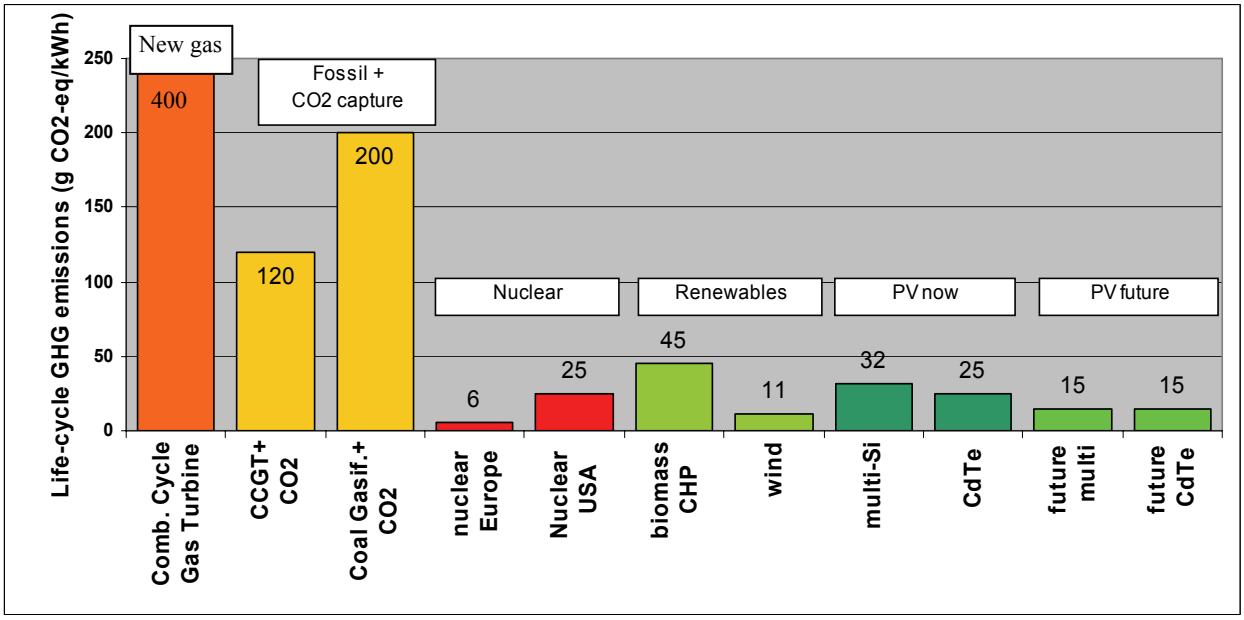

Figure 9: Comparison of GHG emissions of different energy supply options, PV systems installed in S.-Europe (Sources: [12, 13, 14])

If we compare present-day PV technology (at a South – European location) with other energy options we see that PV has considerably lower GHG emissions than all fossil options including fossil + CSS. But in comparison with nuclear and wind energy present-day PV has still relatively high GHG emissions, especially if we install PV systems at lower-irradiation regions. On the other hand we have shown that there are good prospects for further reduction of the GHG emissions, down to a comfortable low value of 15 g/kWh.

Of course sustainability comprises more than only low-carbon emissions, it also implies for example that no burdens are left for future generations, and in this respect PV technology appears to have a better profile than for example nuclear energy or fossil fuel with CSS, provided that we in PV technology are able to close the material loops by developing effective recycling processes. Also one should not forget that PV has a very large potential for application, larger than wind energy and probably also larger than nuclear and carbon storage

6. CONCLUSIONS

We have given an overview of the environmental impacts of present-day PV technology and the effects of probable future developments in (production) technology. Depending on cell technology energy pay-back times are now between 1 and 2 years for a Southern-European locations and between 1.7 and 3.5 for Middle-European locations. Thin film technology are at the lower end of this range. For silicon technology clear prospects for a reduction of energy input exist, and an energy pay-back of 1 year may be possible within a few years.
Hazardous emissions connected to PV technology are primarily related to energy consumption in the manufacturing process, as direct process emissions are almost zero. Therefore cadmium emissions from CdTe technology can be lower than those of most other energy options. Risks from the use of cadmium telluride in modules appear to be quite low, provided that the material is kept well-encapsulated (double-glass encapsulation) and that it can be recovered from waste modules.
PV systems have life-cycle greenhouse gas emissions in the range of 25-35 g/kWh (at S-European location) which is relatively low in comparison with other energy options that have a large application potential.
In conclusion we can say that PV technology is in a very good position to be included in a portfolio of low-carbon energy technologies for a future sustainable energy supply, especially if further cost reductions can also be achieved. Attention to further reduction of energy consumption should also remain a point of attention especially in the areas of silicon feedstock production and ingot growing. Further LCA studies of thin film technology should contribute to create greater transparency and more insight in improvement options for these technologies.

ACKNOWLEDGEMENTS

Part of this work was carried out in the Integrated Project CrystalClear and funded by the European Commission under contract nr. SES6-CT_2003-502583. The cadmium telluride research was conducted within the PV EH&S Research Center, BNL, under contract DE-AC02-76CH000016 with the US Department of Energy.
The authors gratefully acknowledge the help of experts from the following companies: Deutsche Cell, Deutsche Solar, Evergreen Solar, First Solar, HCT Shaping Systems, Isofoton, Photowatt, REC, Scanwafer, Schott Solar, Shell Solar (now SolarWorld) and also other unnamed experts.

REFERENCES

[1]. Fthenakis, V. and E. Alsema, *Photovoltaics Energy Payback Times, Greenhouse Gas Emissions and External Costs: 2004–early 2005 Status.* Progress In Photovoltaics: Research and Applications, 2006. **14**(3): p. 275-280.
[2] E.A.Alsema, M.J.de Wild-Scholten, Environmental impacts of crystalline silicon photovoltaic module production, *LCE2006, 13th CIRP International Conference on Life Cycle Engineering, Leuven, Belgium* (2006) http://www.ecn.nl/library/reports/2006/rx06041.html.
[2] J.E.Mason, V.M.Fthenakis, T.Hansen, H.C.Kim, Energy payback and life-cycle CO2 emissions of the BOS in an optimized 3.5 MW PV installation, *Progress in Photovoltaics* **14** (2006) 179.
[3] M.J.de Wild-Scholten, E.A.Alsema, Environmental Life Cycle Inventory of Crystalline Silicon Photovoltaic System Production - Excel file, **ECN report ECN-E--06-019** (ECN Solar Energy, 2006), http://www.ecn.nl/publications/default.aspx?nr=ECN-E--06-019.
[4] M.J.de Wild-Scholten, E.A.Alsema, E.W. ter Horst, M. Bächler, V.M. Fthenakis, A cost and environmental comparison of rooftop and ground-based PV Systems, this conference.
[5] V.M. Fthenakis, et al. Evaluation of risks in the Life Cycle of Photovoltaics in a comparative context, paper 8.CO.1.2, this conference.
[6] R. Gellings, K. Schmidtfrerick, A. Schlumberger, J. Siemer, Only united we are strong, Supply problems await areas other than silicon, Photon International, July 2006, p.80-89.
[7] B. A. Andersson, , C. Azar, J. Holmberg and S. Karlsson, Material constraints for thin-film solar cells, Energy Vol 23, Issue 5, 1998, P 407-411
[8] M. Shibasaki, personal communication, University of Stuttgart, August 2006.
[9] Müller, A., K. Wambach and E.A. Alsema, Life Cycle Analysis of Solar Module Recycling Process, Proceedings of MRS Fall 2005 Meeting, Boston, MS, Nov-Dec 2005
[10] Fthenakis V.M. and H.C. Kim, Life Cycle Energy Use and Greenhouse Gas Emissions Embedded in Electricity Generated by Thin Film CdTe Photovoltaics, Proc. MRS Fall 2005 Meeting, Boston, 2005.
[11] Fthenakis, V.M., Fuhrmann M., Heiser J. Lanzirotti A., Fitts, J. and Wang W., Emissions and Redistribution of Elements in CdTe PV Modules During Fires, Progress in Photovoltaics, Volume 13, Issue 8 , p. 713 – 723.
[12] V.M. Fthenakis and W. Wang Extraction and separation of Cd and Te from CdTe photovoltaic manufacturing scrap, Progress in Photovoltaics, 14, 363-371 (2006).
[13] B. Metz, O. Davidson, H. de Coninck, M. Loos, L. Meyer, Carbon Dioxide Capture and Storage, IPCC Special Report, Technical Summary, ISBN 92-9169-119-4, www.ipcc.ch
[14] Frischknecht et al., Ecoinvent LCA database, www.ecoinvent.ch
[15] V.M. Fthenakis and Wang W., Emission Factors in the Production of Materials Used in Photovoltaics, 20th EURPVSEC, Barcelona, Spain, June 6-10, 2005
[16] V.M. Fthenakis and Kim. H.C. l, Greenhouse-gas Emissions from Solar Electric and Nuclear Power: A Life-cycle Study, , Energy Policy, in press.
[17] V.M. Fthenakis and Kim. H.C., CdTe Photovoltaics: Life-cycle Environmental Profile, European Material Research Society Meeting (EU-MRS), Symposium O, Invited Paper, Nice, France, May 29-June 2, 2006.
[18] Fthenakis V.M., Life Cycle Impact Analysis of Cadmium in CdTe Photovoltaic Production, Renewable and Sustainable Energy Reviews, 8, 303-334, 2004.

OPTIMIZATION OF THE PERFORMANCE OF SOLAR CELLS WITH SPECTRAL DOWN CONVERTERS

W.G.J.H.M. van Sark
Department of Science, Technology and Society, Copernicus Institute for Sustainable Development and Innovation, Utrecht University, Heidelberglaan 2, 3584 CS Utrecht, the Netherlands,
T: +31 30 253 7611, F: +31 30 253 7601, E: w.g.j.h.m.vansark@chem.uu.nl

ABSTRACT: The inclusion of quantum dots in a plastic layer on top of solar cells increases their performance under standard and non-standard illumination conditions. The quantum dots effectively modify the incident spectrum such that a better match is obtained between the incident spectrum and the spectral response of the solar cells. As solar cell designs have improved over the past years, new optimized converter layers may have to be defined. Investigating new and future designs of multicrystalline silicon solar cells has revealed that the beneficial effect of deploying converter layers is less pronounced, as the new and future designs show an improved blue response. Nevertheless, a relative short circuit current increase of 7.5% is found for optimized converter layers. Combined optimization of solar cell and converter showed that particularly reduction of the front side recombination velocity can result in further performance improvement.
Keywords: Modelling; Fundamentals; Spectral response

1 INTRODUCTION

Under outdoor conditions most of the sun's spectrum is not used for conversion of light to electricity in conventional semiconductor solar cells. Their performance can be improved by a better match of the incident spectrum with the spectral response of the solar cell, which is possible by modification of the spectrum by means of (spectral) down and/or up conversion. In case of down conversion an incident high-energy photon is converted into two or more lower energy photons; for up-conversion two or more low energy photons (sub band gap) are converted into one high-energy photon. Down (or up) shifting is similar to down (or up) conversion where an important difference is that the quantum efficiency of the conversion process is unity, while that of shifting is lower than unity [1].

Spectrum conversion is but one approach of many that are pursued as part of Third or Next Generation solar cell R&D [2], but has been proposed already in the 1970s [3]. At that time plastic fluorescent materials were used and an increase of 0.5-2% was realized in solar cell efficiency as result of an increased UV/blue response. More recently, it has been reported that organic fluorescent molecules incorporated in a coating on a multi-crystalline silicon solar cell lead to an increase in efficiency of 6% [4]. Alternatively, semiconductor nanocrystals (quantum dots, QDs) have been proposed for use in such coatings as their absorption spectrum is very broad in comparison to that of organic molecules, and consequently, a higher increase can be expected when these are employed. In addition, QDs are brighter and more stable [5]. Therefore, renewed interest in the luminescent solar concentrator (LSC), originally proposed also in the 1970s [6], focuses on the deployment of QDs in the LSC [7, 8]. We have been modelling performance enhancement of solar cells resulting from inclusion of QDs in a plastic layer on top of solar cells. Such layer is known as spectral down-converter. Results show a 10% increase in current under AM1.5 [9] and an even higher increase under non-AM1.5 conditions [10, 11]. These results were based on existing designs of multicrystalline silicon solar cells, and the spectral down converter properties (QD concentration and size) were optimized.

In this paper, we focus on the optimum combination of solar cell and spectral down converter. First, the performance of an improved cell design [12] with the optimal down converter as reported in Ref. [9] is analyzed. Possible future improvements in multicrystalline silicon solar cell design are a decrease in front and rear side recombination and increase in rear side reflection as well as an increase in bulk lifetime [12]. As improvements in front surface passivation lead to an improved blue response, the addition of a spectral down converter is expected to be less beneficial. This will be demonstrated. Finally, we will investigate the possible performance enhancement in case both silicon cell and down converter are optimized together to yield the largest possible efficiency.

2 METHODOLOGY

2.1 Device configuration and simulation

The configuration studied is a highly transparent layer containing quantum dots (QDs) on top of a solar cell (Fig. 1) [9]. The size of the QDs is taken such that both blue and green light is absorbed and emitted in the red, which corresponds to an optimum spectral response of the solar cell. Depending on the QD concentration also unabsorbed blue and green light enters the solar cell.

For solar cell simulation we use material and device parameters for the old (status 2002 [13]) and new (status 2005 [12]) standard baseline n-p-p^+ mc-Si cell developed at the Energy research Centre of the Netherlands (ECN), which has parameters that are typical of low-cost

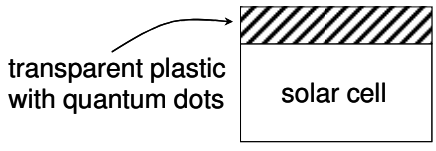

Figure 1: Schematic drawing of the studied configuration. A plastic layer containing QDs is applied on top of a solar cell. Absorption of incident light and emission lead to a modified spectrum incident on the solar cell.

commercial products, including series resistance, shunt conductance and a second diode. The cell thickness is 300 µm, the cell has a shallow diffused emitter, and the 9 µm thick back-surface-field (BSF) has a p^+ doping level of 4×10^{18} cm^{-3}. The front surface anti-reflection coating consists of 71-nm thick silicon nitride with a refractive index n=2.1 deposited by means of an in-line Microwave Remote Plasma CVD process [14]. The performance of the solar cell is simulated with the simulation programme PC1D (version 5.8) [15], using incident spectra that are modified by the spectral down converter layer.

2.2 Spectrum conversion

The incident spectrum, converted to amount of photons per wavelength $\Phi_s(\lambda)$, is modified by absorption of photons in the spectral down converter layer. The amount of absorbed photons in this layer $\Phi_a(\lambda)$ is determined from the QD absorption spectrum, which depends on the QD size, their concentration in the converter layer, and the thickness of this layer. This absorbed amount is subtracted from the incident spectrum. : $\Phi_{sa}(\lambda) = \Phi_s(\lambda) - \Phi_a(\lambda)$. As the QDs re-emit light at a red-shifted wavelength, the amount of emitted photons $\Phi_e(\lambda)$ is calculated from the QD emission spectrum. To this end, data for quantum efficiency (QE=0.8) is assumed, as well as the assumption that ¾ of the emitted photons is directed towards the underlying solar cell, due to internal reflection in the converter layer [16]. The amount of emitted photons then is added to the already modified AM1.5G spectrum: $\Phi_{sae}(\lambda) = \Phi_s(\lambda) - \Phi_a(\lambda) + \Phi_e(\lambda)$, and the resulting spectrum serves as input for the solar cell simulation models. Absorption of photons is calculated by using the Lambert-Beer equation: the photon flux density $\Phi(x,\lambda)$ after passing a distance x in a film with absorption coefficient $\alpha(\lambda)$ is written as $\Phi(x,\lambda) = \Phi^0(\lambda)\ exp[-\alpha(\lambda)x]$, with $\Phi^0(\lambda)$ the incident photon flux density. The exponential term $\alpha(\lambda)x$ equals $\varepsilon_\lambda CD$, with ε_λ the molar extinction coefficient (M^{-1}cm^{-1}), C the chromophore concentration (M), and D the thickness of the film (cm). The molar extinction coefficient is determined by scaling the normalized absorption spectrum such that the molar extinction coefficient ε_λ at 350 nm equals $\varepsilon_\lambda=1.438\times10^{26}a^3$ [17]. The QD radius a is determined from the absorption maximum and the known relation with particle diameter, e.g., [18].

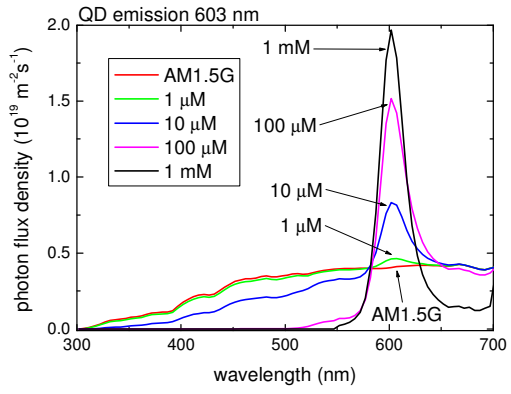

Figure 2: Calculated modified AM1.5 global spectra for QD concentrations from 1 µM to 1mM

The chromophore (QD) concentration varies from the nM to the mM range. The film thickness typically varies between about 1 µm and a few mm. A quantum efficiency of 0.8 is assumed [9]. The result of the procedure for a QD emitting at 603 nm and an AM1.5 global incident spectrum is shown in Fig. 2. QD concentrations were varied from 1 nM to 10 mM at a converter thickness D of 0.1 cm. Starting at a concentration of 1 µM an appreciable amount of photons is absorbed in the blue part of the spectrum, while the modified spectrum is increased at the QD emission wavelength. For higher concentrations this effect clearly is much stronger. As the product CD determines the amount of spectral change, optimum values for QD concentration are related to the thickness of the converter. The effect of QD inclusion on all spectra is similar to the one shown in Fig. 2.

3 IMPROVED CELL DESIGN

3.1 Comparison of cell design

The differences between old and new design mainly are a result of improved recombination parameters, see Table I, and improved front reflectance. The latter is accomplished by applying a newly developed etch procedure (termed T2) which leads to an improved surface texture [12].

The BSF is explicitly modelled in PC1D for the old design, while it can be replaced in the modelling by using an effective rear surface recombination S_{eff} of 3500 cm/s [19]. The doping profiles are compared in Fig. 3. In case of the old design the doping profile was measured. As this is difficult for textured samples it is modelled in PC1D by a combination of two doping levels. Doping profiles are modelled in PC1D using the following error function:

$$N(x) = N_0 \operatorname{erfc}\left(x - x_p \,/\, x_d\right) \qquad (1)$$

where N_0 is the peak doping level, x_p the peak position and x_d the depth factor. For $x<x_p$ it holds $N(x)=N_0$. For the old doping profile, we have fitted the experimental curve to a combination of two doping levels as well, see Fig. 3.

Table I: Old and new cell design and material parameters and resulting performance; further details can be found in Refs. [13] (old) and [12] (new).

	old	new	
area	100	156.25	cm^2
thickness	300	300	µm
emitter	50	75	Ω/sq.
junction	0.63	0.63	µm
doping profile	(see Fig. 3, and Table II)		
texture	no	yes (T2)	
front reflectance, 600 nm	9	8	%
front reflectance, 900 nm	20	8	%
rear reflectance	67	67	%
bulk recombination	50.26	91.9	µs
front surface recombination	5 10^5	2.5 10^5	cm/s
rear surface recombination	3500	350	cm/s
modelled BSF	yes, 9 µm	no, S_{eff}	
open circuit voltage	603	624	mV
short circuit current	31.2	35.4	mA/cm^2
fill factor	0.771	0.773	
efficiency	14.5	17.1	%

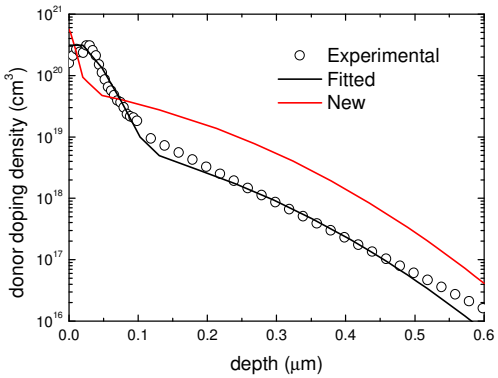

Figure 3: Doping profiles for the new and old solar cell design.

Table II: Doping profile parameters

	old	new	
1st profile (*n*)			
concentration	3	5	10^{20} cm^{-3}
peak position	0.02	0	μm
depth factor	0.048	0.016	μm
2nd profile (*n*)			
concentration	1	6	10^{19} cm^{-3}
peak position	0.0	0.0	μm
depth factor	0.25	0.25	μm
background doping (*p*)	1	2	10^{16} cm^{-3}

The parameters found and used in the simulations are given in Table II. Clearly, the doping profiles are considerably different.

3.2 Comparison of cell performance

The I-V characteristics for the new and old cell design are compared in Fig. 4. Performance parameters are compared in Table I. Clearly, the new design is an improvement, leading to a cell efficiency of 17.1%, mainly due to the large increase in short circuit current.

The external quantum efficiency (EQE) and reflectance for the new and old solar cell design are shown in Fig. 5. Clearly, the cell response is improved both in the blue and the (infra)red. The improved blue response is due to the improved front surface reflectance, passivation, and partly to the new doping profile. This is optimized to yield a maximum open-circuit voltage as checked with PC1D simulations. The improved red response is due to an improved bulk recombination.

3.3 Inclusion of down converter

It is expected that the improved blue response will lead to a less-effective deployment of spectral down converters. To determine this effect, we used the spectral down converter optimized for the old cell design (QDs emitting at 603 nm, 1 mm thickness) [9] on top op the new design, and varied the QD concentrations from 1 nM to 10 mM. The relative increase in short current density is shown in Fig. 6. We find that the optimum concentrations for both designs is 100 μM, while the relative current increase for the new design is lower (8.5%) than for the old design (10%). This is clearly due to the improved blue response (< 600 nm).

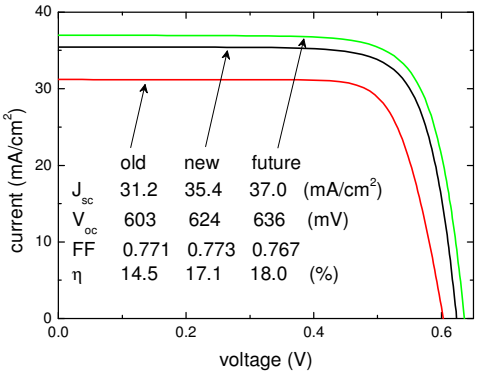

Figure 4: Current-voltage characteristics and performance parameter for the old, new, and future solar cell design

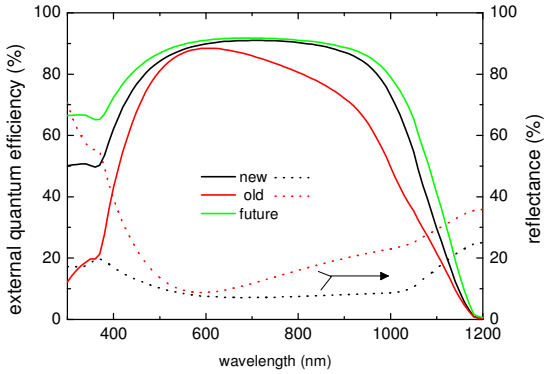

Figure 5: External quantum efficiency and reflectance for the old, new, and future solar cell design

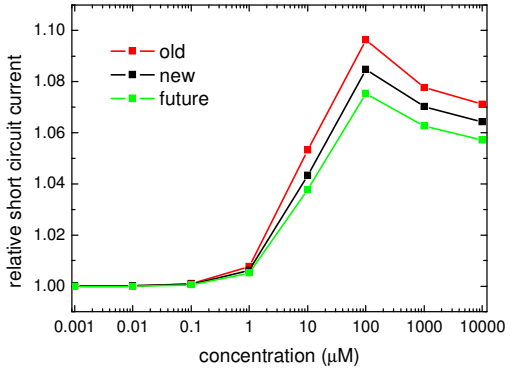

Figure 6: Relative short circuit current increase for modified AM1.5 global spectra for QD (λ_{em}=603 nm) concentrations from 1 nM to 10 mM for the old, new, and future solar cell design

3.4 Future design

Further improvements have been detailed which are expected to yield a cell with an efficiency of 18 % [12]. Expected improved material parameters that are within reach are: bulk lifetime τ_{bulk} = 150 μs, front surface

recombination velocity S_{front} = 5×10^4 cm/s, rear surface recombination velocity S_{rear} = 200 cm/s, and rear reflectance R_{rear} = 80%. Except for these parameters, all parameters used in PC1D are kept identical, and resulting I-V characteristics and spectral response are shown in Fig. 4 and 5, respectively. Both blue and red response are improved with respect to the new (and old) design.

Application of the down converter on the future design leads to a relative increase in short circuit current, albeit lower (7.5%) for the optimum QD concentration of 100 µM than for the old (10%) and new (8.5%) design, see Fig. 6. Apparently, the use of a converter optimized for the old design still leads to performance improvement.

4 OPTIMIZATION OF CELL AND CONVERTER

Further optimization modelling of the combination of the converter and cell is performed starting with the future design with parameters detailed in Section 3.4, and with the doping profile listed 'new' in Table II. From the above we conclude that the converter with QD concentration of 100 µM is optimum. Also, only parameters that influence blue response are considered. Employing PC1D's batch operation we thus varied doping profile, bulk lifetime, and front and rear side recombination velocities. The batch operation allows for simultaneous variation of up to four parameters.

4.1 Doping parameters

Varying only the concentration of doping peak 1 shows that the optimum concentration equals 2.2×10^{20} cm^{-3}, leading to an increase in power and current of only 0.2% with respect to the concentration of 5×10^{20} cm^{-3} for the future design. This optimum is found for both a cell without as well as with converter. The position of doping peak already is found optimal. The doping depth factor is found optimal at 0.002 µm, for the cell both without and with converter, with a relative current increase of 0.5 and 0.3%, respectively. The optimum concentration of the second peak was found to be 1.0×10^{19} cm^{-3}, leading to a current increase of 0.4%, independent of the presence of the converter.

Variation of concentration, position, and depth factor together resulted in values of 8.5×10^{20} cm^{-3}, 0, and 0.002 µm, respectively for a cell without converter, and 7×10^{20} cm^{-3}, 0, and 0.002 µm, respectively for the cell with converter. The current increase amounted to 0.9% and 0.5%, for a cell without and with converter, respectively. The optimum doping profile is thus found to be shallower than used in the new and future designs.

4.2 Recombination parameters

Increasing the bulk lifetime and/or decreasing the rear surface recombination results in performance improvement, but the presence of a converter has a small effect only as the spectral response improves in the red.

Further lowering of the front surface recombination velocity may be pursued in R&D efforts as the lower S_{front} the better the solar cell performance. This is a result of an improved spectral response, as shown in Fig. 7, where the external quantum efficiency is depicted as a function of wavelength for various values of S_{front}, ranging from 10^6 to 10^3 cm/s. Further decrease of the front surface recombination velocity of the future design (S_{front} = 5×10^4 cm/s) will improve the spectral response, albeit only slightly.

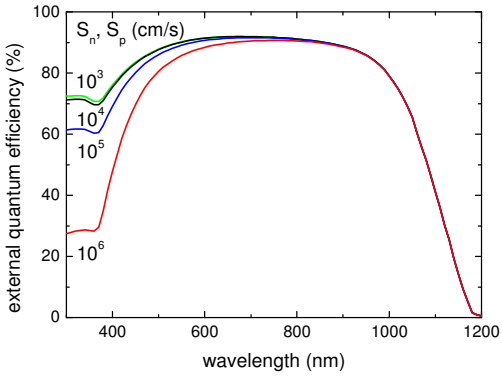

Figure 7: External quantum efficiency for various values of front side recombination velocities for the future solar cell design

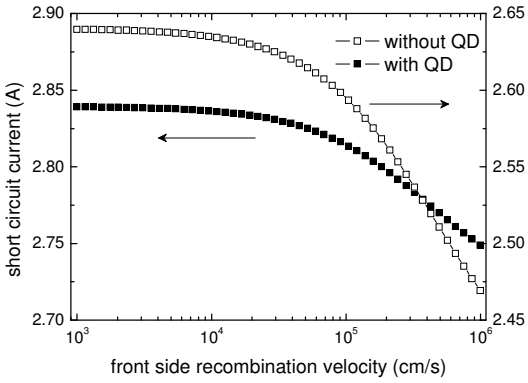

Figure 8: Short circuit current as a function of front side recombination velocity for a bare cell and a cell with converter. Note that the *y*-axis intervals are identical, while a different offset is present for the left- and right-hand *y*-axis

Optimization of the front side recombination velocity for a cell without and a cell with converter shows that the short circuit increase is less in the case of a cell with converter, see Fig. 8. The absolute current increase for a cell with converter is 90.2 mA when comparing the current values at S_{front} = 10^6 and at 10^3 cm/s; for a cell without converter the current increase is 170.5 mA. Relative increases are 3.3% and 6.9%, respectively. However, the absolute values for the short circuit current in the case of a cell with converter are for all values of S_{front} larger than in the case of a cell without converter.

5 CONCLUSION

We have studied the effect of deploying a spectral down converter on top of multicrystalline silicon solar cells by means of modelling. A comparison of old, new, and future cell designs has shown that the beneficial effect of a converter is less pronounced. This is due to the

fact that the cells' blue response has improved as a result of material parameter and cell design optimizations. Inclusion of an optimized converter leads to a current increase of 10, 8.5, and 7.5%, for the old, new, and future design, respectively, using an AM1.5 global spectrum.

As a spectral converter especially modifies the blue part of the spectrum, further optimization of solar cells that is directed towards improvement of blue response (i.e., front-side parameter improvement) should be done in combination with converter optimization. A combined optimization of solar cell and converter showed that modification of the doping profile may lead to a maximum increase in short circuit current of <1%.. In particular reduction of the front side recombination velocity can result in further performance improvement of >3% current increase with respect to the future design.

ACKNOWLEDGEMENTS

We gratefully acknowledge Cees Tool and Arthur Weeber (Energy research Centre of the Netherlands (ECN)) for interest and advice on cell design, and the European Commission for financial support as part of the Framework 6 integrated project FULLSPECTRUM (contract SES6-CT-2003-502620).

REFERENCES

[1] B.S. Richards, Solar Energy Materials and Solar Cells 90 (2006) 2329.
[2] M.A. Green, *Third Generation Photovoltaics, Advanced Solar Energy Conversion*, Springer Verlag, Berlin, Germany (2003).
[3] H.J. Hovel, R.T. Hodgson, J.M. Woodall, Solar Energy Materials 2 (1979) 19.
[4]. T. Maruyama, J. Bandai, Journal of the Electrochemical Society 146 (1999) 4406.
[5] W.G.J.H.M. Van Sark, P.L.T.M. Frederix, A.A. Bol, H.C. Gerritsen, A. Meijerink, ChemPhysChem 3 (2002) 871.
[6] A. Goetzberger, W. Greubel, Applied Physics 14 (1977) 123.
[7]. J.A.M. Van Roosmalen, Semiconductors 38 (2004) 970.
[8]. A. Luque, A. Martí, A. Bett, V.M. Andreev, C. Jaussaud, J.A.M. van Roosmalen, J. Alonso, A. Räuber, G. Strobl, W. Stolz, C. Algora, B. Bitnar, A. Gombert, C. Stanley, P. Wahnon, J.C. Conesa, W.G.J.H.M. Van Sark, A. Meijerink, G.P.M. Van Klink, K. Barnham, R. Danz, T. Meyer, I. Luque-Heredia, R. Kenny, C. Christofides, G. Sala, P. Benítez, Solar Energy Materials and Solar Cells 87 (2005) 467.
[9] W.G.J.H.M. Van Sark, A. Meijerink, R.E.I. Schropp, J.A.M. Van Roosmalen, E.H. Lysen, Solar Energy Materials and Solar Cells, 87 (2005) 395.
[10] W.G.J.H.M. van Sark, Applied Physics Letters 87 (2005) 151117.
[11] W.G.J.H.M. Van Sark, Proceedings 20th European Photovoltaic Solar Energy Conference (2005) 187.
[12] C.J.J. Tool, G. Coletti, F.J. Granek, J. Hoornstra, M. Koppes, E.J. Kossen, H.C. Rieffe, I.G. Romijn, A.W. Weeber, Proceedings 20th European Photovoltaic Solar Energy Conference (2005) 578.
[13] C.J.J. Tool, P. Manshanden, A.R. Burgers, and A.W. Weeber, Solar Energy Materials and Solar Cells (in press).
[14] W. Soppe, H. Rieffe, A. Weeber, Progress in Photovoltaics: Research and Applications 13 (2005) 551.
[15] P.A. Basore, D.A. Clugston, Proceedings 25th IEEE Photovoltaic Specialists Conference (1996) 377.
[16].A.J. Chatten, A.J., K.W.J. Barnham, B.F. Buxton, N.J. Ekins-Daukes, M.A. Malik, Proceedings Third World Congress on Photovoltaic Energy Conversion (2003) 2657.
[17] Leatherdale, C.A., W.-K. Woo, F.V. Mikulec, M.G. Bawendi, Journal of Physical Chemistry B 106 (2002) 7619.
[18] B.O. Dabbousi, J. Rodriguez-Viejo, F.V. Mikulec, J.R. Heine, H. Mattoussi, R. Ober, K.F. Jensen, M.G. Bawendi, Journal of Physical Chemistry B 101 (1997) 9463.
[19] C.J.J. Tool, C.J.J., A.R. Burgers, P. Manshanden, A.W. Weeber,B.H.M. Straaten, Progress in Photovoltaics: Research and Applications 10 (2002) 279.

PV MARKET AND INDUSTRY DEVELOPMENT IN CHINA
IMPACTS OF THE CHINA REDP PROJECT, OTHER PV PROGRAMS AND TECHNOLOGY IMPROVEMENT

Emil ter Horst [1], Zhang Cheng [2]
[1] Horisun Renewable Energy Strategies, D.B. Goerionstraat 42, NL-3573 XP UTRECHT, The Netherlands,
phone : +31-62.8818888 ; fax. +31-30.2760381; e-mail: eth@horisun.nl
[2] PMO WB/GEF China REDP, NDRC, A2105 Wuhua Plaza, A4 Che Gong Zhuang Dajie, Xi Cheng District, Beijing 100044 P.R.China, e-mail: zhangcheng@ndrcredp.com

ABSTRACT: China is THE global rising star up in the PV field. This concerns PV market but even more PV industry development. Especially since 2004 the PV supply chain has developed explosively. A drawback seems that the national industry is orienting towards export, with the risk of neglecting (partly due to high PV prices and to shortage in modules and manpower) the home market especially the market of rural applications.
The NDRC/World Bank/GEF China Renewable Energy Development Project (REDP) is 'running' from 2001 to 2006. The PV component is aiming at developing the rural market for PV in six north-western provinces.
The TI component encourages technology improvement that will lead to lower cost and better quality of components for PV and PV/wind systems. The in-official aim of the TI is also to give the Chinese industry a better chance at competing with western industries in the renewable energy market in general and the Chinese PV market.
China had several quality problems in the PV market around 2000, such as the mal functioning due to lacking quality of the PV modules, of essential other components (esp. the controller) or due to slow service. By the REDP much attention was paid to quality in the Chinese market in the supply and service chain. REDP substantially affected the quality of PV components produced in China and the professionalizing of Chinese PV industry.
Around the year 2000 the NDRC/WB/GEF China REDP has also been crucial for the attention of the Chinese authorities and industry for PV. Now the China REDP ends new programs take over the guiding and trendsetting role, paving the way for China to be one of the top-3 countries in the global PV field before the year 2010.
Keywords: National Programme, PV Market, Rural Electrification

1 INTRODUCTION

In China the attention for PV has grown strongly. This can be noticed both in the local PV markets but much more in the development of PV industry. Especially since 2004 a growth explosion can be seen, the end is not yet within view. The new companies are orienting towards export and less towards the market of rural applications. The development of PV is paralleled by stimulation programs by the Chinese national, provincial and municipal governments.

Before 2004 a special role in this development was plaid by the World Bank/GEF China Renewable Energy Development Project (REDP). The REDP is a cooperation between the Chinese Government, GEF (Global Environment Facility) and the World Bank. The project aims at reducing CO2 emission, slowing down the global climate change and improving the living standard of the people who have no access to electricity in remote areas. The project consists of three parts: Wind component, PV solar home system component and Technology Improvement Component (TIC).

The first two components are market development programs aiming at developing the rural electricity market for wind and PV in six north-western provinces. The third TI component encourages technology transformation and technology transfer. Support is provided to finance technology improvement activities that will lead to lower cost and/or better quality of components for PV and PV/wind systems.

The REDP has been prepared from 1997-2001. The project's components are 'running' from 2001/2 to 2006 and open both for Chinese and for foreign industries. Together with Chinese pioneers from the first hour the REDP has been paving the way for the Chinese PV development and for new stimulation programs.

2 THE CHINA PV MARKET

2.1 Status RE 2005

Since 50 years China has been using small and micro hydro-power for the electrification of villages in rural areas. The accumulated installed capacity to date is 23,000 MW. The attention to RE in the past decade has resulted in about 500 MW of wind farms, 500 MW of biomass cogeneration and several other RE power plants with smaller capacities.

The attention to PV since the late nineties resulted in over 500,000 Solar Home Systems (SHS's), installed mainly in the six remote north-western provinces and added to about another 300,000 existing small decentralized micro-wind (170,000) and micro-hydro systems (150,000).

2.2 PV market 2005

The distribution of sales and installed capacity of PV in China is given in Figure 1 and Table 1.

The national PV market in China is developing as follows:

- before 2000 the PV market was small with professional applications (e.g. telecom) as the largest market segment
- due to the REDP and the growing attention for village electrification with PV now (end of 2005) the internal PV market is dominated by rural applications of PV
- the rural PV market segment is expected to be the largest for the coming decade until the majority of villages in the western provinces will be connected to the grid in 2020
- new programs will stimulate the development of Rooftop and Building Integrated PV in the eastern provinces and the development of large PV power

stations in desert areas (section 5). Grid connected PV is expected to take the lead 10 years from now.

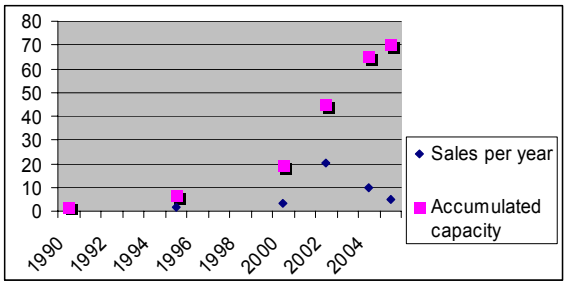

Figure 1a: Installed capacity of PV in MWp per year
1b: Cumulative installed capacity of PV in MWp

Year	Annual Installed Capacity (kW)	Accumulative Installed Capacity (kW)
1976	0.5	0.5
1980	8	16.5
1985	70	200
1990	500	1780
1995	1550	6630
2000	3300	19000
2002	20300	45000
2004	10000	65000
2005	5000	70000

Table I: PV market development in China 1976-2005

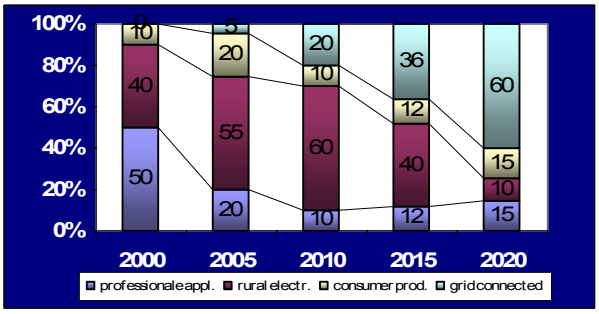

Figure 2: Relative share (real + projected) of PV market segments in China

3 THE CHINA PV INDUSTRY

3.1 Status PV industry

Since the first PV cell was made in China about 50 years ago, industrial activities started for space, telecommunication, defense and petroleum related energy supply systems. In the mid-seventies China started to produce the typical small portable solar home boxes for rural areas. This market has (without any subsidy until 2000) developed successfully.

Before 2000 there were 7 PV manufacturers with a 2 to 3 MWp/yr production capacity, enough for the home market of mainly professional and rural applications. Halfway 2004 (just before the PV boom) there were about 20 PV module manufacturers with about 20 MWp annual production (claiming a capacity of 100 MWp /yr).

Year	National sales	Totally installed	Produced cells	Produced modules	Cell pr. capacity	Module capacity
1999	1	16	1	1	10	
2000	3	19	2,5	2,5	10	
2001	4,5	23	4,3	4,3		
2002	21,5	45	16,5	16,5		
2003	10	55	>10	10	80	80
2004	10	65	>50	?	100	>100
2005	5	70	145	284	>150	857
2006					1450	>1000
2007						
2010	80	500	100			
2020	500	5000	2750			

Figure 3: Overview of national sales, production of cells and modules and production capacity of PV in China in MWp/year

3.2 Polysilicon production

By the end of 2005, the production capacity of polysilicon material in China was about 400 tons. In 2005 the amount delivered reached only 80 tons. There is a big gap between the production and market demand in China and most polysilicon material was imported abroad.

In 2006 China is adding 200 tons of production capacity. For 2007 1960 tons of capacity will be added, while for 2008 another 2000 tons added are estimated.

Polysilicon per year demand and production	2004	2005	2006 (proj.)	2008
Demand semiconductor industry (EG) (tons)	910	1092	1200	
Demand by solar PV industry (SG) (tons)	650	1729	3640	
Total demand (tons)	1560	2821	4840	
Delivery value of polysilicon (tons)	57.5	80	300	
Net imported (tons)	1500	2741	4540	
China production capacity estimate (tons)	?	400	600	4600

Figure 4: National demand and production of polysilicon for semiconductor and solar industry in China in tons/yr

3.3 Silicon ingot manufacturing

The ingot manufacturing industry (for both semiconductor and solar industry) develops very fast recently by an annual growth of 70%. By the end of 2005, the production capacity of poly- and single-crystalline ingots has exceeded 5000 tons in China. Ningjin Jing Long Group has had a production capacity of about 2000 tons and became the biggest ingot manufacturer in the world.

At this moment (2005/6) the total capacity is 5792 tons (divided over 4800 tons of single-crystalline silicon and 992 tons of poly-crystalline silicon); the real output in 2005 has been 2436 tons (divided over divided over 2086 tons of single-crystalline silicon and 350 tons of poly-crystalline silicon).

3.4 PV cell manufacturing

Since 2004 PV industrial activities in China started to boom. The total production of solar cells during 2004 was exceeding 50MWp, which was 4 times the value of 2003.

In 2005 the total production was about 145 MWp, of which Wuxi Suntech delivered 82 MWp, then ranking the eighth biggest cell supplier in the world. However the manufacturing of solar cells would have developed even faster if the supply of silicon material would not have been a limiting factor.

It is estimated that the production capacity already in 2006 will reach 1450 MW, which is almost 10 times the value of 2005.

3.5 PV module manufacturing

In 2005, the module manufacturing capacity in China was 857 MW while the real production and delivery was 284 MW. This is about 15% of the total global production of PV.

Because of the shortage of solar cells in China, more than 50% of the solar cells were imported.

The module production capacity is easy to upscale due to the large share of hand labor, but therefore rather difficult to prognosticate, even for 2006. However the capacity is now (halfway 2006) already over 1000 MWp.

4 THE NDRC WB/GEF CHINA RENEWABLE ENERGY DEVELOPMENT PROJETC (REDP)

4.1 Project Background

The REDP project was set up at the end of the 1990's. Observations in the Chinese SHS market around 2000 were:

- attention for PV and wind (larger wind and a bit less for small wind) especially in the academic sector and some 'new market' parties was growing rapidly
- sales of wind turbines was growing to over 100 MW/year
- sales of PV was growing above 1 MWp per year, increasing with 20% per year
- a unique Chinese portfolio of PV SHS products:
  - very small PV systems of 5-50 Wp per SHS
  - total-service-in-one-box concept
  - competition on price per service; not per Wp or kWh
  - quality and maintenance issues differ from SHS PV markets in other countries
- market development of SHS (and also other RE as solar hot water systems) was not financially stimulated yet
- improvement of quality of PV products was not supported
- no quality assurance (QA) system was used in China

For the prices of SHS in China around 2000 it was found:

- that PV modules >50Wp were sold at world market prices but with lower quality
- that PV-modules <50Wp (mainly laser cut cells) were much cheaper than elsewhere
- that PV solar home systems from China belong to the cheapest on the world market

Furthermore in 2000:

- China's economy and society was changing rapidly
- 20,000 villages and 20 million people did not have access to electricity.

In this situation a small dynamic PV distribution business was emerging, consisting of people from research institutions in Beijing, Shanghai and other eastern cities (knowledge), from provincial institutions (distribution) and sales people in the provinces (knowing the market). On one hand the national rural market was quickly expanding; but on the other hand PV suffered sometimes from lack of quality or deficient after-sales service due to the growth.

4.2 Project Intentions

The China REDP aim is to use state-of-the-art and cost-effective (wind and) PV technologies to supply electricity to remote areas in China in an environmentally sustainable way and to develop a persistent sustainable market.

The REDP will support 10 MWp of PV totally. It concerns about 300,000 PV systems mainly SHS for the north-western provinces and regions Tibet, Qinghai, Xinjiang, Gansu, Sichuan and Inner-Mongolia. See map of China (Figure 6).

The specific objective of the Technology Improvement (TI) component is to lower cost and to improve the quality of PV equipment in China. An important secondary (unofficial) aim of TI is to give the Chinese industry a better chance at competing with western industries in the renewable energy market in and outside China. Being more or less the only program with this goal from 1999 to 2004, Technology Improvement and Quality Assurance issues were of highest relevance.

Figure 5: Participating provinces (blue) in China

4.3 PV Market Impacts

Up to now the following successful (✓) or not-successful (–) market impacts of the REDP were preliminarily assessed.

✓ *To provide basic energy services to remote areas*

- At the end of REDP far over 300,000 extra customers will have access to basic light;
- REDP was an important example to convince the Chinese government that PV is one of the prime technologies to bring electricity to remote areas, leading to new dedicated stimulation programs.

✓ *PV market acceleration*

- Establishment of a market-driven sales (& service) system for SHS: over 25 PV companies are now equipped to sell quality PV in China;

- The costs of SHS were reduced from 80-100 Yuan before 1997 down to 50-60 Yuan per Wp. PV market has grown from 2MW in 1997 to 10 MW in 2004.

? *Sustainable development both for market as for technology development*
  - This impact is not clear on the longer term yet. On the one hand it is clear that PV companies are able to adopt improved technology, but improved (more expensive?) SHS's were not easily adopted by the customers;
  - Due to high prices of PV on the world market prices of SHS's did not go down in China from 2004 to 2006;
  - As the start of new stimulation programs was delayed, the national PV sales went down from 2003 to 2005.

Impacts on quality and Quality Assurance (QA)

✓ *Improvement quality level without raising prices*
- For improvements for which the cost of the purchase was not higher, such as improved battery controllers, this impact was reached in an absolute way: Also several suppliers had to improve their quality as they were losing market share to a competitor with a higher quality or better features at the same price.
- The impact is also reached for improvements, where the higher price for the purchase in absolute sense can be justified by clear savings on short term. It was possible to convince the market e.g. for improved DC-lights. In other improvements with a higher absolute price, the market was not convinced (☹).

✓ *Quality level and best Chinese market players*
- The extensive PV knowledge base already existing made it possible to assess the national state-of-the-art throughout the country rather quickly. The quality level chosen as the minimum level in the REDP was the quality level of eastern China and of PV institutes in Beijing and Shanghai. This forced local PV suppliers to work together with provincial institutes (with access to eastern China's technology) or with national institutes in eastern China.

✓ *Jumpstart through a List of Qualified Suppliers*
- It was possible to train 17 PV suppliers and to do simple and quick tests of qualified components by national testing centers to make a first list of Qualified Suppliers and qualified products. The short-cut on QA in principle worked very well. The lists were ready in a short period, and the project started with a limited but well-working QA-system within a year.
- In 2005 the List of Qualified Suppliers had over:
  - 27 PV manufacturers
  - 27 controller manufacturers
  - 22 inverter manufacturers
  - 10 DC saving light manufacturers
  - And 37 storage battery manufacturers.

– Quality in Chinese PV market to reach international level
  - As said before the quality of PV products which are **offered** has been improved substantially, this can not be said for what is finally **sold**. In general the Chinese market tends to buy a cheaper alternative, even though the quality is lower. Differentiation of the portfolio and competition at the low-end of the market is very high. Education of the consumer is needed to have the market really adopt the improved products. It can be concluded that for all improvements that lead to a higher price of purchase, the advantages have to be communicated much better with the customers.

Figure 6: Two successfully adopted TI products by the market were the improved DC light and the controller

Industrial impacts in China

✓ *PV technology to reach international state-of-the-art*
- Several PV manufacturers have reached the international level for the production of cells and modules. Also on the system level the international state-of-the-art for quality will be reached. For SHS-systems below 50 Wp, the Chinese manufacturers are leading the international state-of-the-art, as well as for selected components as DC-lights and LED-lights.

✓ *Improved competition against western PV industry*
- We see that in 2004 Chinese PV modules can compete for the first time on a substantial level with western modules in the German market;
- Before 1997 there were 7 PV manufacturers with a 2-3 MWp year production; begin of 2004 this has grown to 20 manufacturers with about 20 MWp annual production (and 100 MWp production capacity);
- Since 2004 PV industry is booming especially for export. Of course besides the impact of the REDP there are several other success factors.

Fair competition in REDP projects and Chinese PV market

✓ *Modern competitive project selection*
- This impact was reached by establishing an effective management of the REDP and proposal selection mechanism and criteria. The competitive element is limited mainly to that between Chinese companies, as foreign companies turned out to be at the same project quality more expensive even when the work is carried out in China.

– Equal chance for foreign and national PV suppliers
  - There is no equal chance for foreign PV suppliers in the Chinese PV market of SHS's, except for some professional or selected subsidized niche-

markets, where a higher quality level is demanded. This may be due to the fact that foreign PV suppliers did not develop a product portfolio with a better price/per-formance and/or aiming at the low end of the market.

4.4 Use of Standards

In the China REDP it was chosen not to use internationally available quality standards, but to develop own standards:

- partly because international standardization process was very slow and quality standards for controllers, inverters, batteries were under development for many years, but were not available (IEC, GAP) and wer not able to deliver standards in time;
- partly because some areas important for the Chinese market were new for the international 'QA' community, such as dc-lights and LED-lights;
- also because the Chinese suppliers of PV modules could not reach the international quality level at that time.

The Project Management Office (PMO) of the REDP project established a quality standard, a first quality check and a quality verification system as a part of the overall project management system. The QA system functions up to now overall very well. This is due to the fact that all actors take the use of the standards very serious as the award of the subsidy is depending on the (verified!) use of qualified components.

Though all standards were developed for use in the REDP, they are now widely used in other projects in China and in the rest of the world. De facto the REDP standards are now widely recognized, accepted and used by actors in the whole PV market. The Chinese government has used the REDP standards as if they were national standards.

National standards (situation 2004)

Before 2003 there was no official Chinese standard for SHS's. On the subject the PMO organized expert's meetings with the relevant national standardization committee. It was decided to proceed as follows:

1. If there was a national standard existing (PV modules and batteries) the national standard will be the base for testing.
2. For components without a national standard (controllers, inverters, DC-saving-lights and SHS's on the system level) the REDP standards will be the base for testing.

A PV SHS or component can only be certified if a qualified test center will carry out the test. If a product fulfills the test requirements it will be certified according to the national standards, but automatically the PV product/supplier will also be listed on the List of Qualified Suppliers of REDP.

At the end of 2003 a draft 'National Technical Conditions and Test Methods for PV Solar Home Systems' was made based on the above policy, which was approved to be the formal national standard in 2004.

REDP has developed training programs for disseminating knowledge on this new standard in 2004 and 2005.

Module certification

Until 2004 most Chinese manufacturers sold PV modules which were tested against the Chinese standard GB-9535-1988. In 2004 and 2005 the TI component offered support to about 10 manufacturers to test their modules against the international standard IEC-61215. With this an important chapter (taking only about 5 years from the start of the REDP) in the race of the Chinese PV actors to catch up with the international state-of-the-art for PV modules was closed.

Since mid-2004 daily reality has overtaken this important success: only one to two year later every self-respecting Chinese PV manufacturer is testing now against international standards.

4.5 SHS Factory Check within REDP

Within the REDP the PMO controls the quality of SHS's through an established Qualified Components Supplier List.

The system integrators have to purchase components from the list in order to get the subsidy. The list is established by the PMO mainly based on test reports issued by a test lab accredited with IEC/ISO 17025. Starting from July 2006, in order to strengthen the manufacturing and management capability of the suppliers, the PMO requires module manufacturers and controller and inverter manufacturers to conduct a so-called Factory Check when they apply to be a 'Qualified Supplier'. Only the manufacturers who pass the Factory Check will get onto the list.

The findings of the Factory Check are as follows:

- generally, most of the manufacturers have obtained ISO 9001 certificate, thus, the quality control system is complete and the documentation is quite good;
- manufacturers paid great attention to the Factory Check. The manufacturers were informed of the importance of controlling the quality by improving management and manufacture process, and many manufacturers increased their investment in quality control facilities;
- the type of the products varies from one manufacture to another. It turned out to be is difficult to test all the products according to one standard. There is a need to define the new procedures for new types of products;
- in general the financial and management capabilities of the manufacturers have been largely improved since the REDP project just started;
- overall the REDP was successful in improving product quality although there are still quality issues to be solved.

System test and certification

In order to further improve the current SHS technology on the system level, increase system performance and efficiency as well as to help SHS integrators optimize their system design, the REDP initiated and developed a test on SHS's based on IEC 62124. The test focuses on the comparative testing of the performance of different brands and types of SHS's.

The results will be used to educate the customers on product quality as well as to help the SHS integrators to improve the system design, to reselect system components and to improve their system performance according to the test data.

Parallel the PMO supports the China General Certification Center to establish a national certification

system on PV products with the aim to issue a SHS quality mark. The manufacturers will get the mark for those solar home or other PV systems if the systems pass the test as well as the Factory Check. In this way the achievements of the China REDP project can be made sustainable after 2006.

5 CONCLUSIONS AND FUTURE OUTLOOK

The China REDP project substantially improved the quality of PV components produced in China and the professionalizing of Chinese PV industry. The REDP also has been crucial for the attention of the Chinese authorities and industry for PV in the beginning of this decade.

Other programs and investments have been 'triggered' by REDP; these programs might have had even more impact on industry and market development than REDP, such as:

- the Brightness-program (parallel to REDP)
- the Tibet Sunshine project (parallel to REDP)
- the PV Township program (from 2002, 20 MWp).

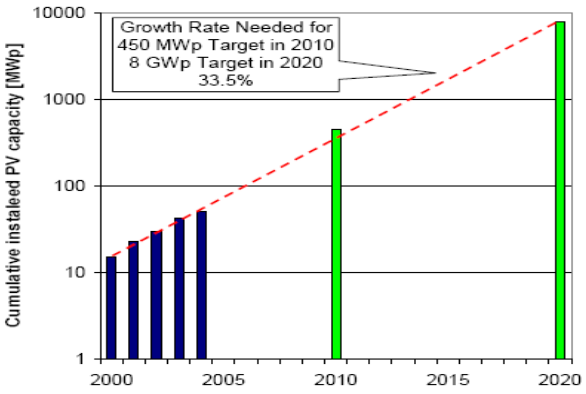

Figure 7: Possible development of cumulative installed capacity of PV in MWp in China derived from policy under discussion.

Relevant policy drivers are:

- China's diversification policy and wish to have a lower dependency on oil and coal
- The need to bring electricity to rural western provinces in China
- China's ambition to be a world market player in this future gigantic market

In the last couple of years several policy statements have been made and discussed:

- 2010: in total ~500 MWp PV solar to be installed
- 2020: PV capacity in China ~4 to 30 GWp installed
- the 'Market-Oriented Reform in China's Energy Sector' called for an improved legislation to stimulate RE
- Olympic Summer Games in Beijing in 2008 are baptized the 'Green Olympics'

The 'Renewable Energy Law' has been approved in February 2005 and is active since 01/01/2006. The effect for PV is not clear yet.

The NDRC WB/GEF China REDP will be ending in 2006. Several new programs are on their way or under consideration:

- China - Renewable Energy Scale-up Program (CRESP)
- National Villages program (28.000 villages ad 5kWp)
  - until 2020: 140 MWp
- Green Rooftops Plan (100.000 rooftops ad 5kWp)
  - 4.000 in 2006-2010: 20 MWp
  - 96.000 in 2010-2020: 480 MWp
- Desert PV program (100 PV Power Plants ad 10 MWp)
  - 8 in 2006-2010: 80 MWp
  - 92 in 2010-2020: 920 MWp

If these programs and incentives are carried out, they will pave the way for a respectable Chinese home market of 1 to 5% of the global market.

Chinese industry has shown since 2004 that they can do better than that: they are making up for a 10-50% share of the global PV production.

REFERENCES

1. Emil ter Horst and Zhang Cheng, "Impacts of Technology Improvement and Quality Assurance in the WB/GEF China Renewable Energy Development Project on PV industry and market development in China", 15th International Photovoltaic Science and Engineering Conference, Shanghai, China, 2005.
2. World Bank, "China Renewable Energy Development Project, project appraisal report", World Bank, Washington-US, 2000.
3. Anil Cabraal, "Strengthening PV businesses in China", Renewable Energy World, May-June 2004.
4. PMO of the China Renewable Energy Development Project, "Solar PV Systems and PV/Wind Hybrid Systems Specifications and Qualifying Requirements", SETC, Beijing-CN, 1998.
5. PMO of the NDRC/GEF/WB Renewable Energy Development Project, "Mid-Term Review Evaluation Report", NDRC, Beijing-CN, 2004.
6. Emil ter Horst, "Technology Improvement Mid-term Evaluation Report", Horisun, Utrecht-NL, 2004.
7. Several interviews during 1998-2005 with WB, SETC and PMO/REDP (NRDC) staff.

ACKNOWLEDGEMENTS

The authors are grateful to the PMO (NDRC) and the WB/GEF program management of the China REDP, making it possible to collect the findings of this paper during several missions. More information on the REDP can be found on the project web site: http://www.ndrcredp.com/english/PMO.asp

This paper is partly an actualization of a case study carried in 2005 (see ref. 1). Financial support by the European Union for this case study through the project Tackling the Quality in Solar Rural Electrification (TaQSolRE) is gratefully acknowledged. More information on the TaQSolRE project is found on: http://www.itpi.co.in/vhosting/taqsolre/home.asp

SIMULATION OF PV-POWERED PRODUCTS: *i*PV-Sim

N.H. Reich, W.G.J.H.M. van Sark, E.A. Alsema

Department of Science, Technology and Society, Copernicus Institute for Sustainable Development and Innovation,, Utrecht University, Heidelberglaan 2, 3584 CS Utrecht, the Netherlands,
T: +31 30 253 7637, F: +31 30 253 7601, N.H.Reich@chem.uu.nl

ABSTRACT: Nowadays only a few indoor operated PV-powered consumer devices exceed power demands of the µW range. Many modern consumer applications, however, show larger power demands in the mW power range. For such devices it is difficult to reach a viable energy balance, especially if low annual irradiation conditions and heavy device usage coincide. We present a new tool, named ***i*PV-Sim**, to enable product designers and engineers to evaluate appropriate designs of (indoor) PV devices in a simple way, nevertheless accounting for the specific system conditions including weak light solar cell efficiency. An annual time step simulation using a step size of one minute is performed to evaluate a broad range of possible consumer systems equipped with PV. Device power specifications can be split into three energy management levels, which can be used to map the large variety of existent power demands of state of the art electronic devices. Specific device use times and light profiles can be designed such that low, medium, and heavy device use as well as any irradiation intensity pattern compared to hourly outdoor light intensity datasets based on measurements can be distinguished. Solar cells are modeled using the two-diode model. Predefined solar cell characteristics extracted from a study on commercially available solar cell performances including the efficiency dependency on light intensity as well as spectral responses are thus available.
Keywords: Modelling; PV system; Software

1 INTRODUCTION

Since already many years, PV-powered consumer applications such as calculators and watches are well known, but the range of possibilities for device integrated PV in consumer and professional applications is much broader. Attempts are underway to integrate PV in prototypes of mobile phones or PDAs [1] and a PV powered wireless keyboard has become commercially available recently [2].

Up to now, however, only few *indoor* operated PV devices exceed power demands of the µW range, and most modern consumer systems have power and resulting energy demands that are three orders of magnitude higher. For such mW-systems it often becomes more difficult to reach a viable energy balance. As the overall energy flow increases, difficulties arise in the design process of integrated PV, especially when calculating energy balances to test the solar powered product for its energetic feasibility:

- large variations of device use times result in large ranges of energy demands;
- uncertainty of available irradiation (patterns) for the solar cells to generate charge currents lead to uncertainty in energy generation;
- increasing system complexity due to higher energy densities (more technical requirements with need for an optimized design, such as an appropriate charge controller, sufficient storage dimensioning, and fitting a PV module configuration to the electrical system over a large irradiation range).

Due to the system complexity it becomes difficult to model all system components; irradiation and device energy demand ranges add additional uncertainty. Therefore we question whether a possible mass production of devices in the mW power range might only be hampered by *uncertainty* of whether or not a 100% solar powered supply can be achieved. We argue, that a lot of possible products can be operated autonomously by implementing PV cells. To reduce the uncertainty of possible PV energy yields and resulting solar fractions in the energy supply of such consumer systems, we developed the simulation tool ***i*PV-Sim** presented in this paper.

By using a time step based computer simulation tool, energy flow calculations become much easier. Arbitrary irradiation and device use time profiles can be defined, so that a detailed simulation of system energy streams can be performed much faster and more accurate than with conventional calculation methods based on e.g. spreadsheet programs. For product designers and industrial design engineers it becomes possible to evaluate appropriate designs of indoor PV devices more accurately and faster. As the tool facilitates the modelling of such devices and because most design engineers are no PV experts, this tool might help to increase the already vast application range of product integrated solar cell applications. However, it is a basic concept of the simulation tool to have a large variety of involved parameters modified by the designer behind the keyboard. This allows for simulation of many different types of possible PV powered products.

This paper is organized as follows: first the PV and storage unit modelling is described; second the editors for device usage and irradiation conditions. Then an example is given of usage of this tool, i.e., a wireless PV powered computer mouse. The results are discussed and lead to conclusions and recommendations for future work.

2 PV AND STORAGE UNIT MODELLING

The simulation model is based on a PV and a storage unit as well as a coupling unit between these two, to account for different charge controller types and behaviors. For the storage unit a simplified battery model that accounts for battery self discharge and charge efficiency is used.

For the PV unit, light intensity dependent solar cell efficiencies and voltages are considered, because indoor PV (iPV) devices will be operated under much lower irradiation conditions compared to the outdoor environment.

2.1 PV modelling

Solar cells are modelled using either the one- or the two-diode model. The single diode model of the solar cell assumes the *pn*-junction as well as the surrounding depletion region to have a negligible recombination loss. In the two-diode model it is possible to account for these losses, because physical device properties of the solar cell causing these losses can be linked to the model parameters [3, 4]. This is an important issue for low light cell efficiency modelling, because with decreasing light intensity junction voltage changes become relatively high, and *pn*-junction recombination losses become more important.

Figure 1 shows the two-diode model of a solar cell. As

well in the figure as also in the further equations, the one-diode model can easily be derived by ignoring the second diode. As shown in Figure 1, both diodes (D_1, D_2) are associated with correlated diode currents ($I_{0,1}$, $I_{0,2}$) and ideality factors (n_1, n_2), whereas n_2 often is assumed to equal 2. A parasitic (lumped) shunt resistance R_{Sh} is related to the ohmic drop within the device. The (lumped) series resistance R_{Se} accounts for the specific cell current conductance properties. The generated current is denoted I_{Ph}. Detailed descriptions of the one- and the two-diode model, respectively, can be found in literature [5, 6].

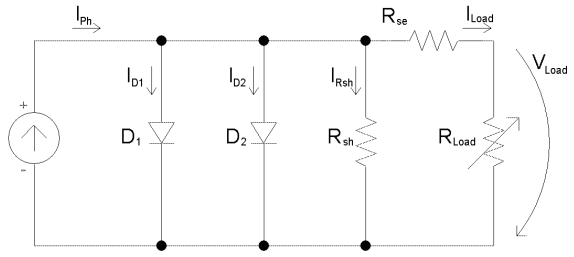

Figure 1: Equivalent solar cell circuit diagram according to the two-diode model

Solar cell voltage depends logarithmically on light induced current, and can be analytically expressed under open circuit conditions ($I_{Load} = 0$) as the open circuit cell voltage V_{oc}:

$$V_{OC} = \frac{nk_BT}{q} \cdot \ln\left(\frac{I_{Ph} + I_0}{I_0}\right) \quad (1)$$

where k_B is Boltzmann's constant (1.38 10^{-23} J/K), T temperature (K), q elementary charge (1.602 10^{-19} C). At room temperature $V_T = kT/q = 25.67$ mV. Under non open circuit conditions, however, the load current I_{Load} induces a voltage drop at the internal series resistance, thus reducing the actual output voltage available at the cell contacts by the factor I_{Load} (solar cell operating current) times R_{Se} (solar cell series resistance). This 'inner' cell voltage is thus higher than the actual open circuit voltage, which has to be accounted for when calculating the current loss related to the shunt resistance (equation 2) and the diodes (see equation 3):

$$I_{Rsh} = \frac{V + IR_{Se}}{R_{Sh}} \quad (2)$$

The cell current I_{Load} can be derived by the sum of all currents listed in Figure 1, which results in the so called 'operation equation' or IV characteristics, wherein the current is expressed as a function of operation voltage (I=f(V)):

$$I_{Load} = I_{Ph} - I_{0,1}\left[\exp\left(\frac{V + IR_{se}}{n_1 V_T}\right) - 1\right] - I_{0,2}\left[\exp\left(\frac{V + IR_{se}}{n_2 V_T}\right) - 1\right] - I_{Rsh} \quad (3)$$

By solving equation 3 with respect to a specific light induced current, which is assumed to be linearly dependent on light intensity, cell efficiency can then be calculated by the well known specific parameter set: fill factor (FF) open circuit voltage (V_{oc}), maximum power point voltage (V_{mp}), short circuit current (I_{sc}) and maximum power point current (I_{mp}).

$$\eta(G) = \frac{I_{mp} \cdot V_{mp}}{G} = \frac{FF \cdot I_{sc} \cdot V_{oc}}{G} \quad (4)$$

The industrial solar cell parameter set uses the one diode model parameters to characterize solar cells and the resulting shape characteristic parameters. As this characterization neglects recombination currents, either the two-diode model must be used or the one-diode model modified, to account for these losses, which become of more influence the lower the light intensity and, as a consequence, the light induced current decreases [3, 4, 7]. Therefore the two-diode model parameter set is used within ***i*PV-Sim**. The two-diode model parameter sets have been validated or modified to account for efficiency at low light intensity to be as good as possible. To that end, measurements of commercial available solar cells at varying light intensities have been used that were presented earlier [8].

Up to now, commercially available crystalline solar cells offer much better efficiencies than most commercially available thin film technologies. For example, amorphous silicon cells (a-Si:H) show STC (standard test conditions) efficiencies around 7% maximum, compared to a 13-17% range STC efficiencies of commercially produced multicrystalline silicon cells. Monocrystalline silicon cells with up to 20% STC efficiency are commercially available at relatively low costs.

However, solar cell efficiencies decrease towards lower irradiance, as is shown in Figure 2. Even specific a-Si:H cells can perform better if very low light intensities prevail..

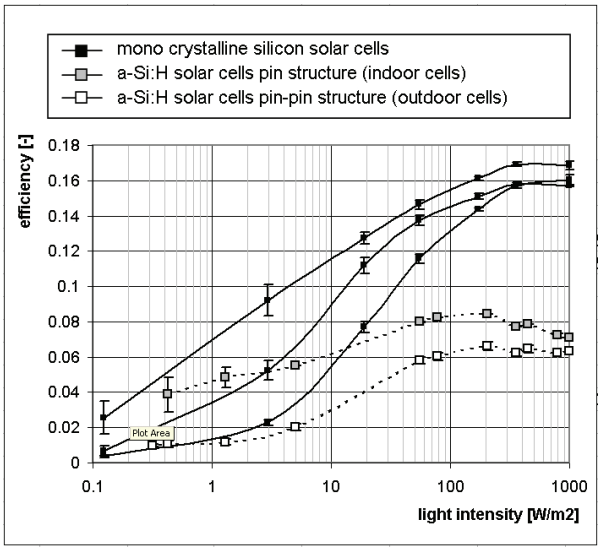

Figure 2: Solar cell efficiencies as a function of light intensity for three different mono crystalline silicon cell manufacturers and for two different a-Si:H solar cell types.

2.2 Device demand modelling

Device power demand can be distinguished in three different heights to account for up to three different energy management system (EMS) levels applied in modern consumer electronic products. These EMS levels are implemented to reduce consumption with respect to often-limited battery capacity and thus runtime of these products. As we found in the design of a prototype application for solar powered consumer systems [9], consumption can either be linearly related to battery voltage for the case of high efficient device implemented DC/DC conversion units, or almost constant with respect to current drain for the case of often very inefficient voltage regulators. A minimum device operation voltage can be defined to identify timeframes in which the device cannot be operated any longer, or to define the time of battery replacement. With these values, all basic device parameters needed for the tool are available, as device energy consumption is actually determined by user defined load profiles (see section 3).

2.3 Storage unit modelling

The storage unit is modelled by using a state of charge dependent battery voltage in combination with a battery current dependent voltage change. Therefore an internal battery (series) resistance is used. This effect is often referred to as battery charge efficiency, because due to the internal battery resistance battery voltage during battery charging

becomes higher compared to the battery base voltage under open circuit conditions, and lower for the case of battery discharge, respectively. Therefore battery energy flows, expressible in watt-hours approximately become a factor 0.8-0.9 smaller than battery charge flows expressed in ampere-hours.

To account for battery efficiency in actual product operation conditions also battery self-discharge has to be considered. Battery self discharge is modelled using a parallel battery resistance parameter. This parameter can be specified with dependency on battery state of charge (SOC), battery age as well as charge flow (aggregated sum of either the battery charge or battery discharge currents), whilst battery series resistance can only be changed dependent on battery age and charge flow. The user can specify all these parameters; standard battery parameter sets are provided for the standard battery types NiCd, NiMH, Li-Ion, SLA (sealed lead acid) and finally RAM (rechargeable alkaline manganese).

Other battery parameters, and many more exist with a lot being very battery type specific, are consciously ignored to keep the model simple and understandable. Especially battery temperature, however, *should* be of interest. Although temperature ranges in consumer devices are not supposed to have temperature ranges as high as in PV systems installed outdoors, it is our intention to implement battery temperature profiles in future versions of this simulation tool, as in many battery types it is temperature that has high influence on the overall battery lifetime.

2.4 Charge controller options

It is possible to distinguish three charge controller configurations that describe the different possibilities to couple solar cells to a battery unit, with an additional 4th option to have maximum power point tracking (MPPT) applied within the charge controller unit.

1. a simple diode (only granting no battery discharge occurs over the battery connected PV module)
2. 'on/off'-switching charge controller (disconnecting the PV module from the battery to protect the battery from overcharge or deep discharge)
3. a current regulated charge controller (that additionally controls the height of the battery charge current as the battery gets charged completely and can allow trickle charge currents to keep a fully charged battery charged)
4. a voltage stepping unit (that operates the PV module at or closer to the maximum power point (MPP))

A single diode (1) is always required for the case of a solar cell that is directly coupled to the battery and a system not containing any charge controlling. A 'on/off' switch options (2) enables the simulation-tool user to enter voltage or battery SOC values at which the PV unit is disconnected from the battery unit to protect the battery from overcharge and deep discharge. A current regulated charge controller (3) accounts for e.g. pulse width modulation (PWM) controlled limits of charge currents. These limits are split into two different sections, whereas 'final charge current' accounts for the timeframe during which the battery gets charged completely, and 'trickle charge current' that accounts for the maximum (and often desired) current that is needed and allowed to keep a fully charged battery charged at 100% SOC without overcharging the battery.

Finally, to account for the possibly implemented MPPT within the charge controller unit, a single value of MPPT efficiency can be defined.

3 DEVICE USAGE AND IRRADIATION PROFILES

3.1 Device profile editor

Device use times can be defined by the user on a minutely basis for a weekly profile. Due to the large variations in energy demands caused by different device use times, large demand ranges should be taken to simulate product energy streams rather than an average device consumption. Therefore it is possible to define usage scenarios for any case, with the three distinct cases light, medium and heavy device usage advised to be used. Figure 3 shows a screenshot of a daily profile for the heavy device usage class.

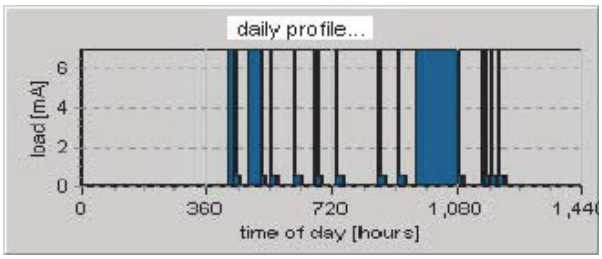

Figure 3: *Daily device use profile example on minutely basis*

Device use profiles are automatically linked to the defined device power demands, as a means to facilitate construction of consumption scenarios. Thereby a good overview on energy consumption characteristics can be immediately provided, e.g. power averages and overall energy demands on a daily, weekly and annual basis. Figure 4 shows an example of a weekly demand profile.

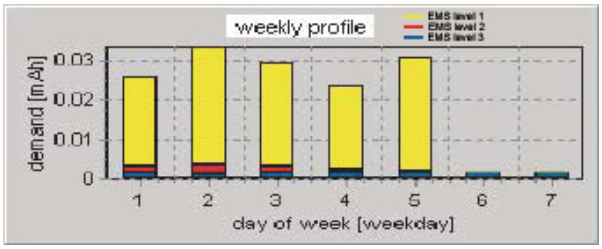

Figure 4: *Screenshot of a weekly device use profile; the energy demand is split into the three different EMS levels*

Device usage can also be linked to irradiation conditions, by defining a linear de-rating factor to account for possible shadowing during device usage.

3.2 Irradiation profile editor

In the irradiation profile editor a so-called 'background' daylight factor (DF) is used to de-rate outdoor irradiation datasets, that are provided within the tool. Typical DFs in indoor environments can be anywhere in the range of 0% (for the case of a room without windows) up to the transmission factor through windowpanes of between 30 and 90% (for the cases at, or very close to the windowsill). However, applying a linear de-rating factor is over-simplifying indoor irradiation conditions. This approach is nevertheless assumed to suffice, as PV performance at low light levels is one of the most important parameters influencing system efficiency.

The final irradiation profile used in the simulations is based on the defined background DF, but can also be adapted on a minutely basis. Arbitrary DFs can be set on user defined timeframes to set up a weekly irradiation profile. Thereby the simulation of 'sun-bathing' PV powered consumer systems is possible, e.g. during lunch breaks or during the weekend. The smaller DFs become, the more important such 'sun-bathing' at e.g. the windowsill is for ensuring that PV energy yields are at reasonable high levels. For example, assuming 1000 kWh/(m^2a) as the outdoor annual irradiation sum, a constant DF of 10% yields a very easy to calculate annual irradiation sum of 87.6 kWh/m^2a. Additional sun-bathing of one hour at noon at a DF of 60% yields over three times as much irradiation, namely between 270-295 kWh/(m^2a), dependent on the geographical location and the related irradiation distribution with respect to timeframes of sunbathing (to calculate the effect, sun bathing each day between 11:30 and 12:30 o'clock at 35 different

measurement locations in the Netherlands was assumed).

4 SIMULATION EXAMPLE

The ***i*PV-Sim** tool was used within the design process of a solar powered mouse (SPM) prototype to estimate the energetic performance of such a device, as also presented at this conference [9].

Energy demands of commercial mouse products found in market research varied with a factor four to five, as shown in Table 1.

EMS-Mode (1-active, 2-sleep, 3-deep sleep state)	*1*	*2*	*3*
Type of mouse	*Power Demand [mW]*		
Wireless optical 1	*7.0*	*0.57*	*0.09*
Wireless optical 2	*36.8*	*2.11*	*0.47*
Wired optical	*500*	*n/a*	*n/a*

Table 1: *Power ratings of two state of the art wireless computer mice [10] and wired mouse data for comparison.*

As in most other A-Brands, three energy management system (EMS) levels are used to minimize energy consumption in the selected mouse product. Device energy demand ranges are calculated based on expected device use times for 4, 18 and 27 hours mouse motion per week [10] accounting for light, medium and heavy device usage, respectively.

To compare energy balances of a mouse for the different device use times, figure 5 shows the battery SOC as a function of time for the three cases. Simulation results are based on a constant DF of 5%, a 28 cm^2 solar cell with efficiency at STC conditions of 6%, a NiMH battery with a capacity of 3000 mAh and a self discharge of 15% per month, and hourly averaged outdoor irradiation data (de Bilt, Netherlands, year 2005).

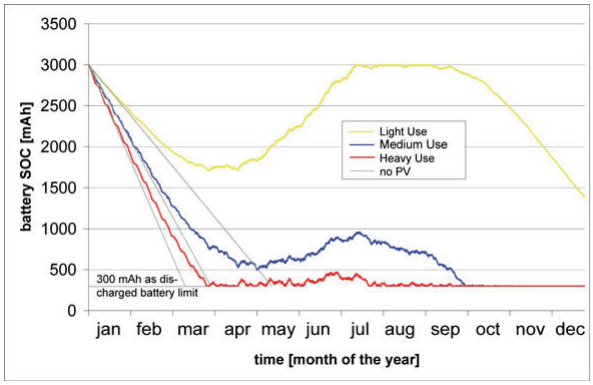

Figure 5: *Battery state of charge over a whole year for light, medium and heavy device use without 'sun-bathing'*

Only for light device use the mouse will operate energetically autonomous, as for the case of a very low DF of 5% and high energy consumption, PV generated charge does not suffice to increase battery SOC during summer. Therefore, the same calculations are redone, now assuming "sun-bathing" of the SPM. Sun-bathing the SPM is assumed to occur each working day between 11:30 and 12:30 o'clock, e.g. during a daily lunch break, and during the whole weekend. Here, a DF of 60% is assumed to account for irradiation conditions at a bright place at the windowsill.

As indicated in figure 6, "sun-bathing" the SPM can result in an autonomously solar powered product, even for heavy device use times of 27 hours a week. For this case, also battery capacity could be much smaller, i.e. a capacity of 1500 mAh, which is only half the capacity of the battery capacity used in the working mouse prototype [9].

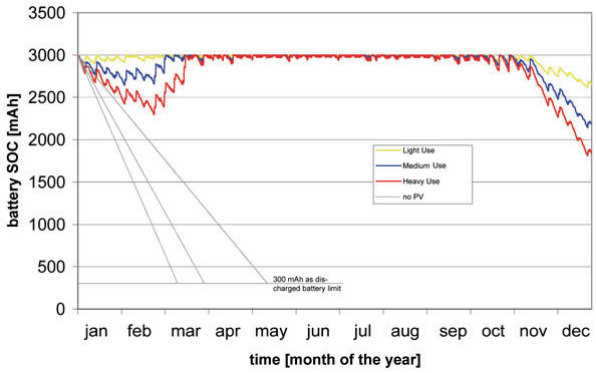

Figure 6: *Battery state of charge over a whole year for light, medium and heavy device use with 'sun-bathing'*

5 DISCUSSION

Although ***i*PV-Sim** enables a fast and easy simulation of system energy streams in PV powered consumer systems, it cannot reduce the uncertainty regarding available irradiation and device use patterns. For example, the battery SOC as a function of time shown in the simulation example of the previous section is based on a DF of 5%, but the PV powered wireless computer mouse in theory can be used in any light condition and usage environment for work with a computer. The average background daylight factor of five percent might be too pessimistic, and 'sun-bathing' the solar powered mouse for one hour each day might be too optimistic, or vice versa, or even completely different. Nevertheless, the tool enables to visualize this uncertainty by means of calculating specific scenarios covering the possible device use circumstances. By doing so, for instance dimensioning of battery capacity is rather based on carefully considered scenarios then on rough estimates that could lead to products not functioning properly and being even disappointing to the end user. This we regard as an important issue to overcome for PV powered products, especially because of the educational role such products might have for the attitude of people towards photovoltaics in general.

Scenarios also allow comparisons of products that are PV powered with those that are not. Figure 7 shows such a comparison for again the case of a PV powered wireless computer mouse. The scenario of a product without PV is based on a battery unit containing two primary batteries of 2500 mAh capacity. The scenarios of a product with implemented PV are based on parameters as outlined in section 4, with the only parameters differing: a DF of 10%, a battery capacity of 5000 Ah (and a start value of 2750 mAh) as well as an additional scenario for a reduced overall battery capacity of 1500 mAh (2 batteries of 750 mAh), respectively. To keep the graph simple, only results for heavy device usage equal to 27 hours a week are shown.

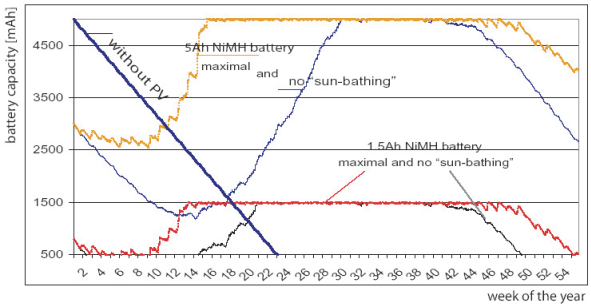

Figure 7: *Battery state of charge over a whole year for light, medium and heavy device use with and without 'sun-bathing'*

The device that is *not* PV powered obviously needs battery replacement on a regular basis; in the example given replacement is needed every 3 months. For the PV powered device, simulated battery SOC as a function of time suggests a battery capacity of between 2500 mAh (sun-bathing) and 3300 mAh (no sun-bathing) for the case of a constant DF of 10%. However, because so many parameters are uncertain, battery capacity should be as high as possible in order to take advantage of a possibly seasonal energy buffering that could grant an energetically autonomous device operation. On the other hand, environmental concerns are satisfied much more by a battery capacity as small as possible, as discussed in detail in the paper on the PV powered mouse prototype [9]. This trade off might very well illustrate the principle problem of system component dimensioning for PV powered consumer systems, namely, that it is complex to satisfy all wishes and demands of the many details that are to be taken into account.

6 CONCLUSION

The presented computer simulation tool ***i*PV-Sim** enables product designers and industrial design engineers to evaluate designs of indoor PV devices in more detail compared to conventional dimensioning methods, and still in a simple way. An annual time step simulation using a step size of one minute can be performed to evaluate a broad range of possible consumer systems equipped with PV.

Device power specifications can be split in up to three energy management levels, which can be used to map the large variety of existent energy management systems in state of the art electronic devices. Device use times and specific light profiles can be designed such that low, medium, and heavy users can be distinguished.

Solar cells are modelled using the one or the two-diode model of solar cells with user-adaptable parameter sets. Predefined solar cell characteristics extracted from a study on commercially available solar cell performances and spectral responses are made available within the program.

An irradiation editor allows for the simulation of a constant background DF as well as user-adaptable DFs within arbitrary timeframes to be able to include 'sun-bathing' PV powered products. Although in principle any irradiation intensity profile can be entered by the simulation tool user, the tool still needs further development to account for more realistic indoor irradiation patterns, i.e. allowing the user to select wavelength dependent absorption characteristics of window panes to easily account for indoor solar irradiation spectra. Finally, artificial light sources and associated spectra of emitted light need to be implemented. However, as the simulation environment has proven to work fast and reliable, the implementation of these details as well as other new detailed features desired by the users of this tool will be rather simple.

A free download of the current version of this computer tool is made available at the internet website at http://www.nils-reich.de.

ACKNOWLEDGEMENT

This work is part of the SYN-Energy project, which is financially supported by the NWO/SenterNovem Energy Research programme.

REFERENCES

[1] H. Schmidthuber: "Verkapselung von kristallinen Silizium-Solarzellen", Dissertation, FernUniversitaet – Gesamthochschlule Hagen, 2003
[2] RWE Schott Solar / Cherry Keyboard http://www.cherry.com, 2005
[3] M.A. Green, "Solar Cells", Prentice Hall, 1982.
[4] A.H.M.E. Reinders, V.A.P. van Dijk, E. Wiemken, W.C. Turkenburg, "Technical and Economic Analysis of Grid-connected PV Systems by Means of Simulation", Progress in Photovoltaics: research and applications 7 (1999) 71.
[5] L. Castaner, S. Silvestre, "Modelling PV systems using PSPICE", Wiley & Sons, 2002.
[6] F. Lasnier, T.G. Ang, "Photovoltaic Engineering Handbook", Adam Hilger, 1990.
[7] L. Stamenic, E. Smiley, K. Karim, "Low light conditions modelling for building integrated photovoltaic (BiPV) systems", Solar Energy 77 (2004) 37.
[8] N.H.Reich *et al.*, "Weak light performance and spectral response of different solar cell types", Proceedings 20th European Photovoltaic Solar Energy Conference (2005).
[9] N.H.Reich *et al.*, "Industrial Design of a PV powered consumer application: Case study of a solar powered wireless computer mouse", this conference (2006).
[10] Percept Technology Labs, Boulder Colorado, 2004.

INDUSTRIAL DESIGN OF A PV POWERED CONSUMER APPLICATION: CASE STUDY OF A SOLAR POWERED WIRELESS COMPUTER MOUSE

N.H. Reich[1], M. Veefkind[2], E.A. Alsema[1], B. Elzen[3], W.G.J.H.M. van Sark[1]

[1]Dept. Science, Technology and Society, Copernicus Institute, Utrecht University, Heidelberglaan 2, 3584 CS Utrecht, the Netherlands, T: +31 30 253 7637, F: +31 30 253 7601, E: N.H.Reich@chem.uu.nl

[2]Industrial Design Engineering, Delft University of Technology, Landbergstraat 15 2628 CE Delft, the Netherlands, T: +31 15 2783795, E-mail: M.J.Veefkind@io.tudelft.nl

[3]Dept. Science, Technology and Society, University of Twente, P.O.Box 217, 7500 AE Enschede Tel: (+31) 53-489.4221; Fax: (+31) 53-489.4734, E-mail: B.Elzen@utwente.nl

ABSTRACT: A prototype of a PV powered wireless computer mouse has been built. Both, an optimized technical implementation and requirements to achieve a good design are investigated. The main design criteria are an appropriate selection of integrated PV cell type, battery capacity and battery type as well as PV-battery coupling. Material criteria and mechanical incorporation of PV into the products encasing is investigated as well as light trapping issues to minimize reflection at the product surfaces. Appealing design aesthetics with respect to good sun harvesting properties are addressed by user research, as to stimulate the user to optimize catching light is found to have high influence on the energy balance. Life cycle aspects of the product are evaluated with regard to potential energy savings, showing that standard energy payback time calculations can hardly assess the environmental impact of PV implemented into consumer systems. Finally, a possible economic feasibility is estimated; PV powered consumer applications are identified as a very interesting niche market with possible high profits, with a solar powered wireless computer mouse as just one of many possible PV powered consumer products.
Keywords: Stand-alone PV Systems; Battery Storage and Control; Consumer Product

1 INTRODUCTION

The research objective of the SYN-Energy project is to improve the basic understanding of solar-powered electrical devices. In this paper, the implementation of solar cells into a wireless computer mouse is investigated as case study for this type of products. An introduction to the SynEnergy project, including the selection method leading to a wireless computer mouse as a prototype, was published earlier [1]. However, the selection of a solar powered mouse (SPM) as a product still often leads to discussions, whether or not a SPM is a good product for device integrated PV. A *"complete energy supply by integrated PV"* is argued to be inevitable for such products. Due to variations of device use patterns and ambient light conditions, the energy balance is very uncertain indeed, as we will show.

Achieving a positive energy balance is one of the most critical issues for an SPM. The integration of solar cells into the mouse surface in an aesthetically pleasing and energetically acceptable way is another challenge. The design of an SPM is in our view a good example to gain experience with, because it is a complex process to develop such a solar powered product. In this paper we will present technical engineering solutions in combination with correlated industrial design processes. This also comprises research and analysis of user requirements. This integrated approach may contribute to improve the product design of PV powered devices, which might help to open up further markets for solar cell applications.

2 DEVICE CRITERIA

It proved difficult to define specific device criteria; in a first approach scattered, non-uniform lists of wishes and demands for the many possible details to be implemented in the SPM resulted. Therefore a first analysis phase ("quick scan") was used to define a "*program of wishes and demands*" for further design. This phase includes market research (existing products, market segmentation, and corridor of price), exploratory user research (observational research, interviews, and focus groups), and rough energy balance calculations.

2.1 Preliminary energy balances

For manufacturing the SPM prototype a commercial available wireless mouse, yet without integrated PV, was selected to function as the prototype base. Energy demands of commercial mouse products found in market research varied with a factor four to five. The selected product, indicated in table 1 as 'Wireless optical 1', is sold by Microsoft (MS) under the product name 'Intellimouse' and proved to have the lowest energy demand of all tested products.

EMS-Mode (1-active, 2-sleep, 3-deep sleep state)	*1*	*2*	*3*
Type of mouse	*Power Demand [mW]*		
Wireless optical 1	*7.0*	*0.57*	*0.09*
Wireless optical 2	*36.8*	*2.11*	*0.47*
Wired optical	*500*	*n/a*	*n/a*

Table 1: *Power ratings of two state of the art wireless computer mice [2] and wired mouse data for comparison.*

As in most other A-Brands, three energy management system (EMS) levels are used to minimize energy consumption in the selected mouse product, by e.g. adapting LED light intensity dependent on the specific underlay material, or turning the LED off if the device is not used. An implemented DC/DC converter increases battery runtime, with the device still functioning at (primary) battery voltages down to 0.6 Volt. Interestingly, this product is not equipped with a simple 'on/off'-switch, as correlated potential energy savings are supposed to be marginal. Device energy demand ranges are calculated based on expected device use times between 4 and 27 hours mouse motion per week [2].

PV generated charge depends on several parameters. Therefore we developed a computer tool to simulate PV powered consumer systems [3]. Light intensity dependent cell efficiency is thereby considered, as irradiation intensity has a high impact on expectable PV energy yields [4]. An assumed constant daylight factor (DF), defined as the ratio of irradiation indoors compared to outdoors, is used to account for indoor irradiation levels. Other parameters of interest, such as battery charge efficiency, battery self-discharge, and efficiency of the used electronic circuitry were also considered by applying constant de-rating factors.

Several simulations with different system configurations, cell efficiencies and device use patterns have been performed. To compare a mouse device with and without integrated PV,

figure 1 shows battery state of charge (SOC) over a whole year for the two cases and three usage scenarios. Simulation results are based on a constant DF of 5%, a 28 cm^2 solar cell with efficiency at STC conditions of 10%, a NiMH battery with a capacity of 3 Ah and a self discharge of 15% a month, the range of expected device use of 4 (light use), 18 (medium use) and 27 (heavy use) hours a week, and finally hourly averaged outdoor irradiation data (de Bilt, Netherlands, year 2005).

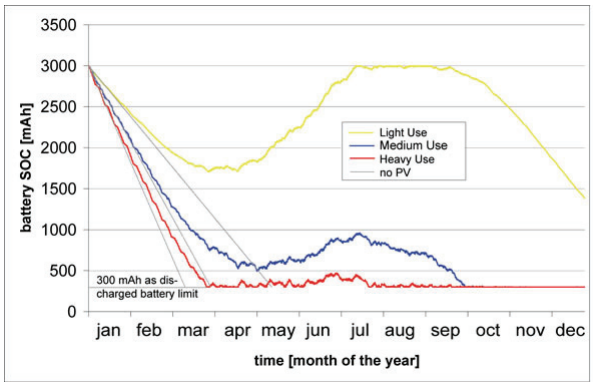

Figure 1: *Battery state of charge over a whole year for light, medium and heavy device use with and without integrated PV*

For the SPM, thus a mouse with integrated PV, battery runtimes is obviously increased. The calculated battery SOC clearly reflects higher irradiation intensities during the summer period. With the assumed medium and heavy use patterns, however, PV generated charge does not suffice to increase battery SOC during summer. Therefore, the same calculations are redone, now assuming "sun-bathing" of the SPM. Sun-bathing the SPM is assumed to occur each working day between 11:30 and 12:30 o'clock, e.g. during a daily lunch break, and during the weekends. Here, a DF of 60% is assumed to account for irradiation conditions at a bright place at the windowsill.

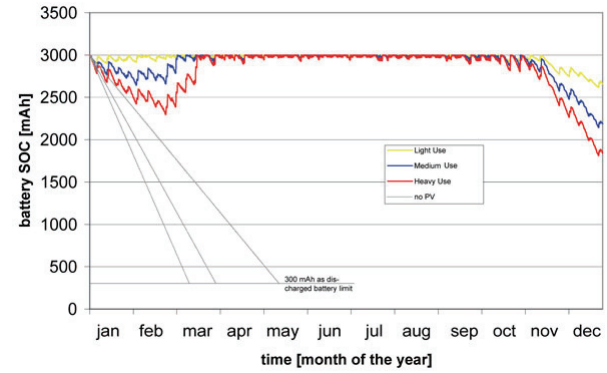

Figure 2: *Battery state of charge over a whole year for three use classes with daily sun-bathing the SPM*

As indicated in figure 2, "sun-bathing" the SPM can result in an autonomously solar powered product, even for heavy device use times of 27 hours a week.

2.2 Design analysis

The analysis first part ("quick scan") and especially the energy balance calculations clarified that the development of the wireless pointing device can take three directions:

1. The development of a "worry free" SPM for "light use"
2. The development of a SPM for "heavier use" that requires special care of the user
3. The development of a SPM that has a larger surface area than traditional mice

Ad. 1. This track leads to a SPM that is expected to be energetically auto-sufficient without need for special care.

Ad 2. This track leads to a SPM that is designed to be "sun-bathed" once a while; taking advantage of higher daylight factors and direct light if placed at the windowsill.

Ad 3. Logically, this product should be "worry free" since "sun-bathing" a larger product would be inconvenient. Most probable this leads to a flat mouse pad kind of product.

In an early stage the project team decided to continue with direction two, for two reasons. Firstly, it is technically and economically the most feasible option. Secondly, the concept of a product that needs to be sunbathed is interesting from a user interaction viewpoint. A design that enables the adoption of such a behavioral change might even open up a new category of PV-powered consumer products.

2.3 Design criteria

Following the design analysis for a SPM that requires special care of the user, we identified a "*program of wishes and demands*":

- The SPM must be designed as if it was to be produced in a commercial setting. Its design should allow for mass production and meets the current corridor of price for wireless mouse devices (30-70 Euro), as well as environmental standards (RoHS).
- When fully charged, the SPM must allow an average user (2.5 hrs. of active use daily) to work five days without irradiation.
- The SPM's design must indicate the user that sun-bathing is required, especially before the battery runs out. It is desired that the design stimulates to sunbath the SPM pro-actively.
- The users must perceive the SPM as a quality product, in contrast to a large fraction of the PV powered products that are in the market and have a gadget character.

A so-called focus group research, in which potential users have been interviewed, allows a closer interpretation of the last criterion. The SPM's perceived quality depends highly on the integration of the PV-cell in its encasing. Figure 3a/b/c shows three of the several possible designs used in the focus group.

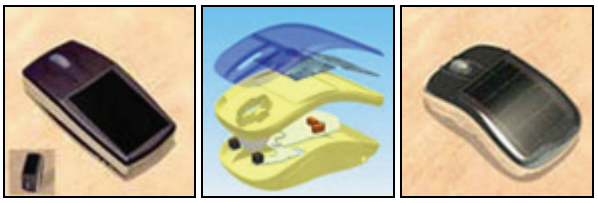

Figure 3a/b/c: *Integration of different PV cell types using different encasing shapes and cell technologies, with (a) flat panel integration as part of outer encasing; (b) crystalline series connected cell integration; (c) bent a-Si:H on foil cells.*

According to the respondents, the PV-cell must follow the encasing's shape. PV-cells that do not do so, are perceived as vulnerable and less reliable. This is particularly critical since the same focus group research points out that ergonomics is the user's most important criterion, while organic, rounded shapes are perceived as most ergonomic. It also shows that rectangular mice are no option.

3 COMPONENT SELECTIONS AND SYSTEM DESIGN

With the acquired list of wishes and demands, several system components are dimensioned and distinct system setup decisions made. These issues can be mainly summarized as PV cell type, battery type and their electronic coupling.

3.1 Battery / Storage

To select an appropriate battery type, the team evaluated different battery types based on available handbooks. A relationship matrix is used to evaluate commonly used

battery parameters [5-8]; Chemistry, energy density [Wh/kg] and [Wh/cm^3], cycle life, charging time, overcharge tolerance, self-discharge, cell voltage, maximum discharge rate (max. load current), operation temperature, maintenance requirement, price, efficiency, cycle depth characteristics, available capacities, discharge profile and calendar life. The evaluated battery types are: Nickel-Cadmium (NiCd), Nickel Metal Hydride (NiMH), Lithium Ion (Li-Ion), Sealed Lead Acid (SLA) and Rechargeable Alkaline Manganese (RAM). For further assessment, a relationship matrix with the following five categories has been used:

- Costs (battery and required electronics)
- Efficiency
- Design freedom
- Durability
- Environmental issues

Within this relationship matrix, NiMH is the only battery type that does not have a bad score in any of the categories. Li-Ion is a very good candidate except for its costs and temperature dependent aging (durability). Although prices for Li-Ion batteries show a decreasing trend, they are not yet considered as a feasible option. Other battery types show such shortcomings in one or more categories that they are not further considered.

Although the overall performance of the NiMH battery is not bad in any category, it requires additional electronics to protect against overcharge and over-discharge. Due to the flat discharge profile, it is difficult to estimate the load condition. A further disadvantage is the high self-discharge rate (15-25% per month), which lowers the SPM's system efficiency and makes it difficult to sell a NiMH equipped SPM in (partly) charged condition. The NiMH battery is available in different shapes and capacities, and voltages are multiples of 1,2V. Therefore the choice for NiMH allows a lot of freedom if it comes to the rest of the system.

3.2 PV technology

The selected PV cell type should be feasible from both energetic and economic viewpoints. For an economical evaluation, two different PV technologies can be identified, namely thin film technology providing encased modules, and crystalline cells with the need for further module assembling. Module assembling is considered to have a strong negative impact on costs, as a round design rather than a rectangular module shape was defined as obligatory in the program of wishes and demands. Crystalline solar cells, however, offer much better efficiencies than most commercial available thin film technologies. For example, amorphous silicon cells (a-Si:H) show efficiencies determined standard testing conditions (STC) around 7% maximum, compared to a 13-17% range STC efficiencies of commercially produced crystalline cells, with cells up to 20% STC efficiency commercially available at relatively low costs. Solar cell efficiency, however, decreases towards lower irradiance, and as the SPM will be used in indoor environments, this effect should be taken into account. We have reported earlier that some a-Si:H cells even perform better than specific crystalline solar cells at light intensities below 10 W/m^2 [3,4].

Other PV technology investigated was found not to match the demands of the SPM. Thin film cells on foils have the advantage to be bendable and thereby allow higher freedom in solar cell integration into the products encasing, but show a bad energetic performance. Other thin film technologies show rather high efficiencies at higher light intensities, such as Cu(In,Ga)Se$_2$ (CIGS) and CuInS (CIS) cells, but bad weak light performance. For example, measured CIS cell efficiency rapidly decreases towards weaker light intensities with efficiencies below 1% for irradiation below 10W/m^2 [4]. However, it was shown that bad weak light performance of these solar cells can be overcome by additional process steps in cell manufacturing for CIGS cells [9]. If CIS and / or CIGS cells can proof to have high cell efficiencies also at weaker light intensities, both technologies are good options for device integrated PV.

3.3 Charge Controller and micro controller features

The charge controllers' basic function is to protect the used battery from overcharge and deep discharge. The actual control strategy very much depends on the specific battery setup and type. Although specific voltage ranges, voltage thresholds, battery trickle charge currents and time constants vary dependent on battery type, battery capacity and nominal battery voltage, the working principle is more or less the same. A micro controller is used to measure battery voltage and possibly battery currents to control battery (dis -) charging by switching one or more field effect transistors.

With a micro controller (µC) implemented into the charge controller, additional features can be realized:

- Battery status indication
- Data logging capabilities
- PV maximum power point tracking (MPPT)

Whilst the battery status indication is defined to be obligatory in the program of wishes and demands, data logging capabilities have been excluded to keep charge controller electronics simple. A battery status indication was realized based on measured battery voltage, indicating a full and an almost empty battery state of charge.

The operating voltage of the selected µC is 2 V minimum, which turned out to complicate the implementation of the µC into the selected product. The MS mouse electronics operate at voltages well above 2 V, but due to the implemented DC/DC converter this voltage is not directly available. Several solutions for a µC power supply have been identified, including a separate power supply or charge pump. A battery configuration above 2 V is possible as well, because power demand of the MS mouse was found not to increase towards higher battery voltages of 2 to 2.6 Volts. With higher voltages, power demands of the µC increases slightly, but nevertheless remain at an acceptable low value of 0.13 mW for the simplest mode and 0.45 mW for an implemented MPPT calculation feature.

3.4 Maximum power point tracking

Whether or not MPPT makes sense very much depends on the gained energetic benefit. To calculate this possible benefit, increased power demand of the µC as well as DC/DC transformation efficiency has to be considered and compared to the increased operation performance of PV. MPPT efficiency usually is around 90% and better, e.g. [10], but with an own consumption of needed electronics in the Watt power range. For the SPM, high MPPT efficiency depends on a low own consumption of the micro controller (µC), which is due to the very low power transmissions.

The chosen µC [11] has a minimal operating voltage of 2 Volts and a current drain of 50 µA in its most simple configuration. Power demand of the µC, however, varies dependent on what functions it performs. An additional 125 µA is needed for enabling integrated A/D converters needed for MPPT, as the delivered PV power (PV current and voltage) must be measured in order to determine the maximum power point voltage. Furthermore, for measuring the PV current, a voltage drop at a needed shunt resistance of up to 60-100 mV occurs. With the own consumption of the µC of 0.5 mW, an irradiation of 3 W/m^2 can be calculated to power the µC's MPPT feature. As the SPM is supposed to be operated under higher irradiation intensities than 3 W/m^2 to provide solar powered operation, and also might be sunbathed once a while, we expect the potential benefit of an MPPT feature to be positive, however, with high uncertainty remaining.

3.5 Incorporation of the PV cell; the optics of the encasing

The PV-cell is a relatively large part of the SPM and it

needs to be mounted in such a way that it receives as much light as possible. Basically four ways of incorporating the PV-cell exist:

- Placement in the encasing, under a transparent cover
- Placement directly against a transparent cover
- Placement outside or as a part of the encasing
- Placement at the edge of a light collector

All alternatives include one or more interfaces between media, so that additional reflection occurs. In order to tackle this problem, we developed a first order simulation model based on Fresnel's equations. It allows a fast understanding of reflection effects without the need of introducing the product's exact geometry. For the direct light component, solar elevation determines the incident angle. Figure 4 shows an example of angle dependent light transmission through to the incorporated PV cell, placed under a transparent cover.

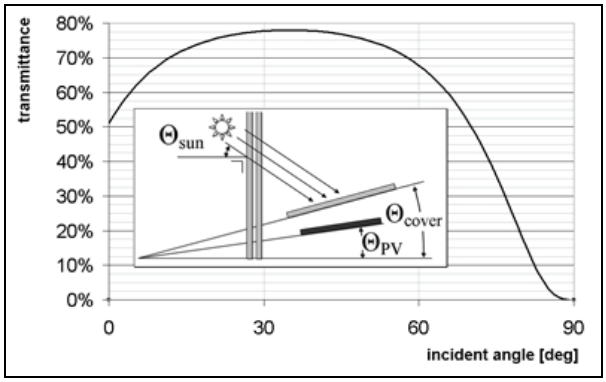

Figure 4: *Transmission as a function of incident angle*

Light originating from indoors sources, lamps or reflecting objects can also be assumed to arrive at the product's cover. Only direct lamp light, however, is considered to cause enough irradiation to allow PV-charge generation. In the case of a horizontally mounted PV-cell in combination with an also horizontally placed transparent cover, losses due to reflections of indoor lighting are about 10-15%. Reflection losses for sun-bathing are much higher: 20-25% at 45 degrees incident angle, than almost linearly increasing to 100% for low solar elevations due to total reflection.

Therefore, "sun-bathing" will be little effective in winter months, if nothing is being done in order to avoid reflection on the SPM's cover at low solar elevations. A relatively small tilt of 15 degrees already results in a large improvement. Higher tilts, however, were found to reduce the SPM's performance for light from indoor origin. Second best options are a tilted cover only, filling the space between the cover and the cell, and finally a wedge-shaped cover. Coatings and the use of low refraction index material provide little improvement.

3.6 Environmental considerations

Beside design issues also environmental aspects need attention. One might expect an additional "green" benefit from this kind of product in comparison with standard battery-operated mice. An obvious advantage would be, if some energy savings can be realized with the SPM.

One has to realize, however, that typical irradiation levels for the SPM will be far lower than for outdoor PV systems. For roof-top, grid-connected (outdoor) PV systems, the Energy Pay-Back Time (EPBT) of solar cells is in the range between one and four years, depending on technology and location [12]. If we assume an average daylight factor (DF) of 10% this would result in EPBT of solar cells a factor ten higher; an energetically amortization of integrated PV cells would occur after ten to forty years. It is obvious that consumer devices have much shorter life. Therefore, solar cells implemented into the SPM will most probably not deliver as much energy as was needed to produce them.

Standard wireless computer mice, however, are not powered with grid electricity, but usually by primary (i.e. non-rechargeable) batteries. Primary batteries are very energy-intensive to be produced. Although literature and transparent calculations on this issue are very scarce, primary battery efficiency - defined as electricity output related to primary energy input - is reported to be as low as two and three percent [13]. This means "displaced" electricity supply is much less efficient than for grid-connected PV systems. With such data, the energy balance of a solar mouse becomes much more positive and EPBT between half a year and one and a half years may be realized, depending on the type of solar cells (Fig. 5).

In the case of secondary batteries, also charger standby losses carefully have to be considered. Charger standby losses are in the order of 0.5 – 1 W [14] for efficient chargers. If the charger is only connected to the grid while actually recharging the secondary batteries, standby losses will be rather marginal. In reality, however, re-chargers often tend to be continuously connected to the mains (e.g. by a separate mouse recharging or docking station belonging to the product). Charger losses of 4 - 9 kWh a year can then easily result (see figure 5, "worst case charger losses"). It will take a very short time only, until more energy is wasted by the re-charger losses, than would be needed to produce solar cells powering a SPM. Depending on amounts of time associated to charger standby losses, impressively low relative EPBT of less than one hour result (Fig. 5).

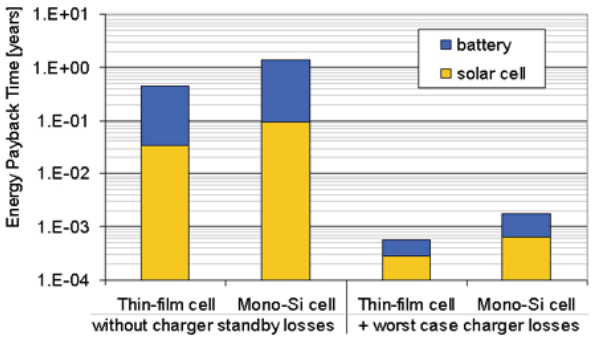

Figure 5: *Relative energy payback times for solar cells in a SPM resulting from a comparison to a system without PV with maximum possible and without charger standby losses*

This example shows that standard EPBT calculations for solar cells are difficult to apply on PV powered consumer systems. The many possible system setups complicate calculations on possible environmental benefits, as it is difficult to define a base case scenario. An additional environmental benefit is caused by less battery wastage for solar powered compared to standard powered products. This benefit, however, is difficult to quantify.

3.7 Economic feasibility

In a commercial setting, the SPM's solar design might have an added economic value because of two reasons: at first a "*green image*", but also possible lower operation costs. Whilst the "green image" can be related to end consumers, lower operation costs will be of interest for purchasers, e.g. trading IT products for big companies. Such target groups can rather be convinced by monetary terms, e.g. if it can be shown that a SPM will enable considerably lower battery demand.

To calculate the possible economic benefit related to less battery costs over the product lifecycle, we assume primary battery costs to equal 1€ for one standard AA battery, based on the Energizer E91 Alkaline battery product (1.5 V, 2.85Ah, 3.5Wh energy capacity). Depending on device use times between 4 and 27 hours a week, an overall primary battery demand between 2 and 53 batteries, respectively, over an assumed four years product lifecycle result. The large range in primary battery consumption and associated cost is

due to variations in device power demands of the different products (see Table 1) and device use time ranges.

For PV costs, the implemented solar cell area of 28 cm^2 outlines 0.28 Wp and 0.56 Wp for a module with 10% and 20% efficiency, respectively. Cost calculations for very high efficiency solar cells designed for consumer systems result in module costs in the range of 80 to 140 €/W_p [15]; high efficient solar cells constitute about 50% of the consumer product cost. For industrial produced silicon cells, having a moderate efficiency, costs in the range of 2-5€/Wp for the cells and "mini-module" costs around 10-30€/Wp are found. Assuming a moderate 15% cell efficiency and 0.4 Wp integrated PV, costs between 4 and 12 € for the solar cells result. Although a detailed economic analysis is beyond the scope of the current project, this first order estimation shows additional costs for manufacturing an SPM in the range of 4 to 12€ for the PV cell and 5 to 10€ for additional electronics. This rough comparison on costs thus identifies an economic saving potential in the range of 2-53€ per product over its lifetime, with initially increased costs of 9-22€.

4 DECISION DEPENDENCIES

In the previous sections the different design issues and technical aspects are described independently. Dependencies, however, exist between

- the storage and the module set-up (battery voltage must match the module's working voltage);
- the module set-up and PV-technology (multiple cell modules require interconnection of cells);
- the PV-technology and its incorporation into the SPM (since the encasing must be curved, the use of a rigid cell excludes placement directly against a transparent cover)

One way to represent the mutual dependencies of design areas is the composition of a graph of different areas and their relations. In Figure 6, arrows represent the mutual dependency of the different design areas. Two networks can be distinguished, with both the electro technical configuration and the mechanical incorporation determined by the module setup and its geometry.

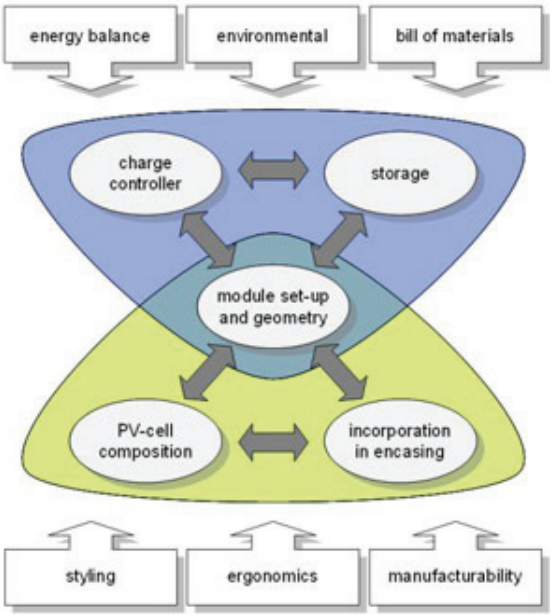

Figure 6: *Coupling of design areas*

Decisions in the 'technical' network depend on criteria that concern energy balances, environmental issues and bill of materials. The combination of storage and a module set-up determines whether a DC/DC converter is required. Therefore, not all combinations that only include a diode to couple module and storage are possible. Other options, which are most logically thought in combination with DC/DC conversion and MPPT, include battery protection and battery charge indication. The 'design' network mainly concerns the SPM's encasing design. This is due to the fact that the PV-cell's surface area is a large fraction of the SPM's total surface. Decisions depend on criteria that concern styling, ergonomics and manufacturability. Similar to the 'technical' network, decisions on each of the design areas limit the possibilities in the other network, with PV technology selection and cell composition influencing all sections.

5 FINAL CONCEPT

For incorporation of the PV cell and electronics, the inner space of the mouse encasing has been designed to incorporate a flat, rigid PV module, as shown in figure 7a/b.
In order to improve the "perceived ergonomics" the final concept is dominated by curved lines and double curved surfaces. Straight lines and flat surfaces are avoided as much as possible. Figure 8a/b shows the front and the top-side view of the SPM's final design, yet without implemented PV cells.
The final concept of the SPM includes one single PV-cell, with a curved outline. This way the PV-cell fits well with the SPM's curved encasing and maximizes the PV-cells surface area. Since PV-cells with this shape are not available, this must be a dedicated part. Cutting of cells is the only way to manufacture not rectangular or circular wafer based cells, with the parts cut off most likely being discarded. The single cell module is preferred over the dedicated multiple cell module, since its production requires less initial cost.

One should keep in mind that, for optimal conversion, individual cells connected in series must have an equal surface area, which complicates production. For the prototype, the team decided for a Schott Solar a-Si:H cell, as laminating a module using crystalline cells would have needed more research, planning and time. The mechanical set-up, however, in principle can work with both a mono-crystalline cell as well as thin film modules. For the sake of higher energy yields, a single crystalline cell performing well under weak light conditions, battery- coupled using an adequate voltage converter, should be used.

The evaluation of different battery chemistries pointed out that both Li-ion and NiMH are suitable for the SPM. Li-ion batteries are more efficient and are expected to have a better performance at shallow discharging in combination with float charging, slow- or trickle charging. NiMH has the advantages of a lower price, better resistance against high operation temperatures and a lower voltage.

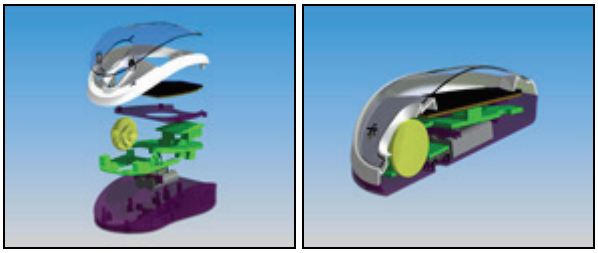

Figure 7a/b: *Final design of the SPM – detailed assembling of the individual components*

Figure 8a/b: *Final design of the SPM – front and side views*

Additionally, it is easier for consumers to replace NiMH batteries as they are easily available at almost any place where batteries are sold. At the end the team opted for two AAA 750 mAh NiMH batteries connected in series, especially because of fear that Li-ion gets deteriorated due to high temperatures (sunbathing) and cannot easily be replaced by the end user. The two batteries are connected in series, in order to have enough voltage to power the charge controller without any need for additional electronic circuits.

The selection of a single cell module set-up implies the use of a DC/DC converter. A boost converter transforms the voltage in order to charge the batteries. The implemented microprocessor executes a routine every minute, which sets the PV-cells voltage close to its maximum power point. Thereby losses at the shunt resistance to measure PV power output are minimized. Moreover, the micro controller enables a battery status indicator, and protects the battery against overcharging and deep discharge.

The placement of the solar cell behind a double curved transparent plastic cover causes losses due to reflection. These losses become very high for irradiation at low solar angles. However, the cover and module's tilt angles result from a trade-off between the SPM's ergonomics and the required space for electronics, batteries and mechanics. In the final concept the module is tilted 10 degrees. In this way a relatively large cell can be incorporated without sacrificing to much internal space, while improving the SPM's performance under low solar angle conditions. To enable sunbathing, a simple support structure enables to vertically position the mouse at e.g. a windowsill (see Figure 9a/b).

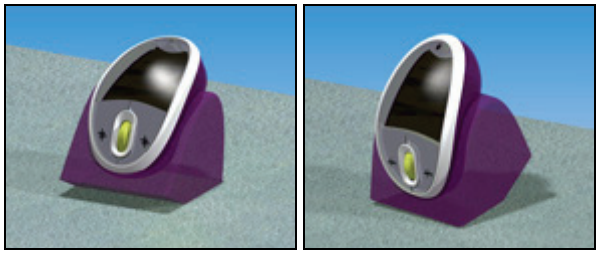

Figure 9a/b: *Support for vertically placing the SPM at a windowsill*

6 Conclusion

The design process led to a final concept for the SPM, as well as a working prototype. Like all new products, however, the SPM prototype involves a number of imponderables. As a result of this, it is yet unclear which design decisions are better than others. The knowledge base used did *not* allow the identification of an *optimal* technical set-up. In other words, it did not allow the SPM to be designed "first time right." For the full understanding of the SPM along with possible improvements and better system configuration options, further research is required. This includes, amongst other things, user research with working prototypes, as some of the imponderables are due to the yet unknown user behavior.

Even if assuming certain user behavior and light conditions, however, it is not possible to indisputably determine a technically optimized design. An important doubt that rose during the design process is whether or not a DC/DC-converter featuring MPPT is energetically beneficial. It is still unclear, in how far the extra earnings due to MPPT warrant the required electronic circuits and their energy consumption. Further research, including experiments and light intensity measurements under 'real-world' product environments are needed in order to optimize decision-making on this issue.

Another technical issue with need for further investigations is the encasing's optical properties. Although two-dimensional simulations provide a basic insight, this approach does not allow sufficient information for optimization of double curved transparent covers. Ray-tracing, which is a common technology in the 3D-CAD software used to design the SPM's encasing, allows such simulation. Within the 3D-CAD environment, however, ray-tracing is used to *create* the images (rendering) and *not* to create quantitative data on surface's irradiation.

Finally, user research has convinced the SYN-Energy team that users willing to sunbath their product exist. However, exact user behavior is still unknown. In combination with the variety of possible light conditions, thereby the simulation of the SPM's energy balances is hampered. Future user tests with SPM prototypes will help to fill these knowledge gaps. It will then be possible to assess, if specific user behavior like "sun-bathing" of the mouse will be necessarily dependent on device use times, in how far such actions may be elicited by the mouse design, and finally, whether such requirements to the user can be considered acceptable.

ACKNOWLEDGEMENT

This work is part of the SYN-Energy project, which is financially supported by the NWO/SenterNovem Energy Research programme.

REFERENCES

[1] Alsema *et al.*, Proc. 20th European Photovoltaic Solar Energy Conference, Barcelona 2005.

[2] Percept Technology Labs, Boulder Colorado, 2004

[3] Reich *et al.*, this conference

[4] Reich *et al.*, Proc. 20th European Photovoltaic Solar Energy Conference, Barcelona 2005, p.

[5] Buchmann: "Batteries in a portable world", EC & M Books, 1997

[6] Crompton "Battery Reference Book", Butterworth-Heinemann, 2000

[7] Electus distribution catalogue 2001, Soanar Plus Ltd.

[8] Linden & Reddy: "Handbook of Batteries", McGraw-Hill Handbooks, 2002

[9] Virtuani, Proc. 19th European Photovoltaic Solar Energy Conference, Paris 2004.

[10] Santos, Antunes, Solar Energy 80 (2006), 772-778

[11] Microchip Technology Inc.: "PIC16F785 data sheet"

[12] Fthenakis, Alsema, Progress in Photovoltaics 14 (2006) 275-280.

[13] Scholl, Baumann, Muth, INFU, University of Dortmund, 1997

[14] EPA / DOE (U.S.) Climate Protection Partnerships Division, "ENERGY STAR Program", 2006

[15] Schmidhuber, PhD thesis, FernUniversität – Gesamthochschule – in Hagen, 2003

THE FIRST PV-DIESEL HYBRID SYSTEM IN THE MALDIVES INSTALLED AT MANDHOO ISLAND

W.G.J.H.M. van Sark[1], E.H. Lysen[2], D. Cocard[3], P. Beutin[3], G.F. Merlo[3], B. Mohanty[3], J. van den Akker[4], A. Razzak Idris[5], A. Firag[5], A. Waheed[5], A. Shaheed[5], M. Latheef[6], A.Wajeeh[7]

[1]Dept. Science, Technology and Society, Copernicus Institute, Utrecht University, Heidelberglaan 2, 3584 CS Utrecht, the Netherlands, T: +31 30 253 7611, F: +31 30 253 7601, E: w.g.j.h.m.vansark@chem.uu.nl
[2]Utrecht Centre for Energy research (UCE) Heidelberglaan 2, 3584 CS Utrecht, the Netherlands, T: +31 30 253 7614, F: +31 30 253 7601, E: e.h.lysen@chem.uu.nl
[3]French Agency for the Environment and Energy Management (ADEME), 2, square La Fayette, B.P. 90 406, 49004 Angers Cedex 01, France, T: +33 1 47652123, F: +33 1 46383141, E: damien.cocard@ademe.fr; mohanty@vsnl.com
[4]Auroville Renewable Energy (AURORE), Centre for Scientific Research (CSR), Auroville 605101, Tamil Nadu, India, T: +91 413 2622749, F: +91 413 2622057, E: jos@auroville.org.in
[5]Ministry of Environment, Energy and Water (MEEW), Majedhee Magu, Henveyru, Malé, Republic of Maldives, T: +960. 333 1695, F: +960. 333 1694, E: abdulrazzak@meew.gov.mv
[6]State Electric Company Limited (STELCO), Ameenee Magu, Malé, Republic of Maldives, T: +960. 332 0982, F: +960. 332 7036, latheef@stelco.com.mv
[7]Ministry of Transport and Civil Aviation (MTCA), Huravee Building, Ameer Ahmed Magu, 20.05 Malé, Republic of Maldives, T: +960. 332 3993, F: +960. 332 3994, wajeeh@transport.gov.mv

ABSTRACT: A grid-connected PV-diesel hybrid system has been designed and installed at one of the Outer Islands of the Maldives, as part of the SMILES project. Matching of demand and supply was thoroughly examined using the HOMER optimization programme. Data on daily load and efficiency of present diesel generators were collected as well as data on solar irradiation. The system simulations showed that with a daily load of 207 kWh/day the combination of a 12 kWp PV system with a battery backup capacity of 108 kWh would be optimum, given the most convenient strategy for the use of two differently sized diesel generators now present. Future demand growth can be accommodated by only a slight change in diesel generator operating strategy.
Keywords: small grid-connected PV Systems, hybrid, sizing

1 INTRODUCTION

The Republic of the Maldives is comprised of 1192 coral islands in the Indian Ocean, located South-West of India. The combination of the small sizes of the islands and their low height above sea level make the Maldives one of the most vulnerable countries to the projected impacts of climate change: it was the first country to sign the Kyoto protocol. It also suffered considerably from the December 2004 Tsunami. The Maldives depends overwhelmingly on imports of diesel oil for their electricity production, which creates serious economic and financial difficulties, as is typical for small island developing states [1, 2].

The Government of Maldives (GoM) is therefore committed to promote sustainable energy and has been actively pursuing several inter-related initiatives to overcome the existing barriers to the utilization of Renewable Energy Technologies. Examples are the RETDAP project (Renewable Energy Technology Development and Application, funded by the GEF (Global Environment Facility) and UNDP (United Nations Development Programme)) and the SMILES project (Strengthening Maldivian Initiatives for a Long-term Energy Strategy co-funded by the European Commission under the Asia Pro Eco Programme).

The aim of the SMILES project was to assist the Ministry of Communication, Science and Technology (MCST) in strengthening its capacity to enforce sustainable energy development goals through demand side and supply side management strategies. Presently, a ministry reform showing the Maldivian commitment, has led to the creation of the Ministry of Environment, Energy and Water (MEEW). Within SMILES, know-how and expertise have been shared with various Maldivian stakeholders in order to adopt policies and strategies for lowering the rapid growth in fossil fuel demand while ensuring energy access to more remote and less economically advantaged islands. Interaction with national stakeholders will help to increase the efficiency of energy generation and its utilization in the power sector, and lower the import rate of fossil fuels by exploiting renewable energies and improving efficiency of the transport sector. Specific targets under the SMILES project included increasing the efficiency of energy generation and its utilization in the power sector (activity 1), lowering the import rate of fossil fuels by exploiting renewable energies, (activity 2) and improving efficiency of the transport sector (activity 3).

Within the framework of the RETDAP and SMILES projects, the potentials of available solar and wind resources in the country for electricity applications were assessed and quantified. In addition, a study was performed to define and evaluate optimal renewable energy systems, which showed that 100%-renewable energy systems are not financially viable. Hybrid systems, in which existing or new diesel generators are combined with photovoltaic (PV) solar panels and electricity storage (battery banks) could lower the price of electricity by 0.05-0.10 US$/kWh on the smaller-sized so-called Outer islands. Assuming that these latter systems, which have a high probability of adoption, indeed are implemented on the majority of the Outer Islands, about 10% of the electricity demand of the Maldives could be supplied by RE based systems in a cost effective way [3, 4].

Demonstration of a working hybrid PV-diesel system with storage backup was identified as crucial for raising

awareness and building up know-how among the Maldivians. Therefore it was decided to design and set up a pilot hybrid PV-diesel system in one of the islands. After reviewing a number of islands and assessing their suitability for installing such a system, the Maldivian partners selected the island of Mandhoo. The system is expected to serve as an interesting learning experience for the Maldivian partners before setting up similar installations in future in other islands. This paper describes the designing and implementation process that took about 14 months, starting from December 2004 just prior to the Tsunami. In the design phase, the HOMER simulation tool has been extensively used in order to compare and optimize the electrical demand to the electrical energy that the system is able to supply, on an hourly basis [5].

2 PRESENT ELECTRICITY SYSTEM

Mandhoo Island is located about 100 km South-West of the capital Malé in the South Ari Atoll at 3'41" N, 72'42" E. The annual average temperature on the island is around 30°C year round, with a minor variation of a few degrees. The relative humidity levels are around 70-80%. The island is inhabited by about 40 families (250 persons) that are all connected to the island grid. The PV system is planned to operate in conjunction with the existing diesel power generating systems on the island, whereby the PV system in principle provides power during the day, and the diesel systems during the evening and night.

Figure 1: Existing diesel sets: back 31 kW, front 22 kW

The island has two diesel generators (G1 of 31 kW and G2 of 21.6 kW capacity, see Fig. 1) that were provided by the Ministry of Atolls Development (MoAD), while the Island Committee has financially contributed to the building of the powerhouse, distribution network and connection the households, a few other buildings such as the island office, school, mosques, health post, etc. The Island Committee is in-charge of operating and maintaining the existing powerhouse. Electricity is metered and sold to the households and the commercial clients at a rate (2005) of 4.5 Rf (0.35 US$) per kWh. Another important electrical load is the street-lighting in the island during night time. The generators are used alternately, and a manual switch is used to change the load from one to the other generator. The small diesel engine G2 runs during the day, meeting a demand which is around 6-8 kW, and the large diesel G1 is switched on around 18:00 hours to serve the peak load of about 16 kW during the evenings, with incidental peaks above 20 kW, and a night time demand of 12 kW. It is switched off at 6:00 hours.

Based on the gathered information, a load curve was derived. Electricity supplied by the generators amounted to 75 555 kWh in 2005, with an average of 207 kWh/day. The local operator of the power plant was instructed in December 2004 to collect daily data on electricity production and fuel consumption in a special book. The logged data enabled to reconstitute quite accurately the efficiency curves of both generators, as depicted in Fig. 3. As a result, the existing system could be well modelled using the HOMER software. Key data resulting from the HOMER simulations are summarized in Table I. The most important assumptions are a diesel fuel cost of 0.5 US$/l, an interest rate of 12%, and a project lifetime of 15 year.

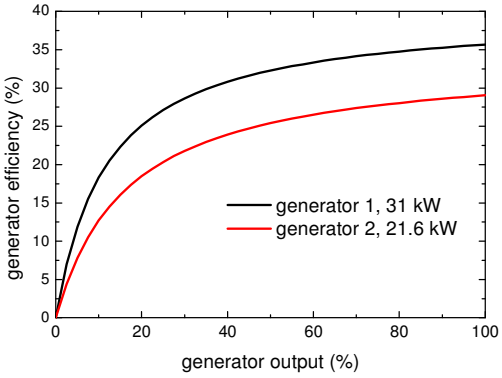

Figure 2: Generator efficiency as a function of relative output

Table I: Key data for the power generating system at Mandhoo (performance in 2005)

	G1	G2	Total
Generated electricity (kWh)	48846	26709	75555
Amount of fuel (l)	16529	12743	29272
Specific fuel usage (l/kWh)	0.338	0.477	0.387
Average efficiency (%)	30.0	21.3	27.0
CO_2 emission (kg/year)			77450
Electricity cost ($/kWh)			0.342

3 HYBRID DESIGN

3.1 Considerations

Integrating the PV system with battery back-up in the current island grid was considered as a suitable way to introduce renewable electricity supply, as PV/battery systems are simply add-ons to the existing infrastructure. The system should be as simple and sturdy as possible and easy to operate for the present operator. Therefore it was decided to go for an independent PV-battery system, i.e. either the PV system provides electricity to the distribution system, or one of the diesel generators. This is to be implemented through a manual switch-over between the two systems, in the same way it is being done at present, with a manual switch-over between the

two diesel generators in the morning and in the evening. Synchronization was not opted for, given the added complexity and the need to add synchronization units for the diesel generators as well.

The way the operator of the power station operates the system has been integrated into the simulations of the PV-diesel system. The underlying constraints for designing the system are as follows:

- one should not expect to introduce too many changes in the operator's habits;
- both diesel generators should be turned off during a certain period of the day, so that the surrounding population may feel (*hear*) the difference once the PV system is installed;
- both diesel generators should be kept in operating condition throughout the year (theoretically, one genset is sufficient to meet the load, but maintenance requires that they will be used alternatively);
- the PV system should ideally be placed nearby the power house in order to minimize the transmission losses as well as to facilitate the maintenance of the entire system.

The PV system should supply power to the network during daytime, from 07h00 until 18h00, with the objective of avoiding the use of a diesel generator during that period and reducing the dependence on fossil fuel. As the PV system would operate during sunshine hours, the size of the storage batteries can be minimized, thus reducing the battery investment and replacement costs. On an average day the battery will start feeding the network (through the inverter) and with higher solar radiation, the PV panel gradually takes over the load, and also starts recharging the battery when extra power is available. On cloudy days, this may not be the case; then the battery will have to supply most of the load throughout the day. The HOMER model runs showed that on certain days the battery is not able to meet the demand because they will reach a depth of discharge below 50% around midday. The operator will be instructed to switch on the diesel engines by midday on cloudy days. He will be guided by a simple indicator showing the state of charge of the battery. On a normal sunny day the operator makes a manual switch-over to one of the diesel generators at 18h00. The same switch will reverse the energy flow in the converter, thereby starting to recharge the batteries. The batteries should be fully charged again before 07h00 of the next day. As an example of HOMER simulation results, Fig. 3 shows monthly averaged demand and supply curves.

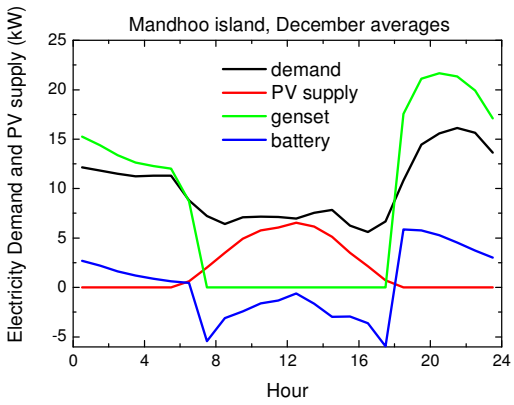

Figure 3: Daily demand and supply curves for Mandhoo in December. During this month, the PV system meets the full demand at noon, the rest being supplied by the batteries that are fully charged during night by the generator.

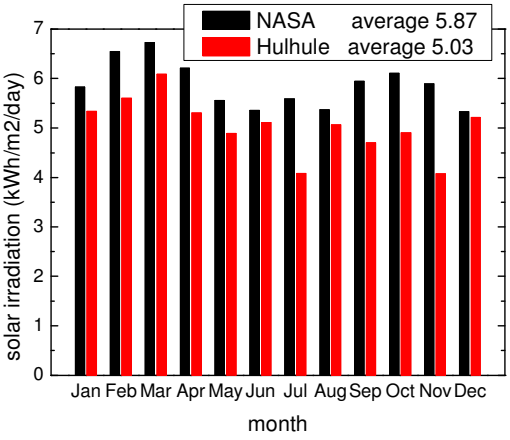

Figure 4: Solar irradiation (in kWh/m^2/day) at Hulhule' airport

3.2 PV system

On the basis of local inspections and analysis with the HOMER model, the following design specifications were found to be optimal for a solar penetration of about 25%: PV capacity of 12 kWp, battery capacity of 108 kWh (50 batteries, 360 Ah, 6 V), and 12 kWp converter. The solar regime was taken from measured (2003-2005) data at Hulhule' airport which is about 100 km away from Mandhoo. The average daily irradiance is 5.03 kWh/m^2 day, providing 1650 kWh/kWp. The measured data are about 15% lower than the data from the NASA solar irradiation data set [6, 7], see also Fig. 4. This data set comprises 10-year average irradiance data, which were derived from satellite images that were measured from July 1983 to June 1993.

In the ideal case, the PV panels should be located near the power station, but the site is not ideal as it is shaded by trees in the afternoon. Therefore, a street between the school and the health centre, running from east-north-east to west-south-west was selected. This location is partly shaded by trees, but only in the early morning and late afternoon. The PV panels are mounted on a self-standing elevated roof-like structure, which is designed to withstand winds of up to 20 m/s. The structure is equipped with two gutters to lead the rain away from the edges of the panels. People are able to walk or bicycle easily below the structure.

Given the need to concentrate on the maintenance and the physical switchover between PV and diesel generators in the powerhouse itself, it was decided to have the batteries and the converter installed in the powerhouse. This implies a long (200 meter) DC connection between PV panels and the rest of the system, which results in some DC transmission losses. The converter should be able to withstand the daily manual switch-over of the load, without voltage surges on the network.

The system was to be equipped with a monitoring system, which can be read from the MEEW office in Male'. This is presently the case with the monitoring of weather data from three masts in the country: each data-logger sends a daily e-mail to the Male office at 24h00 with the data recorded that day. In a similar manner, the monitoring system is to transmit the required 10-minute average data, thus allowing to properly monitor the PV-diesel system. The monitoring system is located in the powerhouse and monitors the solar radiation (based on a global radiation pyranometer), the DC voltage and current from the PV panel to the batteries, the DC voltage and current to or from the battery bank, the DC voltage and current to or from the converter, and the outgoing AC power (three phases).

4 REALIZATION

In the first mission to the Maldives in December 2004, the European experts visited the island of Mandhoo and took or arranged data to be taken. Also, preliminary HOMER simulations were performed. During the second mission in February and March 2005, a final system design was defined together with Maldivian partners, based on acquired data of the daily load and commercially available PV and converter components. A one day visit to Mandhoo, together with the SMILES partners from MCST, MoAD and STELCO, marked a vital step in the introduction of the PV-diesel system in the island. The Maldivian partners had organized a meeting with all inhabitants of the island, during which a detailed presentation was made about the PV-diesel hybrid system in Dhivehi, the Maldivian language. The inhabitants unanimously voted in favour of the installation of the system (Fig. 5).

Figure 5: Mandhoo inhabitants during the presentation on the PV–diesel system

In the months thereafter, the experts assisted MCST in preparing a tender document which was sent to well-known European solar system providers, inviting them to submit proposals with price quotations. Just after summer, a supplier was selected, and shipments to Malé were planned for November. In December, local workers constructed the steel support structure, and after transport of PV panels and converter to Mandhoo, installation of the PV system was carried out around Christmas, and finalized on 31st December 2005. Figure 6 shows a photograph of the finalized PV system. The structure was

Figure 6: PV system at Mandhoo

erected on the planned site, between the school and the Mandhoo Health Center. This will thereby serve the double purpose of providing shelter against rain or double purpose of providing shelter against rain or sunshine for those waiting in line for the Health Post and at the same time be of educational value for the children and teachers of the school. The installed system consists of PV capacity 12.8 kWp PV (160 pieces, 80 Wp, 12 V, BP), battery capacity 54 kWp (120 pieces OPzS solar 450, 450AhC120), converter 20 kW (2 pieces, 10 kVA, Ainelec Energy Bay).

5 EVALUATION

During the final mission of the European experts in December 2005, it was found that the daily load of the island had substantially increased as a result of an additional air-conditioned communication centre. The estimate for the daily consumption as used in the HOMER modelling exercise therefore had to be revised and was increased to 275 kWh/day (100375 kWh/year). Also, as the actual PV system is somewhat different from the optimum system simulated in Section 3.2, new HOMER runs were required. As the actual electricity consumption is expected to increase in the coming years, a few runs were made with a future value of 350 kWh/day (127750 kWh/year) to analyse the effect this higher consumption will have on the behaviour of the PV-diesel system. Results show that in both cases the most convenient solution for the operator is to let the generator G1 run longer in the morning, i.e., until 07h00 for the load of 275 kWh/day or until 08h00 for the future load of 350 kWh/day). On cloudy days, the small generator G2 should be switched on, and this should perhaps be done every week for a few hours in order to prevent corrosion of the engine.

During the installation, it turned out that the converter system was not functioning well as a result of faulty printed circuit boards. These were returned to the manufacturer. During their absence, the system was damaged by lightning, and presently the system is still not functioning. This is absolutely unacceptable, and may have repercussions on the future deployment of PV systems in the Maldives.

6 CONCLUSION

We have been successful in designing and realizing the first grid-connected PV system in the Maldives. Thorough system design was possible using the HOMER programme, and MEEW employees are now capable of using it for future installations. Load curves and efficiency curves of diesel generators are indispensable in determining the most optimum configuration, as well as actual measurements of the solar regime. It really is a pity that the system is not functioning yet, but actions are being taken to get it up and running as soon as possible.

ACKNOWLEDGEMENTS

Thanks are due to the many Maldivians who were very supportive of our work. The work of Klaas van Alphen as UNDP intern is highly appreciated and served as indispensable input. Further, we would like to gratefully acknowledge the financial support from the Asia Pro Eco Programme of the European Commission for the SMILES (Strengthening Maldivian Initiatives for a Long-term Energy Strategy) project, ADEME for financing the PV system., and GEF and UNDP for the RETDAP (Renewable Energy Technology Development and Application) project.

REFERENCES

[1]. T. Roper, *Small Island States – Setting an Example on Green Energy Use,* Reciel 14 (2005) 108-116.

[2] D. Weisser, *Power sector reform in small island developing states: what role for renewable energy technologies?* Renewable and Sustainable Energy Reviews 8 (2004) 101-127.

[3] K. Van Alphen, W.G.J.H.M. Van Sark, M.P. Hekkert, *Renewable energy technologies in the Maldives - determining the potential,* Renewable and Sustainable Energy Reviews (2007) (in press).

[4] K. Van Alphen, M.P. Hekkert, and W.G.J.H.M. Van Sark, *Renewable energy technologies in the Maldives - realizing the potential,* Renewable and Sustainable Energy Reviews (2007) (in press).

[5] T. Lambert, P. Gilman, P. Lilienthal, *Micropower system modeling with HOMER*, in *Integration of Alternative Sources of Energy*, F.A. Farret, M.G. Simões, Editors, Wiley: New York, USA, 2006, 379-418. (see also website: http://www.nrel.gov/homer)

[6] W.S. Chandler, C.H. Whitlock, P.W. Stackhouse Jr., *NASA Climatological Data for Renewable Energy Assessment,* Journal of Solar Energy Engineering, 126 (2004) 945-949.

[7] NASA Atmospheric Sciences Data Center, see website: http://eosweb.larc.nasa.gov/sse.

CONTROL OF THE GROWTH OF TEXTURED Ag AND Ag:AlO_X BACK REFLECTORS FOR n-i-p SOLAR CELLS

R.H. Franken, R.L. Stolk, H. Li, C.H.M. van der Werf, J.K. Rath*, R.E.I. Schropp
Utrecht University, Debye Institute, SID - Physics of Devices, P.O. Box 80.000, 3508 TA Utrecht, The Netherlands,
\Tel : 0031 (0)30 2532964, Fax 0031 (0)30 2543165, e-mail: R.H.Franken@phys.uu.nl,

ABSTRACT: Rough reflecting back contacts, like texture-grown Ag, are generally used to enhance the short-circuit currents of substrate type n-i-p solar cells. The roughness of the interfaces (both the vertical as well as the lateral properties) is considered to be the key to efficient light trapping. Therefore it is important to understand and control the growth process of these metal layers. We studied the growth evolution of Ag layers deposited by RF magnetron sputtering at various substrate temperatures and indicate the different growth zones with the help of the structure zone model. Additionally we consider sputter-deposited Ag layers containing AlOx impurities (inhibitors) that block the growth of Ag crystals and prevent restructuring of the texture of the surface. This makes it possible to increase the period in which competitive-texture-growth is dominating the growth and hereby we can create surface features with higher *rms* roughness and smaller lateral sizes, which are considered to be more effective for the scattering of visible light. Ag:AlO_x layers are deposited at relatively low substrate temperatures, below 300^{o}C, and a microcrystalline silicon n-i-p solar cell is obtained with an efficiency of 8.1 %.
Keywords: Back contact, sputtering, polycrystalline

1. INTRODUCTION

Rough reflecting back contacts are normally used to enhance the short circuit current in substrate type n-i-p solar cells. A commonly used material is polycrystalline Ag.. Metals of this kind can be grown with texture as deposited. No additional treatment steps are needed. The roughness of these layers is considered to be the key for efficient light trapping [1, 2].

From the literature, it is known that both the vertical as well as the lateral dimensions of the surface of front TCOs are important for effective light scattering in superstrate type of solar cells [3,4]. Moreover, for substrate type of solar cells, specifically microcrystalline silicon (μc-Si:H) solar cells, we find a strong correlation between the morphology of back contact layers and the current generated by long wavelength light [5]. This specific technological application requires a well-designed morphology of the back contact. Therefore, it is essential to have a better understanding and control of the growth process of these texture-grown polycrystalline metal layers.

Extensive studies on the correlation between deposition parameters and film structure over the past decades have given insight and understanding in the film formation process. It has led to the structure zone model (SZM) that explains the structural evolution of film during growth. The SZM has been reviewed in literature [6, 7, 8]. In this study we have used the theoretical description of the SZM to understand and control the growth of texture development of sputtered Ag back reflectors.

We will present here a growth evolution study of texture-grown Ag layers. We will indicate the different growth zone regimes and explain the differences in texture evolution. Furthermore, it is demonstrated how to control both vertical and lateral sizes of the surface texture in order to engineer a more efficient light scattering back contact.

Nowadays many industries opt for thin flexible substrates in highly cost effective roll-to-roll production processes [9, 10, 11]. The flexible substrates are made of high temperature resistant plastics (up to 300 ^{o}C). We show a method in order to grow an effective light scattering back reflector at a sufficiently low substrate temperature (T_{sub}).

2 FUNDAMENTAL

The literature describes the fundamental growth phenomena of polycrystalline films [12, 13]. Various growth regimes for metal film formation are distinguished and the texture development for crystal growth is explained on the basis of four different growth zones (Figure 1), which are mainly temperature related. Additionally, differences in the growth process of pure metal (basic SZM) and multiphase or impurity containing metal films (real SZM) are shown [14, 15].

The evolution of microstructure in thin films proceeds through consecutive steps that include nucleation, island growth, coalescence of islands, formation of polycrystalline islands, development of a continuous structure and film growth.

During the stage of crystal coalescence, coarsening of the film, through diffusion of the sputtered particles and grain boundary motion, will play a dominant role on the texture development depending on the temperature and sizes of the crystals. From this stage onwards, the texture of the film will evolve according to two selection mechanisms. The selection can either be influenced by: 1) restructuring of the grain surfaces during growth or 2) competitive growth.

1: Restructuring of the surface starts when the grain boundaries are highly mobile and bulk diffusion is significant. There will be a pronounced selection of the orientation during the coalescence of the islands. This is also called normal grain growth and is led by the minimization of the surface and interface energy. It can be followed by abnormal grain growth, during which the grain boundaries will migrate and larger feature diameters with columnar crystals and flat surfaces will be obtained.

2: When the grain boundary migration is limited a competition between the growth of neighboring grains is started. The faster growing crystals will overgrow the slower growing ones and a V-shaped crystal is formed. As a consequence there is a variation in morphology with increasing film thickness. Additionally, competitive

* Corresponding Author: J.K.Rath@phys.uu..nl

texture growth can occur if incorporated inhibitors (impurities) prefer to block certain crystal orientations, which allows other orientations to grow faster. In case of aluminum material containing oxygen, it is known that certain crystal orientations are not blocked by the impurity species [16, 17].

These different growth mechanisms are part of the SZM described in the literature [6, 12]. In each zone a different type of mechanism will be dominant depending on the substrate temperature and impurity level. Four different types of zones for polycrystalline evolution are distinguished and can be visualized, as shown in Figure 1.

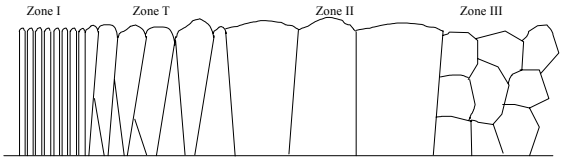

Figure 1: Four different zones for polycrystalline material evolution are distinguished in the structure zone model.

1: Zone I corresponds to a very low temperature interval, typically $0 < T_{sub} / T_m < 0.2$, where T_{sub} and T_m are the substrate temperature and the melting point of the metal respectively. In this temperature range the surface diffusion of atoms is negligible and a fiber like structure is developed.
2: At a higher temperature range (zone T) $0.2 < T_{sub} / T_m < 0.4$, surface diffusion is increased and grain coarsening of small islands occur. This is followed by a competitive growth evolution.
3: Zone II is characteristic for high substrate temperatures $T_{sub} / T_m > 0.4$ where the effect of grain boundary migration becomes dominant. The growth in zone II can evolve in two different ways; normal grain growth and abnormal grain growth [13, 18, 19].
4: Zone III consists of nearly spherical grains, due to the continuous blocking of the crystal growth and the successive development of new nucleation sites. This zone is typical for the high temperature region; however, it can exist at any substrate temperature depending on the "inhibitors" present. This can be obtained by the use of co-deposition of impurity species.

3 EXPERIMENTAL

Ag polycrystalline films have been deposited by reactive magnetron sputtering of a 99.99 % pure Ag target. The samples have been prepared on Corning 1737F glass substrates. With fixed deposition parameters layers were grown at various substrate temperatures of 90, 180 and 270 ^oC. The temperatures are chosen in the range for structure zones T and II and around the transition of these zones. The accompanying T_{sub} / T_m values are respectively 0.30, 0.37, 0.44, considering the melting point for Ag of 1235 K. Several thickness series (with thicknesses of around 200 – 500 – 1000 , and 2000 nm) were studied.

Furthermore a 99.99% Ag:Al(1%) target has been used for depositing Ag:AlO_x material. Sputtering of Al from the target in an Ar atmosphere containing 0.3 % oxygen leads to incorporation of AlO_x inhibitors during the growth of Ag films. Samples have been made with the same thickness variations at two temperatures, 180 and 270 ^oC (Zone T, Zone II).

The surface structure of the samples has been analyzed by atomic force microscopy (AFM) measurements. X-ray diffraction (XRD) has been used to analyze the structure.

4 RESULTS

4.1 Texture evolution

Figure 2 shows the evolution of *rms* roughness with increasing layer thickness, indicated by the arrows. In the basic SZM, a T_{sub} of 90 ^oC is considered to be in the middle of zone T. As indicated with the solid squares, in this case, clearly both *rms* roughness and feature sizes are small and they keep increasing with increasing film thickness. The vertical as well as lateral sizes of these surface features show a positive linear correlation in growth, which can be an indication of V-shaped grains and indicates that deposition takes place in the competitive texture growth regime in the real structure zone T. Both T_{sub} of 180 (solid cirlces) and 270 ^oC (solid triangles) show a structure zone II behavior: For all of these films the *rms* roughness stays roughly constant at thicknesses above 500 nm (at diameter L = 700 nm and 2250 nm, respectively). The clear increase in feature diameter and leveling off of the roughness indicate that grain boundaries are able to migrate, thus restructuring of the surface takes place. The saturated values of *rms* roughness as well as the feature diameter are higher in case of T_{sub} = 270 ^oC than in the case of T_{sub} = 180 ^oC.

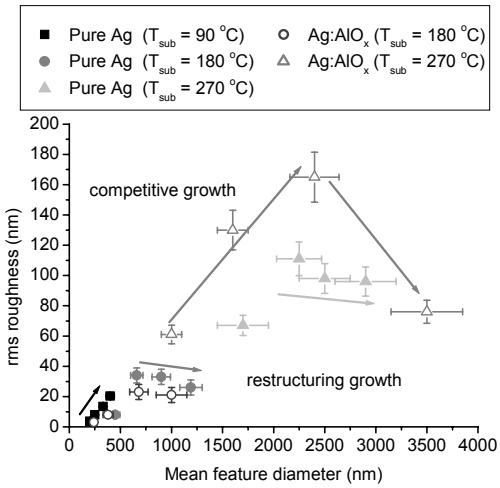

Figure 2: The thickness evolution in *rms* roughness and feature diameter for 'pure' Ag and Ag:AlO_x layers.

In the first stages of the thickness evolution it is observed that the *rms* roughness scales with the lateral feature diameter, which tells that there is enough grain migration and surface diffusion. The features are growing without any limitation in either direction, lateral and vertical. Up to a certain feature diameter, depending on T_{sub}, this growth can occur uninterrupted. At that point a state is reached where it is energetically more favorable to grow in lateral dimension only and coarsening of the grains is blocked. The coarsening should therefore be strongly related to the minimization of either the surface energy or the grain boundary energy. Indeed, a linear

correlation between this saturated value of feature diameter and the kT values of the deposition is seen in Figure 3.

The presented 'pure' Ag layers show that for both growth zone T as well as II the *rms* roughness evolution is limited. Growth zone T shows increasing *rms* with increasing film thickness, however due to a low surface diffusion feature sizes are limited. Growth zone II shows larger sizes with increasing temperature, however due to restructuring of the texture the *rms* roughness shows a maximum at a certain temperature.

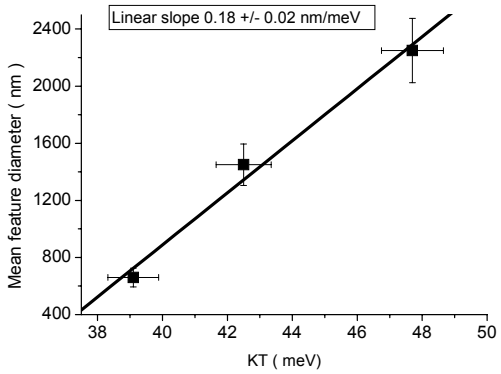

Figure 3: The correlation between the feature size at which restructuring takes place and T_{sub} (kT).

4.2 Introduction of Ag:AlO_x inhibitors

For efficient light trapping it is assumed that high *rms* roughness is needed together with feature sizes that are similar to the wavelengths that have to be scattered (650-1000 nm). A delay in restructuring of the surface roughness and a decrease in the lateral sizes (diameters) of the features can be obtained by blocking the crystal growth with inhibitors. For this purpose we studied the film growth using an Ag:Al(1%) target. The AlO_x will be active in both decreasing the grain mobility and therefore lateral grain growth as well as inducing competitive growth of crystals due to preferred blocking of specific crystal faces.

Ag:AlO_x growth at 180 ^oC indeed shows decreased sizes in both vertical as well as lateral directions compared to the "pure" Ag growth, as can be seen from the open circles in Figure 2. The figure shows a delay in restructuring compared to the 'pure' Ag case. At T_{sub} = 270 ^oC a concomitant increase in *rms* roughness with increasing feature diameters is observed with increasing films thickness. The lateral feature sizes are, compared to the 'pure' Ag case, smaller at a similar layer thickness. This indicates that the grain boundaries are limited in movement. Up to a feature size of 2350 nm a linear correlation is visible, as is generally observed in case of structure zone T, which indicates competitive growth texture induced by blocking of crystal faces in certain directions and resulting V-shaped grain growth. The highest *rms* roughness value obtained is 179 nm. This is significantly higher than in the "pure" Ag case. Above lateral sizes of 2350 nm a complete restructuring of the surface texture takes place, as was also observed for the "pure" Ag case. Furthermore, in contrast to the normal grain growth of "pure" Ag, the restructuring is considered to be due to abnormal grain growth. This inference is supported by the observation that the feature diameter increases drastically while the *rms* roughness (vertical) height levels off, along with a complete recovery of (111) orientation, as measured by XRD.

4.3 Control of the morphology

From the literature, it is known that the average feature sizes of films under both clean and contaminated conditions show an exponential dependence with the reciprocal substrate temperature. Figure 4 shows this dependence for the "pure" Ag and the AlO_x contaminated series. Both figures show also the dependence on thickness. As the increase in diameter with thickness is linear for all the cases, this indeed results in a similar trend that is shifted upwards for thicker layers. A horizontal cross section of this figure tells us at which temperatures and thicknesses a specific average feature diameter can be obtained, independent from structure zones and the different growth regimes. The figure gives a lot of knowledge of the growth of polycrystalline Ag layers and a fingerprint for the growth. Based on this representation the control of the surface feature diameters during film growth at different temperatures is possible.

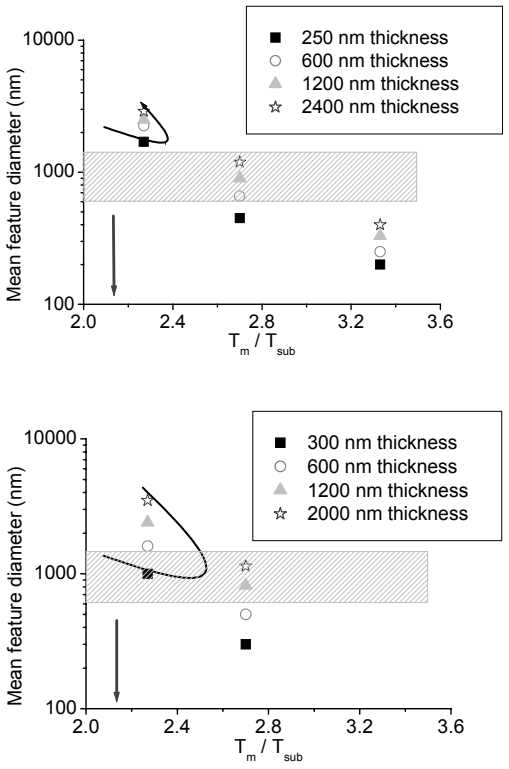

Figure 4: The dependence of the feature size on the reciprocal T_{sub} gives a fingerprint for the structure growth. The required feature size range (rectangle), 80 nm *rms* roughness boundary (line) and 300^oC T_{sub} (arrow) are indicated.

For adequate light trapping, a high *rms* roughness is preferred. For n-i-p silicon solar cells *rms* values between 50-100 nm are considered to be reasonably high. It has been shown that both the *rms* roughness and specific feature diameters are important for efficient light scattering [5]. The patterned rectangle in the figure 4 indicates average feature diameters in the range of 600-1300 nm, which are considered to be appropriate for light scattering in n-i-p solar cells [20]. Furthermore, we

indicated by the curved line the films that show an *rms* roughness above 80 nm. For lower roughness the curve will be widened and shifted down to the right. For higher roughness the opposite trend is seen.

As can be seen clearly for the "pure" Ag series, high *rms* and specified feature diameter are mutually exclusive and thus difficult to obtain. The combination is limited by the *rms* roughness that is limited to 60 nm and the feature diameter that is 2000 nm and higher. In the Ag:AlO_x series higher *rms* roughness in combination with smaller diameters were obtained as explained in the previous section. Therefore, the 80 nm *rms* curve is shifted and it overlaps the diameter rectangle, thus an optimal combination can be obtained. Additionally it is observed that an overlap between the optimal lateral and vertical sizes can be obtained at substrate temperatures below 300 ^oC, for which the position is indicated by the arrow.

4.4 Low temperature Ag films

As is shown in Figure 4, with the use of AlO_x impurities it is possible to obtain an efficient light scattering layer below a T_{sub} of 300^oC. Such substrate temperatures are suitable for deposition on heat resisting flexible plastic foils as used in roll-to-roll production [21]. Two layers of 280 and 700 nm respectively were deposited at 270 ^oC (Figure 5).

A high efficiency of 8.1 % was obtained for an n-i-p µc-Si:H solar cell (consisting of an i-layer of 1500 nm) on the back reflecting contact comprising the 280 nm thin Ag:AlO_x layer and a 500 nm ZnO:Al TCO layer. Table 1 shows the J-V parameters of the best cell. A J_{sc} of 20.9 mA/cm^2 is obtained, which can be regarded as reasonably high for this i-layer thickness [21]. However, the external quantum efficiency measurements indicated a less than expected red light absorption. This is confirmed by total integrated reflection measurements where, over a wide wavelength range, an absorption loss is seen. This is attributed to increased plasmon absorption due to the specific morphology. This plasmon absorption loss is described in more detail in a different paper at this conference [5].

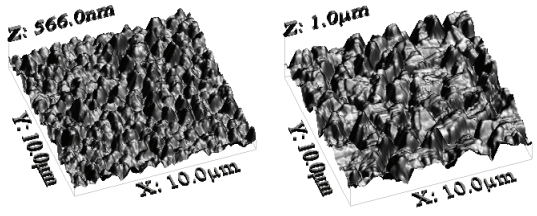

Figure 5: AFM images of 280 (left) and 700 (right) nm thick Ag:AlO_x layers deposited at 270 ^oC . The *rms* is 73 (left) and 122 nm (right), respectively. The mean lateral features sizes are 750 and 1800 nm, respectively.

Table 1: J-V parameters of the best cells deposited on the Ag:AlO_x/ZnO back contacts with different surface roughness of the silver layers.

***rms* roughness (nm)**	**J_{sc} (mA/cm^2)**	**V_{oc} (V)**	**FF**	**Efficiency (%)**
73	20.9	0.57	0.68	8.1
122	21.8	0.55	0.61	7.3

5 CONCLUSIONS

Insight and understanding in grain growth of magnetron sputtered Ag films, especially in the presence of (deliberately incorporated) impurities, is obtained. We observed that the structural evolution for pure films could be explained by the basic growth phenomena and the structure zone model. We observed that for growth zone II films, restructuring of the surface roughness occurs at different lateral surface feature diameters that are linearly dependent on substrate temperature. For higher kT values restructuring can be extended to higher feature diameters. Introducing Al impurity during film growth builds in AlO_x inhibitors at the crystal faces and grain boundaries. This impurity decreases the lateral grain growth and thus delays the restructuring of the surface. The extended competitive growth trend, therefore, increases the *rms* surface roughness to values up to 179 nm.

The dependence of feature diameters on reciprocal temperature plotted for different thicknesses, gives a control of the film growth over a wide range of temperatures. Introducing the *rms* roughness as a contour curve in this picture gives a fingerprint for the surface morphology at different growth parameters. The Ag:AlO_x films show a combination of high *rms* value and small feature diameter, which is believed to be the most appropriate for light scattering in n-i-p solar cells.

These efficient light scattering surfaces can already be obtained at temperatures below 300 ^oC, which is suitable for high temperature resistant plastic substrates that can be used in roll-to-roll production. We have shown a 8.1 % efficiency for a 1500 nm thick µc-Si:H n-i-p solar cell with back reflectors deposited at temperatures around 270 ^oC.

Acknowledgements

The authors thank the Netherlands agency for Energy and Environment (SenterNovem) for financial support.

REFERENCES

[1] O. Kluth, C. Zahren, H. Stiebig, B. Rech, H. Schade, in *proc. of 19th EUPVSEC, Paris,* (2004), pp. 1587.
[2] A. Banjeree and S.Guha, J. Apply. Phys. **69**, (1991) 1030.
[3] T. Dekker, J.W. Metselaar, R. Schaltmann, B. Stannowksi, R.A.C.M.M. van Swaaij and M. Zeman, in *proc. of 20th EUPVSEC, Barcelona,* (2005) , pp 1517.
[4] H. Schade, P. Lechner, R. Geyer, H. Stiebig, B. Rech, O. Kluth, in *Conference record of 31st IEEE Photovoltaic Specialists Conference,* (2005) pp. 1436.
[5] R.H. Franken, R.L. Stolk, H. Li, C.H.M. van der Werf, J.K. Rath, R.E.I. Schropp, *in 21st EUPVSEC, Dresden,* (2006), this conference.
[6] J. A. Thornton, J. Vac. Sci. Tech. **11**, (1974) 666.
[7] P.B. Barna, M. Adamik, Thin Solid Films **317**, (1998) 27.
[8] J. A. Thornton, J. Vac. Sci. Tech. **A4**, (1986) 3059.
[9] A. Gordijn, et al. in *Proc. 4th World conference on Photovoltaic Solar Energy Conversion, Hawaii* (2006).
[10] F. Jeffrey et. al., Int. J. Solar Energy, **18**, (1996) 205.
[11] D. Fischer et al, in Proc. *16th EUPVSEC,, Glasgow*, (2000), pp. 2153.

[12] M. Adamik, P.B. Barna, I. Tomov, Thin Solid Films **359**, (2000) 33.
[13] M. Adamik, P. B. Barna, I. Tomov, Vacuum **61**, (2001) 251.
[14] I. Petrov, P.B. Barna, L.Hultman, J.E. Greene, J. Vac. Sci. Technol. A **21**(5), (2003) s117.
[15] M. Adamik, P. B. Barna, I. Tomov, Thin Solid Films **317**, (1998) 64.
[16] R. Michel, j. Gastaldi, C. Allasia, C. Jourdan, J. Derrien, Surface Science **95**, (1980) 309.
[17] C. W. B. Martinson, S. A. Flodstrom, J. Rundgen, P. Westrin, Surface Science **89**, (1979) 102.
[18] H. P. Longworth, C. V. Thompson, J. Appl. Phys. **69** (7), (1991) 3929.
[19] D.J. Srolovitz, J. Vac. Sci. Tech. **A4** (6), (1986) 2925.
[20] B. Yan, J. M. Owens, C. Jiang, J. Yang, S. Guha, *Mater. Res. Soc. Symp. Proc.* **862**, (2005) A23.3.1.
[21] A.Takano, M. Tanda, M. Shimosawa, T. Wada, T. Kamoshita, Jpn. J. Appl. Phys. **42**, (2003) L1312.

OBSERVATION OF PHOTOGATING EFFECT IN MICROCRYSTALLINE SILICON SOLAR CELLS AND ITS CONTRIBUTION TO DEVICE OPTIMIZATION

Hongbo Li, Francisco Rubinelli[1], Jatin Rath, and Ruud E.I. Schropp
Utrecht University, Faculty of Science, Debye Institute, SID – Physics of Devices, P.O. Box 80.000, 3508 TA Utrecht, The Netherlands *(e-mail: h.li@phys.uu.nl)*
[1]INTEC, Universidad Nacional del Litoral, Güemes 3450, 3000, Santa Fe, Argentina

ABSTRACT: A photogating effect is observed under strong blue bias light in microcrystalline silicon solar cells with an i-layer made by hot-wire CVD technique. Computer simulations point out that this is related to a low internal electrical field due to electronic defects in the i-layer. By improving the i-layer quality, this effect is reduced and an efficiency of 8.52% is reached for a μc-Si: H n-i-p cell.

Keywords: photogating effect, microcrystalline silicon, computer modeling

1 INTRODUCTION

The name 'photogating' for the observed anomalously high quantum efficiency values in amorphous silicon p-i-n structures was proposed by the group at Pennsylvania State university in 1992 [1] but the effect was reported in the 1980s [2] already. The main characteristics of this effect are the observation of anomalous high values in the spectral response for red or blue wavelengths when the external quantum efficiency is measured under blue or red bias light condition respectively. The reason for this remarkable phenomenon can be attributed to the trapping and release of photo-generated carriers in the low electric field region created by the strong bias light. In the case of using blue bias light, this low field region is located in the front part of the p-i-n structure, due to the high absorption coefficient of a-Si: H. While applying a chopped red light (monochromatic beam) that it is uniformly absorbed, the field in the rest part of the device is slightly modulated with the chopping frequency. Because the potential drop between each side of the i-layer stays constant in the experimental configuration, the field in the front also changes with the same frequency. This small change results in the transport of the trapped carriers originally created by the bias beam ("gating"). Therefore, the observed QE values, defined as $QE = \Delta I_m/e\phi_m$, where ϕ_m is the photon flux of the incident chopped monochromatic light, ΔI_m is the synchronously detected AC current, and e is the charge of electron, are enlarged. The exceptionally high quantum efficiency is also called apparent quantum efficiency (AQE) by researchers working on other type of solar cells [3].

In this paper we report, to our knowledge, for the first time the observation of a strong photogating effect in microcrystalline silicon (μc-Si: H) solar cells. Because of its lower band gap and inherently inhomogeneous structure, this effect is stronger than in a-Si:H solar cells, and therefore it opens the opportunity to further utilize this effect in μc-Si:H electronic devices, such as integrated semiconductor photoreceptors with internal gain, or as in the present paper, as a supplement for the existing solar cell characterization technique.

2 EXPERIMENTAL DETAILS

The cells involved in this study have a n-i-p structure: SS/ rough Ag/ ZnO back reflector/ n-type μc-Si:H/ intrinsic μc-Si:H/ buffer/ p-type μc-Si:H/ ITO/ Au (gridlines), with an active cell area of 0.13 cm^2. All silicon layers were deposited in the multi-chamber UHV PASTA system. Intrinsic i-layers were deposited by the hot-wire CVD technique near the phase transition region between microcrystalline silicon and amorphous silicon. Two 0.5 mm tantalum (Ta) filaments were used. The filament current was adjusted to be 10.5 A, with a calibrated filament temperature around 1850 ^oC, which results in a radiatively heated substrate at a temperature of around 250 ± 5 ^oC [4]. Doped layers (p-type and n-type) were deposited by plasma CVD in separated chambers. The substrates used are either Ag/ZnO coated Asahi U-type TCO glass, or Ag deposited at high temperature (for proper roughness) with a ZnO coating made in house by sputtering.

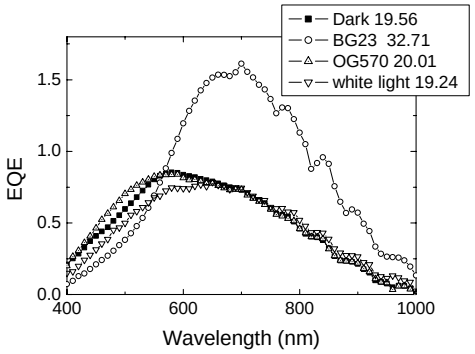

Figure 1 EQE of a μc-Si: H n-i-p cell showing a strong photogating effect. Solid square: the cell measured in the dark (Dark); open circle: measured with blue filter (BG23); up triangles: with red filter (OG570); down triangles: with white bias light (white light). The numbers in the legend show the calculated integrated current density in mA/cm^2 by convolution with the standard AM1.5 spectrum. I-layer thickness is around 1.3 μm.

A spectral response setup with the possibility to apply bias light and bias voltage was used for measuring the external quantum efficiency (EQE) of the solar cells. A Xenon lamp was used both as the source for the monochromator and for the bias beam. A low pass filter,

BG23, and a high pass filter, RG570, were used in the bias light path to obtain blue and red bias light, respectively. The photon flux density of the light, as measured by a calibrated silicon photodiode, was around $5*10^{15}$ cm^{-2} s^{-1} for the bias beam and $3*10^{13}$ $cm^{-2}s^{-1}$, for the monochromatic beam. The intensity of unfiltered white bias light was around 100 mW/cm^2 and was kept constant. Bias light intensity variations were realized by using a set of neutral density glass filters in the bias beam. The current density–voltage (J–V) characteristics of the solar cells were measured at 25 °C under AM1.5 100 mW/cm^2 white light generated by a dual beam solar simulator (WACOM). A 0.3 mm stainless steal mask used for depositing the ITO top contact was also used during the J-V measurement to have a precise definition of the cell area.

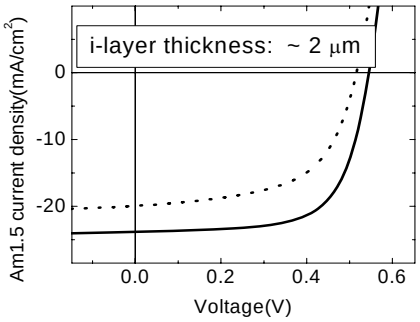

Figure 2 AM1.5 J-V characteristics of μc-Si: H n-i-p cells on stainless steel with textured back reflector. (1) Dashed line: A cell with an un-optimized i-layer shows a strong photogating effect; (2) solid line: A cell with an optimized i-layer, the photogating effect is eliminated and an efficiency of 8.52 % is reached (J_{sc}=23.4 mA/cm^2, V_{oc}=0.545V, FF=0.668).

3 RESULTS AND DISCUSSINOS

3.1 Observation of Enhanced External Quantum Efficiency (EQE)

A typical EQE of a cell exhibiting enhanced external quantum efficiency is shown in Figure 1. Curves marked with solid squares and down triangles are the measurement performed under standard conditions, i.e. in the dark and under white bias light respectively, and with 0 V bias voltage. The integrated current density, using a tabulated AM1.5 solar spectrum, gives a value for the short circuit current J_{sc} of 19.24 mA/cm^2, which is among the typical values for J_{sc} (SR) for a n-i-p μc-Si:H cell on a Asahi/Ag/ZnO substrate. Under blue bias light conditions, a significantly enhanced EQE in the red light region (wavelength from 550 nm to 1000 nm and above) with a peak value ~1.61 at around 700 nm wavelength is observed. Simultaneously, the curve in the blue light region (wavelength < 550 nm) shows a lower EQE value than that obtained under white bias light. The integrated current density shows a value of 32.7 mA/cm^2, which is 70 % higher than that measured under white light. With the orange filter OG570 in the bias light path, an enhanced blue response and slightly decreased red response are observed. Current-voltage measurement with the solar simulator (Figure 2, dotted line) shows as output characteristics: J_{sc} = 19.24 mA/cm^2, V_{oc} = 0.47 V, FF = 0.531 and efficiency of 4.80 %, indicative of a high density of defects in the absorber layer.

3.2 COMPUTER SIMULATION

3.2.1 AMPS analysis

The computer code D-AMPS [5] was used to study this effect. The input parameters were adopted based on the previous work done by J. Strengers *et al.* for a μc-Si: H n-i-p cell study [6]. Important values, such as effective band gap, defect density distribution, carrier mobilities of the intrinsic μc-Si: H materials were adjusted in a limited range, in order to fit our experimental result. Details for the simulation will be published elsewhere.

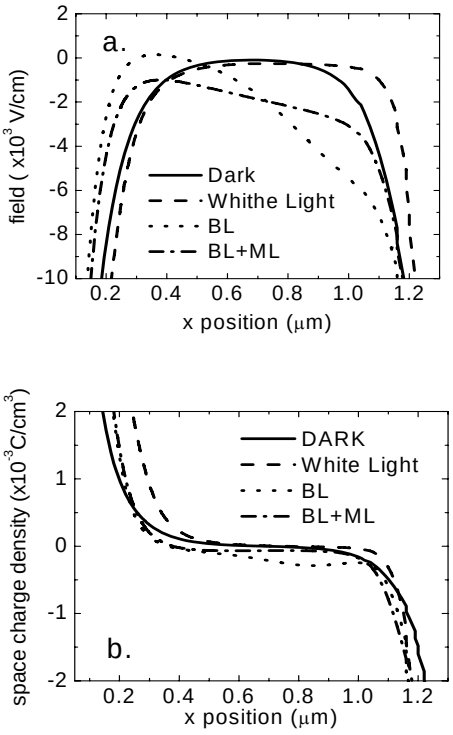

Figure 3 The electric field (a) and space charge (b) distribution in the short-circuit condition for the i-layer only. BL: blue bias light; ML: red monochromatic light.

3.2.2 Simulation result

When the defect density in the i-layer is high or the i-layer is thick, the internal electric field is not homogenously distributed in the intrinsic layer. This can be seen in figure 3a, the simulated internal electrical field profile under the short circuit condition. In the equilibrium state (solid line), a strong electric field exists in the region close to the p/i and i/n interfaces. In the middle part of the i-layer, however, the field is weakened by several orders of magnitude. When the cell is illuminated, part of the defect will act as trapping centers for photo generated electrons and holes, and therefore, they will modify the electrical field distribution in the i-layer. This can be seen in Figure 3b, in the space charge distribution plots, from the dashed curve when the sample is measured under the white bias light. As a result, the shape of the field distribution profile (Figure

3a, dashed line) changes a bit compared to the curve in the dark condition, and the minimum shifts to the rear side of the cell.

When the cell is illuminated with a strong blue bias light (AM1.5 spectrum with a blue filter, photon flux in the order of 1×10^{15} $cm^{-2}s^{-1}$), almost all the incident photons are absorbed in the front part of the cell, due to the high absorption coefficient of the intrinsic μc-Si:H to short wavelength light. As a result, a much weakened electric field is presented in the front part of the i-layer, with a minimum close to zero; the field in the rear side of the cell is, however, increased compared to the dark and white light condition (Figure 3a, dotted line). This is a result of the fixed boundary condition acting on the electric potential.

When a chopped monochromatic red probe beam (ML) with a photon flux in the order of 1×10^{13} cm^{-2} s^{-1} is superimposed on the strong blue bias beam (BL), the photons are nearly homogeneously absorbed in the i-layer due to the low absorption coefficient of the μc-Si:H for the red light. This can again modify the space charge distribution profile, but it will have the largest influence in the rear part of the i-layer. In the front part, the space charge density is dominated by the blue bias light, which is about 2 orders of magnitude stronger than the monochromatic probe beam. This can be seen in Figure 3b, by comparing the doted (BL) and dashed-dotted (BL+ML) lines. This modulated space charge distribution results in a modulated field distribution profile which is in phase with the incident probe monochromatic beam, as is shown in Figure 3a by the dashed-dotted line. One can see that the previously weakened electric field in the front part of the i-layer by the DC blue bias light is now enhanced, although the magnitude is not large. Due to the overwhelming absorption of the strong bias light, the small change in the electric field has a big influence on the carrier transport kinetics. As a result, a decrease of recombination rate in the front part of the cell is observed, which is shown in Figure 4. Part of the photocarriers which were generated by the DC bias light and trapped in the low field region can then flow out of the cell, and be collected by the lock-in amplifier.

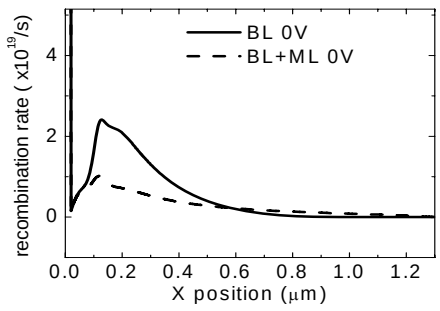

Figure 4 Recombination rate profile when only the blue bias beam (BL, solid line) and both BL and a weak red probe beam (BL+ML, dashed line) are present.

The mechanism of the enhanced QE values is similar to that of the photogating effect observed in amorphous silicon p-i-n structures [1] and Schottky barrier structures [5]. The difference in our case from the previous observations is that the input parameters in our simulations were chosen to fit μc-Si: H solar cells rather than a-Si:H. This difference is mostly characterized by the higher carrier mobilities and the narrower mobility band gap, compared to those of amorphous silicon. Structural characterizations, done by Raman spectroscopy and XTEM measurement, confirm the microcrystalline nature of the studied cells and materials.

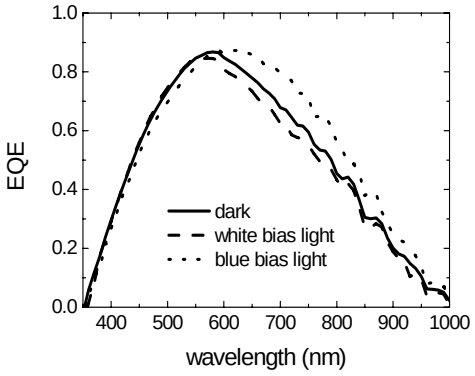

Figure 5 Measured external quantum efficiency for a cell with optimized i-layer. The J-V characteristics of this cell are shown in Figure 2 by the solid line.

4 APPLICATION TO DEVICE OPTIMIZATION

Since the photogating effect is related to the sub-gap defects in the intrinsic layer, the strong photogating effect shows that the i-layer in such cells has high defect density. By using an improved n-layer and a two-step hydrogen profiling technique, however, an efficiency of 8.52 % has been reached for a μc-Si:H n-i-p cell deposited on a stainless steel substrate with textured Ag and ZnO back reflector made in house [7]. Thus far, this is the highest efficiency for a μc-Si:H n-i-p cell with i-layer made with hot-wire CVD. FTPS measurement on the i-layer of this cell gives a sub-gap defect density around 3×10^{15} cm^{-3}. Figure 5 shows the EQE of this cell. One can see that there is still a weak PG effect observable, which means the i-layer can still be optimized. This can also be seen from the relatively low FF of this cell under the AM1.5 sun light (Figure 2, solid line).

5 SUMMARY

The photogating effect is observed for the first time in μc-Si: H thin film solar cells. Computer simulations point out this is due to electric field modulation in the i-layer of the solar cell, where the field is weakened by the strong blue bias light. High defect density and low internal electric field are the main requirements for observing the PG effect. This knowledge has helped us to improve the efficiency of μc-Si: H nip cells with an i-layer made by hot-wire CVD [7].

6 ACKNOWLEDGEMENTS

The authors would like to thank C.H.M. van der Werf for sample preparation, R.H. Franken for the rough back reflector development, Dr. R.L. Stolk for useful discussions. The research was financially supported by the Netherlands Agency for Energy and the Environment (SenterNovem).

7 REFERENCES

[1] J.H. Hou and S.J. Fonash, Appl. Phys. Lett. 61 (1992) 186
[2] H.P. Maruska, M.C. Hicks, T.D. Moustakas, and R. Friedman, IEEE Trans. Electron Devices ED-31 (1984) 1343
[3] M. Gloeckler and J.R. Sites, J. Appl. Phys. 95 (8) (2004) 4438
[4] M. K. van Veen, R.E.I. Schropp, J. Appl. Phys. 93 (2003) 121
[5] F. A. Rubinelli, J.K. Rath, and R.E.I. Schropp, Journal of Applied Physics, 89 (2001) 4010
[6] J.J.H. Strengers, F.A. Rubinelli, J.K. Rath, R.E.I. Schropp, Thin Solid Films 501 (2006) 291
[7] H.Li, R.H. Franken, R.L. Stolk, C.H.M. van der Werf, J.K.Rath, R.E.I. Schropp, accepted for presentation at the 4th international conference on HWCVD, Oct 4-8, 2006, Gifu, Japan

A COST AND ENVIRONMENTAL IMPACT COMPARISON OF GRID-CONNECTED ROOFTOP AND GROUND-BASED PV SYSTEMS

M.J. de Wild-Scholten, m.dewild@ecn.nl, Phone +31 224 564736, Fax +31 224 568214
Energy research Centre of the Netherlands ECN, Unit Solar Energy, P.O. Box 1, 1755 ZG PETTEN, the Netherlands
E.A. Alsema, e.a.alsema@chem.uu.nl, Phone +31 30 2537618, Fax +31 30 2537601
Copernicus Institute, Utrecht University, Heidelberglaan 2, 3584 CS Utrecht, The Netherlands
E.W. ter Horst, eth@horisun.nl, Phone +31 30 257608, Fax +31 30 2537601
Copernicus Institute, Utrecht University, Heidelberglaan 2, 3584 CS Utrecht, The Netherlands
Manfred Bächler, baechler@sonnenstromag.de, Phone + 49 731 140 5410, Fax + 49 731 140 5419
Phönix SonnenStrom AG, Schillerstr. 1/6, 89077 Ulm, Germany
V.M. Fthenakis, vmf@bnl.gov, Phone +1 631 344 2830, Fax +1 631 344 4486,
National Photovoltaic EH&S Research Center, Brookhaven National Laboratory, Upton, NY 11973, USA

ABSTRACT: The environmental impact and total system costs have been investigated for roof-top and ground-based crystalline silicon PV systems by using environmental and cost life cycle assessment.
Greenhouse gas emissions and other environmental impacts from Balance-Of-System components are relatively small, in comparison with those of the total PV system. In-roof systems have lower impact due to credit from avoided roof tiles. With proper design of the mounting structure ground-based systems can have low impacts as well.
Although large ground-based systems use larger weights of mounting structure than small roof-top systems and occupy land, they have lower prices than small-scale roof-top systems due to efficient installation and bulk purchasing.
Keywords: economic analysis, environmental effect, small grid-connected PV systems, large grid-connected PV systems

1 INTRODUCTION

In cost and environmental analyses the contribution of Balance-of-System (BOS) components is often given less attention because its share is smaller than that of the PV modules [1]. However as module costs and environmental impacts decrease, the balance-of system part will become of increasing importance. Also in systems with less efficient modules the contribution of BOS will be higher. Furthermore rooftop systems can have an advantage in BOS costs and impacts over ground–based systems because of the lower material requirements, possible savings on roofing material and multiple area use.

The purpose of this paper is to make a comparison of grid-connected rooftop and ground-based photovoltaic systems, based on an analysis of economic cost and environmental impacts for existing systems in Europe and the USA.

For the cost analysis we will look at the cost for different BOS components and installation requirements for in-roof PV systems, on-roof systems (retrofit above existing roof) as well as a number of large ground-mounted systems in the 0.5-5 MWp range [2,3].

The environmental assessments will be based on a Life Cycle Assessment study for the same type of systems as mentioned above. Among the impact results we will pay special attention to the greenhouse gas emissions.

2 METHODOLOGY

For our analysis we selected a number of photovoltaic systems, which we considered representative for today. The small-scale systems are based on BOS components available in Western-Europe (mainly Germany) and designed as described in section 3. Data on material quantities were collected with the help of mounting system suppliers and other sources of information.

The large-scale systems are actually existing systems: one located in Germany and one in Springerville, U.S.A. The latter system was described in [2,4]. Data for the German system was described in [3] and Phönix Sonnenstrom provided further details.

To determine the environmental impact of the BOS components, an environmental life cycle assessment excluding the end-of-life phase has been done using the software SimaPro 7 with the database Ecoinvent 2.1 (corrections made for list of errors as of 16 March 2006). Since the environmental impact is dominated by the primary energy use, this is calculated by using the Cumulative Energy Demand version 1.03 method. An important environmental effect is the global warming potential, which we estimated by means of the IPCC 2001 GWP 100a version 1.02 method.

3 SMALL SCALE ROOF-TOP PV SYSTEM DESIGN

3.1 PV modules

As a typical example for today's technology we chose for modules incorporating 6 x 10 multicrystalline silicon cells with a size 156 mm x 156 mm. One example of such a module is the SolarWorld SW220 with size 1001 mm x 1675 mm (= 1.68 m^2), 220 Wp, weight 22 kg. Because we focus on BOS aspects in this paper, we restrict our analyses to just this module type; also systems with thin film modules are not considered.

3.2 Array layout and inverter

A 1-phase inverter is chosen with a maximum AC power rating of 5 kW, since this is the largest 1-phase inverter possible in Germany.

Since SMA is the largest European solar inverter manufacturer [5], we calculated the number of the SolarWorld modules possible to a 1-phase SMA inverter with maximum power not exceeding 5 kW, using the SMA Excel tool GenAu.xls version 7.3. This results in 2 strings of 13 SolarWorld modules (area 44 m^2) connected to one SMA Sunny Boy 5000TL HC MS inverter.

Reference houses in the Netherlands have roof surface areas ranging from 47 m^2 to 94 m^2 [6]. Present roofs are dual-pitched, but mono-pitched with optimal orientation and slope for integrating PV modules have been demonstrated [7]. We have multiplied the 2x13 module system by 2 to obtain (1) 4 rows of 13 modules with a total area of 87 m^2 and total PV power of 11.4 kWp and (2) 2 inverters with nominal AC power of 2 x 4.6 = 9.2 kW. The ratio of the inverter power and module power is 0.8. The PV system could be installed on 2 smaller houses with a joint roof or 1 large house, preferable mono-pitched with optimal orientation to the sun.

The modules are oriented portrait, which has the advantage of less accumulation of soil in the profiles and minimizes the amount of mounting material needed related to the total module area as well as the labor needed to install the mounting system. These advantages are also valid for ground-based systems.

3.3 Mounting system

We considered two classes of roof-top mounting systems: on-roof mounting, leaving the existing roofing material in place, and in-roof mounting, where the modules take over the function of the roof tiles. In the latter case an actual saving on roof tile material can be accounted. The mounting structures for the roof-top systems that we selected are all suitable for 30^0 sloped roofs and, in the case of the on-roof system, it is compatible with the type of roof tile called Frankfurter Pfanne.

The two on-roof mounting structures analyzed are:

- Schletter Eco05 profile and EcoG roof hooks (the lightest possible)
- Phönix Sonnenstrom TectoSun

The two in-roof mounting structures analyzed are:

- Schletter Plandach 5
- Schweizer Solrif

According to [8] Schletter is the largest solar mounting system supplier for the German market.

As mentioned the modules are mounted on the roof in portrait direction and 4 rows of 13 modules.

3.4 Cabling and connectors

To connect the modules 4 mm^2 DC cabling is used with total length of 188 meter.

To connect the inverter to the grid 6 mm^2 AC cabling is used with total length of 10 meter.

4 ENVIRONMENTAL LIFE CYCLE ASSESSMENT OF PV SYSTEMS

4.1 Modules

The analysis of the multicrystalline silicon modules was in line with our earlier published Life Cycle Assessment of crystalline silicon modules [1]. No update of module production technology was incorporated in this paper.

4.2 Inverters

Detailed data on material use in inverters are not easy to obtain. From earlier studies [9,10] we had at our disposal a detailed bill of materials for a string inverter, the former Philips PSI 300 (P_{nom}= 300 W). Based on that information the material composition for the highly comparable PSI 500 (P_{nom}= 500 W) could be estimated fairly accurately. In the third place we had material data for a somewhat older inverter, the Mastervolt SunMaster 2500 (P_{nom}= 2500 W). All three inverters have wire-wound transformers as major electronic components (by weight).

In figures 1 and 2 you can see that the weight of the inverter in general decreases with the nominal AC power. This effect is strong for very small inverters with a nominal power below 1 kW. Between 2 and 200 kW the weight per kg depends on the inverter choice and is between 5 and 15 kg/kW. Above 400 kW the weight tends to be below 5 kg/kW. For this reason we can expect a lower environmental impact per rated power for inverters for large-scale ground based systems..

Life cycle inventory data for electronic components, like transformers, capacitors and IC's are not available in the standard LCA database that we use (Ecoinvent 2000). Therefore we based ourselves on LCI data for a number of "standard" electronic components that were collected by Andræ [11] [12]. The representativity of these components for inverter electronics could not be verified. Given the relative importance of electronics on the impact results for inverters, this would be a point for further investigation.

The green house gas emissions per rated power of two of our modeled inverters, Sunmaster 2500 and PSI 500, are presented in figure 3.

Figure 3 shows that the impact per rated power of the 500 W inverter is relatively large, mainly as a result of the relatively high amount of electronics and also by the aluminium casing material used for the PSI 500. Quite remarkable too, is the high share of electronics in our modeled inverters. Very often in LCA analyses of inverters, the electronic components are neglected because they are not know or too difficult to model. Our results suggest that this may lead to gross underestimation of the real impacts of inverters.

For inverters in the higher power class, e.g. above 10 kW, one might expect that the relative impact of the electronic components will decrease, as the amount of control electronics will surely not scale with capacity.

For our roof-top system we would need a 4.6 kW inverter. Because no life cycle inventory data for a commercially available 4.6 kW inverter were available, we decided to use scaled-up data for the Sunmaster 2500 instead.

The real impact of a modern inverter in this power class could be different especially if it is transformerless, i.e. if it contains less copper but more electronics. Given the relatively high impacts of electronic components our approach is likely to give an under-estimate of the impacts of a modern inverter.

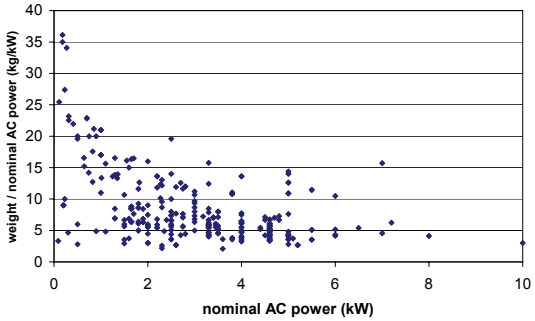

Figure 1: Weight of small inverters (<10 kW)

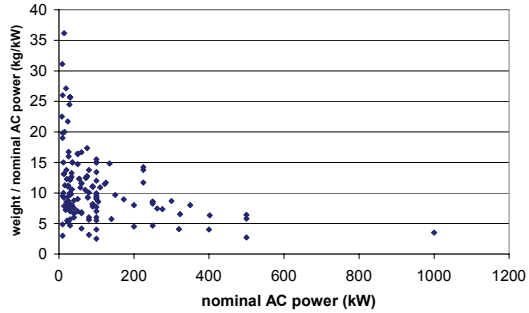

Figure 2: Weight of large inverters (>10 kW)

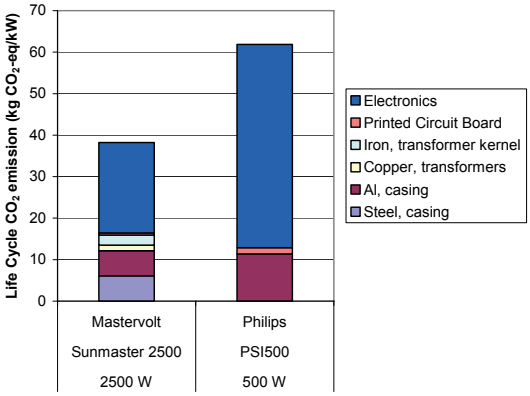

Figure 3: Breakdown of green house gas emissions (in g CO_2-eq/kW) of the inverters Sunmaster 2500 and PSI 500.

4.3 Mounting system

See table I for the inventory of materials used in the various mounting systems.

The different mounting systems investigated may have different static bearing strength for loads like snow/ice and wind (DIN1055).

In figure 4 global warming potential, as expressed by green house gas emissions, is shown. Note that module frames have been included in this figure although these are usually not considered as a BOS component. The reason is that mounting structure design is obviously influenced by the choice for either framed of frameless modules, especially for on-roof or ground-based arrays. Further remark that for those mounting structures that can allow the use of unframed modules, we omitted the frame in our analysis. The impact of the frame alone is often as high as that of the mounting structure. The somewhat heavier design of the frameless-capable mounting structures is more than compensated by the reduction of aluminium use for the module frames. Thus the use of frameless instead of framed modules reduces the global warming potential significantly. One can wonder if a similar advantage could be realized in cost terms.

Also it is interesting to see that the avoidance of ceramic roof tiles in the in-roof systems results in net negative impact scores for the mounting structure, meaning that the global warming effect is decreased. Of the two ground-based mounting structures, although they have comparable weights, the Springerville has lower global warming impact than the Phönix system. The concrete foundations used in Springerville have very little impact, and also less steel and aluminium is used.

Not surprisingly, the roof-top structures have a lower impact than the ground-based ones.

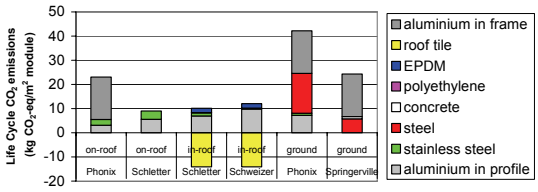

Figure 4: Breakdown of green house gas emissions (g CO_2-eq/m^2 module) for mounting systems including module frame. The "aluminium in profile" is part of the mounting structure, while "aluminium in frame" is the impact of the module frame.

4.4 Cabling and connectors

Cabling and connectors are increasingly being made of halogen free materials and compliant with ROHS [13].

The material composition of the cable used in this LCA are presented in Table II.. Amounts of materials in connectors are not available and therefore are not included in the analysis. The contact materials in the connectors is copper or brass (alloy of copper and zinc) with coating of tin. For the housing of the connectors various plastics are used: polyamide, polycarbonate, polyphenylene oxide, polypropylene, thermoplastic elastomer or thermoplastic polyurethane.

4.5 Total Balance-of-System

See table III for primary energy use of different components of the PV system. The primary energy use is the energy used over the total life cycle of the PV system.

Energy payback times for the different Balance-of-System components are calculated and presented in figure 5 using the following assumptions:
- irradiance of 1700 kWh/m^2/yr (South Europe)
- multicrystalline module efficiency of 13.2%
- performance ratio = 0.75 (http://www.iea-pvps-task2.org/).

The actual performance ratio of PV systems can vary considerably with system design, shading and ventilation. In-roof systems installed in high-temperature areas, may suffer from extra temperature loss, but this depends a lot on the actual roof and mounting design. Because of lacking information on typical loss factors for in-roof systems, we used the same conservative performance

ratio of 0.75 for all system designs.

Based on these assumptions, green house gas emissions are calculated and presented in figure 6 using the following additional assumptions:

- life time of PV system is 30 years
- life time of the inverter is 15 years

A breakdown of the global warming potential of the Balance-of-System components is given in figure 6, again showing that by eliminating the module frame a large reduction of the environmental impact can be obtained. Furthermore ground-based systems generally have a higher impact than in-roof systems, and even if possible extra temperature losses for in-roof systems were taken into account, it seems improbable that this effect would negate the observed advantage.

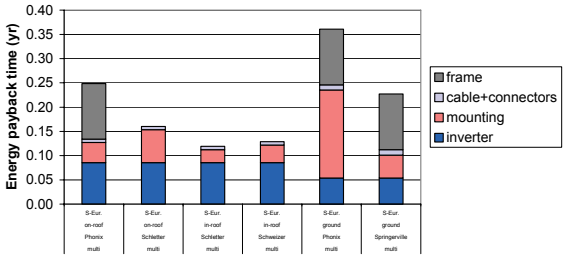

Figure 5: Energy pay back times of Balance-of-System components and module frame of PV systems located in South Europe

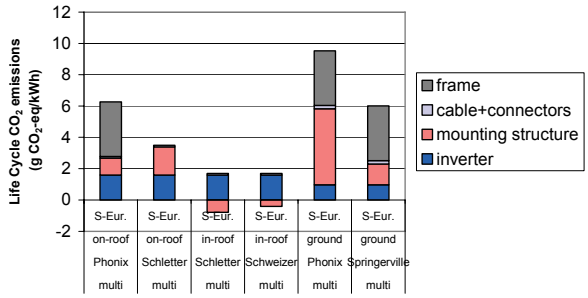

Figure 6: Green house gas emissions (in g CO_2-eq/kWh) of Balance-of-System components and module frames of PV systems located in South Europe

4.6 Total PV system

Figure 7 shows that the global warming potential of the total PV system is still dominated by the module.

For future crystalline silicon technology, where the impact of laminates may be reduced by 50% or more [17], the BOS contribution may increase up to 25% and almost 50% if we consider the frame as well (see figure 8). In this situation an optimized design of the BOS, reducing overall environmental impacts, becomes even more relevant than it is now.

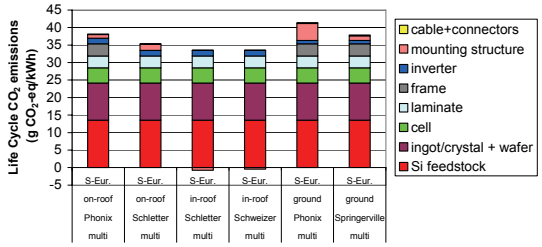

Figure 7: Breakdown of green house gas emissions (in g CO_2-eq/kWh) of PV systems located in South Europe

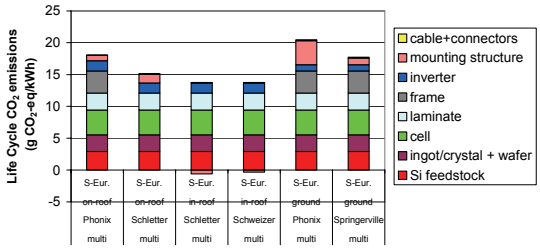

Figure 8: Breakdown of green house gas emissions (in g CO_2-eq/kWh) of future PV systems located in South Europe (17% module efficiency, 150 µm cell thickness, silicon feedstock produced with fluidized-bed-reactor technology)

5 PRICE

All prices mentioned are excluding VAT.

5.1 Modules

Prices of modules [14] are presented in figure 9. For the breakdown of PV system price we assumed a module price of 4 €/Wp (excl. VAT) for small-scale systems and 3 €/Wp (excl. VAT) for large-scale systems.

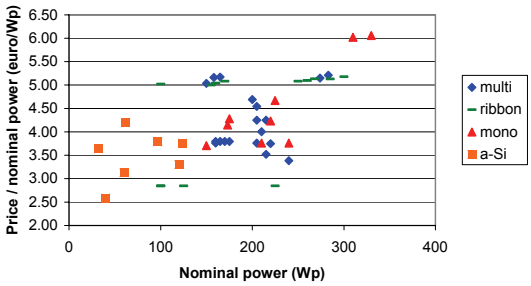

Figure 9: Prices of modules excluding VAT [14]

5.2 Inverters

In figures 10 and 11 it can be seen that the price/kW decreases with nominal AC power of the inverter with the lowest value approaching 0.2 euro/kW.

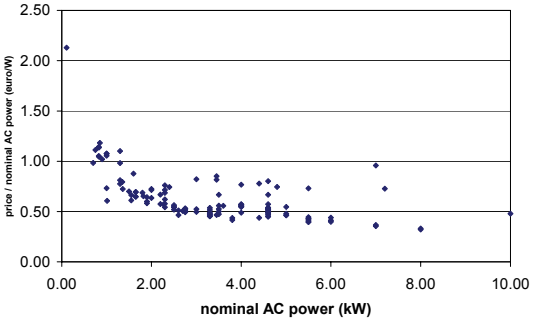

Figure 10: Prices of small inverters excluding VAT

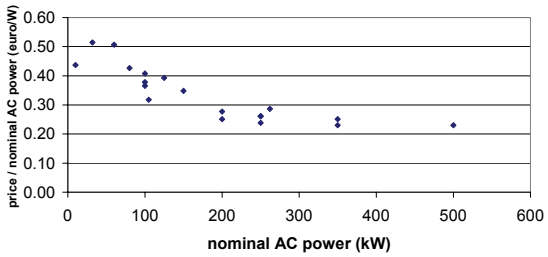

Figure 11: Prices of large inverters excluding VAT

5.3 PV system

Figure 12 shows prices of small-scale PV systems [15]. Figure 13 shows investments of large-scale PV systems [16].

A breakdown of the prices of PV systems is presented in figure 14 using data from [2], [3] and [4] for large-scale PV systems and own estimates for the roof-top systems.

The total Balance-of-System prices of roof-top and ground-based systems are comparable. Although the weight of the mounting structure of the ground-based systems is much larger than the weight of the roof-top systems, the prices are comparable because the components used in ground-based system are made of less expensive materials and can be designed/installed more efficiently. The large-scale ground based systems furthermore have the advantage of bulk purchasing compared to the small-scale roof top systems.

The PV system prices are still dominated by the module price.

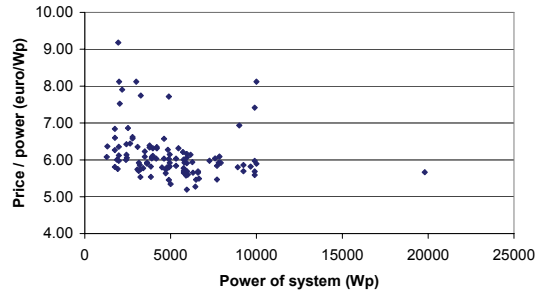

Figure 12: Prices of small-scale PV systems excluding VAT

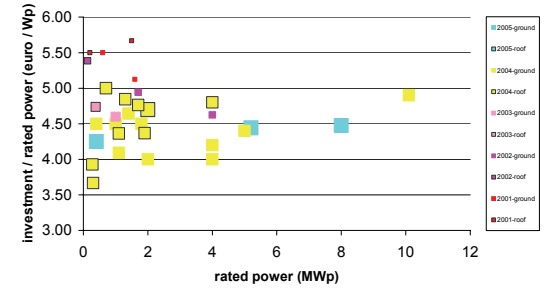

Figure 13: Investments of large scale PV systems

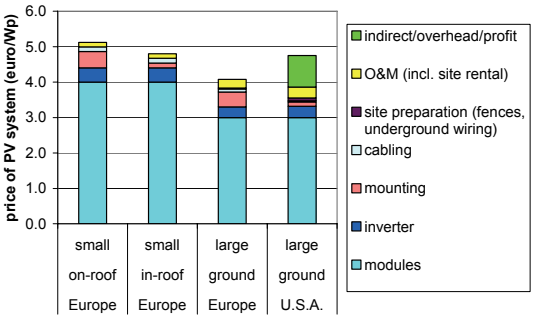

Figure 14: Breakdown of prices of PV systems excluding VAT

6 CONCLUSIONS

The environmental impact and total system costs have been investigated for roof-top and ground-based crystalline silicon PV systems by using environmental and cost life cycle assessment.

Greenhouse gas emissions and other environmental impacts from Balance-Of-System components are relatively small, in comparison with present-day modules.

Frameless laminates are largely preferred from an environmental point of view; the extra impacts from a somewhat heavier mounting structure are more than compensated by the avoided impacts of the frames.

In-roof systems clearly have a lower environmental impact of the Balance-of-System components in comparison to on-roof and ground-based systems. This advantage is due to the credit from avoided ceramic roof tiles. For an in-roof system the greenhouse gas emissions of the balance-of-system components can be as low as 3% of the emission of the total PV system, while the BOS (including frames) of an on-roof system is responsible for about 18% of the emissions of the total PV system..

The BOS (including frames) of ground-based systems are responsible for 16 to 23% of emissions of the total PV system. With frameless modules and a proper design of the mounting structure, ground-based systems will have comparable impacts as *on*-roof systems, but still higher than for in-roof systems. The BOS then produces about 7% of emissions of the total PV system.

If in future the impact of PV laminates will be 1/2 of today's impact, then the relative impact for BOS will be about 8% for in-roof PV and 15% for optimized ground based PV respectively, compared with the emissions of the total PV system.

Among BOS components the inverter seems to cause a relatively large impact, especially in smaller PV systems. Better LCA data on the electronic parts of an inverter would be helpful to reduce uncertainties for this component.

Although large ground-based systems use larger weights of mounting structures than small roof-top systems and occupy land, they have considerably lower prices than small-scale roof-top systems due to efficient installation and bulk purchasing. This effect will be in future lower as it scales mainly with the (falling) module

prices.

On the other hand ground costs (which were taken into account) can be higher in more densely populated areas, thus reducing the cost advantage.

Future PV roof-top systems should try to reduce further on costs and materials for mounting structure, roof tiles and on installation work because the relative impact of BOS will rise with falling module prices.

The environmental life cycle inventory data are available at the ECN website as Excel file [18].

8 ACKNOWLEDGEMENTS

Part of this work was carried out in the project "Technologie- en Milieuverkenningen" with ECN project number 7.4750 financed by the Ministry of Economic Affairs, the Netherlands.

Manuel Schwarzmaier of Schletter Solar-Montagetechnik, Helge Hartwig of Ernst Schweizer Metallbau and Daniel Hahn of Phönix Sonnenstrom AG are acknowledged for providing the amounts of mounting structure materials.

REFERENCES

[1] E.A.Alsema, M.J.de Wild-Scholten, Environmental impacts of crystalline silicon photovoltaic module production, *LCE2006, 13th CIRP International Conference on Life Cycle Engineering, Leuven, Belgium* (2006) http://www.ecn.nl/library/reports/2006/rx06041.html.

[2] J.E.Mason, V.M.Fthenakis, T.Hansen, H.C.Kim, Energy payback and life-cycle CO_2 emissions of the BOS in an optimized 3.5 MW PV installation, *Progress in Photovoltaics* **14** (2006) 179.

[3] M.Bächler, C.Bindel, Cost comparison of large scale crystalline and thin-film PV systems, *20th European Photovoltaic Solar Energy Conference, Barcelona, Spain* (2005).

[4] L.Moore, H.Post, T.Hansen, T.Mysak, Photovoltaic power plant experience at Tucson Electric Power, (2005) http://www.greenwatts.com/Docs/TEPSolar.pdf.

[5] B.Epp, International inverter market 2005, *Sun & Wind Energy* **1** (2005) 52.

[6] NOVEM, Referentiewoningen bestaande bouw, (NOVEM, Sittard, the Netherlands, 2001), http://www.dubo-centrum.nl/publicaties/publicatie.php?kaartNr=1567.

[7] T.Reijenga, Sustainable and solar building (5 MW project) - Langedijk (NL), *17th European Photovoltaic Solar Energy Conference, Munich* (2001) http://www.bear.nl/content/pdf/vb2.6paper.pdf.

[8] J.Zeitner, Gewinn maximieren mit Montagesystemen, *Sonne Wind & Wärme* **6** (2006) 92.

[9] E.Alsema, Duurzaamheid van fotovoltaïsche systemen op basis van geavanceerde silicium technologie, **NWS-E-2003-17** (Utrecht University, the Netherlands, 2003), http://www.chem.uu.nl/nws/www/publica/e2003-17.pdf.

[10] E.C.Molenbroek, P.Deege, Inventarisatie materiaalverbruik BOS-componenten, **E21085** (Ecofys, Utrecht, Nederland, 2002).

[11] A.S.G.Andræ, Environmental life-cycle assessment in microelectronics packaging. (2005). Chalmers University of Technology, Göteborg, Sweden.

[12] A.S.G.Andræ, Life cycle inventory data of electronic components, personal communication. (2006). 3-8-2006.

[13] M.J.de Wild-Scholten, K.Wambach, E.A.Alsema, A.Jäger-Waldau, Implications of European environmental legislation for photovoltaic systems, *20th European Photovoltaic Solar Energy Conference, Barcelona, Spain* (2005) http://www.ecn.nl/library/reports/2005/rx05014.html.

[14] Photon, Gleich und doch nicht gleich gut. Solarmodule - das zentral Element jeder Anlage, *Photon* **Special** (2006) 26.

[15] Photon, Das Angebot an Komplettsystemen ist unbeständig, *Photon* **Special** (2006) 60.

[16] J.Siemer, Prospects for a sunny return. The situation for PV funds is complicated, but the great potential remains, *Photon International* **September** (2005) 18.

[17] E.A. Alsema, M.J. de Wild-Scholten, V.M. Ftenakis, Environmental impacts of photovoltaic technology, a critical comparison of energy supply options, this conference.

[18] M.J.de Wild-Scholten, E.A.Alsema, Environmental Life Cycle Inventory of Crystalline Silicon Photovoltaic System Production - Excel file, **ECN report ECN-E--06-019** (ECN Solar Energy, 2006), http://www.ecn.nl/publications/default.aspx?nr=ECN-E--06-019.

Table I: LCI of mounting systems.

kg / m²	on-roof Phönix TectoSun	on-roof Schletter Eco05 + EcoG[1]	in-roof Schletter Plandach 5[1]	in-roof Schweizer Solrif	ground Phönix	ground Springerville
module size (mm x mm):	1675x1001	1675x1001	1675x1001	1675x1001	1318x994[2]	1892x1283[3]
framed (f) or unframed (u) modules	f	f+u	f+u	u[4]	f	f
Steel	0.00	0.00	0	0.00	11.50	4.01
Stainless steel	0.49	0.72	0.28	0.08	0.17	0.00
Aluminium	0.54	0.97	1.21	1.71	1.26	0.00
Concrete	0.00	0.00	0.00	0.00	0.00	8.03
TOTAL	**1.03**	**1.69**	**1.49**	**1.79**	**12.93**	**12.04**
frame of module	3.04	0.00	0.00	0.00	3.04	3.04
EPDM under-roof	0.00	0.00	1.41	1.41	0.00	0.00
Avoided roof-tiles	0.00	0.00	-40.00	-40.00	0.00	0.00

[1] For the Schletter mounting systems the Excel tool Autokalkulator version 8.22 is used to calculate the amounts of materials.
[2] Phönix ground-based PV system uses Sharp 162 Wp multicrystalline silicon modules.
[3] Springerville ground-based PV system uses ASE 300DG/50 300 Wp multicrystalline framed modules.
[4] The Solrif profiles are fixed to the frameless module (=laminate) in the factory.

Table II: Material composition of cabling

kg / m	Helukabel Solarflex 101 4 mm² DC	Helukabel NYM-J 6 mm² AC
Copper	38.4	173
TPE Thermoplastic Elastomer	29.6	0
PVC	0	147

Table III: Primary energy use of the PV systems

MJ / kWp	Phönix TectoSun on-roof	Schletter Eco05 + EcoG on-roof	Schletter Plandach 5 in-roof	Schweizer Solrif in-roof	Phönix ground	Springerville ground
module size (mm x mm):	1675x1001	1675x1001	1675x1001	1675x1001	1318x994	1892x1283
Si feedstock	13319	13319	13319	13319	13319	13319
ingot/crystal + wafer	9204	9204	9204	9204	9204	9204
cell	3368	3368	3368	3368	3368	3368
laminate	3201	3201	3201	3201	3201	3201
frame	1697	0	0	0	1697	1697
inverters	1267	1267	1267	1267	795	795
mounting system	612	1000	393	534	2682	701
cabling	99	99	99	99	159	163
total	**32766**	**31457**	**30850**	**30991**	**34424**	**32447**